Ph.D. DISSERTATION

Development of Effective Solution-processed Patterning Techniques for High-resolution Display Components

고해상도 디스플레이 구성 요소를 위한 용액 공정 기반의 효율적인 패터닝 기술 개발

FEBRUARY 2023

DEPARTMENT OF ELECTRICAL AND
COMPUTER ENGINEERING
COLLEGE OF ENGINEERING
SEOUL NATIONAL UNIVERSITY

GEONHEE KIM

Development of Effective Solution-processed Patterning Techniques for High-resolution Display Components

고해상도 디스플레이 구성 요소를 위한 용액 공정 기반의 효율적인 패터닝 기술 개발

지도교수 홍 용 택

이 논문을 공학박사 학위논문으로 제출함
2023 년 2 월

서울대학교 대학원
전기 · 정보 공학부
김 건 희

김건희의 공학박사 학위논문을 인준함
2023 년 2 월

위 원 장 정 윤 찬 (인)

부위원장 홍 용 택 (인)

위 원 곽 정 훈 (인)

위 원 유 승 협 (인)

위 원 정 승 준 (인)

Abstract

Development of Effective Solution-processed Patterning Techniques for High-resolution Display Components

GEONHEE KIM

DEPARTMENT OF ELECTRICAL AND COMPUTER ENGINEERING

COLLEGE OF ENGINEERING

SEOUL NATIONAL UNIVERSITY

As the development of the display components is focused on the stable operation of the devices on plastic and elastomeric platform, solution-process has received attention as a prospective deposition technique to supplement the drawbacks of the conventional process. Among them, numerous papers about the printing method of the material ink have been reported due to its high degree of patterning without needing an extra patterning mask. Although inkjet printing is a promising method, a demand for electrohydrodynamic (EHD) printing has emerged for high-resolution patterning technology. In this Ph.D. dissertation, I suggested facile patterning techniques of various elements for next-generation displays by utilizing inkjet printing or EHD printing according to the desired resolution.

First, the complicated patterning process of the silver nanowire (AgNW) transparent electrodes hinders their commercialization. Although AgNWs have

excellent optoelectronic properties and mechanical stability, which can be mentioned as replacements for indium tin oxide, the patterning mask of the AgNWs needs to be replaced for changing the patterns, and the expensive fabrication cost is required for the high-resolution mask. To overcome those issues, I developed a straightforward patterning method of the AgNWs based on the inkjet printing of the adhesive-blended poly(3,4-ethylenedioxythiophene):poly(styrene sulfonate) (PEDOT:PSS) polymer patterns on the target substrate for transfer of AgNWs from the elastomeric stamp. The transfer process of AgNWs only onto the pre-printed polymer patterns enables a facile patterning without needing a patterning mask. The transfer-based patterning technique can be conducted on the plastic substrate, and the patterned AgNWs can be adopted to flexible display applications with superior flexibility.

Second, the resolution limit of the inkjet-printing process and the external force during the lamination of AgNW-coated PDMS stamp interrupted the fine patterning of the AgNWs with a feature size under 30 μm. Therefore, an optimized patterning approach should be needed to enhance the resolution of the AgNW patterns. Poly(vinyl alcohol) (PVA) was selected as an adhesive located under the spray-coated AgNW. When the printed PEDOT:PSS was deposited on the AgNWs, the conductive polymer and underlying PVA layer formed an interpenetration network. As a result, the AgNWs were captured between the PEDOT:PSS and PVA layer, and the AgNWs with a formation of the previously printed PEDOT:PSS pattern remained without damage after the removal process. The EHD printing of the PEDOT:PSS was also implemented to demonstrate precise micropatterns with a width down to 15 μm. Another advantage of the PVA-assisted method is the precise patternability of the AgNWs on the elastomeric substrate. Therefore, this patterning approach can be

applied to highly conductive and stretchable electronics with high resolution.

Finally, I investigated the optimized patterning process of the quantum dot (QD) color conversion structure with EHD printing. To improve the uniformity of the printed QD layer, producing a mixture of photocurable polymer and QD was preceded. The ligand exchange treatment was conducted to prevent the aggregation of QD in the polymer matrix and resulting nozzle clogging during the EHD printing. The ligand-exchanged QD maintained its optical properties, such as emission wavelength and absorbance spectrum. In addition, the composite of polymer and QD showed stable jetting conditions even in the case of a high concentration of the QD. Through the proper surface treatment, the printed color conversion structure was formed in a lens-shaped structure with a diameter from 40 μm to 20 μm. After printing the composite on the micro-LED light sources with the desired thickness, the composite layer demonstrated its color-conversion effect. Furthermore, the blended QD ink can be printed on the surface of the polyimide and elastomer, which can pave the way for next-generation light-emitting devices.

Keyword : Silver nanowire, PEDOT:PSS, inkjet-printing, EHD printing, Quantum dot, Flexible & stretchable electronics
Student Number : 2016-20865

Contents

List of Tables

List of Figures

Chapter 1 Introduction

1.1. Next-generation Display

Visualization of information is the most intuitive technique of sharing knowledge throughout the history of humankind. Beyond transmitting information by series of characters or immovable images, the era of display devices operated by semiconductor-based electronic circuits has arrived to represent video data. While the display technology has advanced, the fabrication strategies of the display have been focused on a rigid platform such as a plasma display panel, liquid crystal display, and organic light-emitting diode (OLED) [1]. However, as the demands for mobile displays and wearable electronics have risen, the innovation of the form factor of the next-generation display is necessary to replace the conventional rigid-display components [2, 3]. Major concerns of the display industries and numerous researchers are developments of devices on the flexible platform and further paving the way for stretchable electronics with free form factors (**Figure 1.1**). In the case of flexible displays, the first commercialization of mobile phones with flexible OLEDs already progressed in 2015, and the manufacturing of various flexible displays has been announced. In addition, the applications of stretchable electronics are expanded to diverse research fields, such as stretchable OLED circuits, electronic skins, and wearable healthcare devices [4-6]. For a demonstration of the next-generation display components, a typical implementation technique or coventional materials has

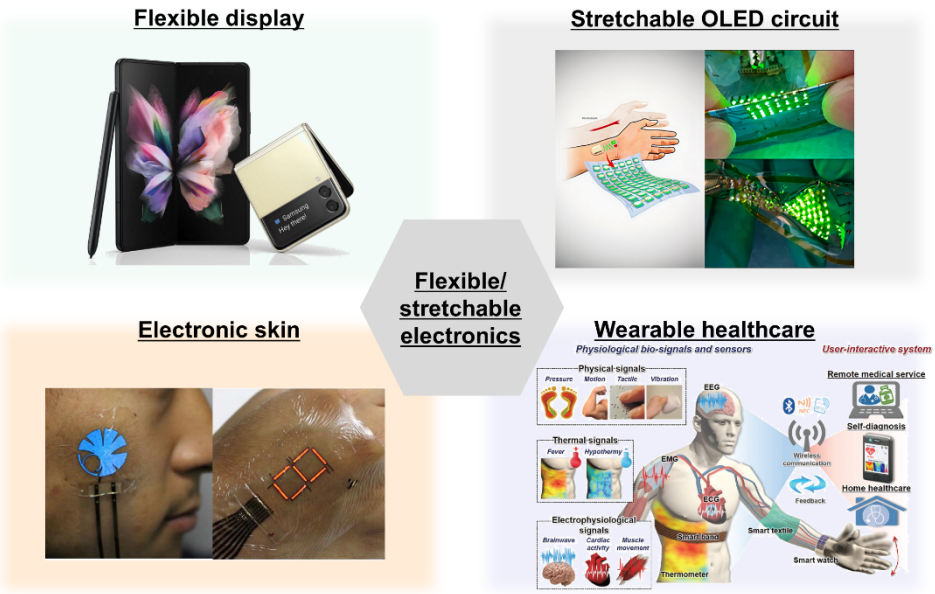

Figure 1.1 Various flexible/stretchable display applications (Source: Samsung Newsroom, [4-6]).

a drawback and limitations, which is why the development of progressive fabrication strategies and the finding replacements of the existing materials are needed. For example, indium tin oxide (ITO) is a widely used material for the electrodes of optoelectronic devices due to both superior conductivity and high transparency [7]. However, the inherent brittleness of the ITO film leads to the degradation of the performance of the flexible and stretchable devices under external strain [8]. In addition, the high deposition temperature of the ITO film for crystallization also causes the deformation of the plastic and the elastomer platform [9, 10]. Therefore, various studies have been reported about the alternative fabrication process and materials suitable for flexible and deformable platforms. In this Ph.D. dissertation, I studied novel deposition methods for several display components for flexible and stretchable electronics. And in the next section, a representative deposition technique

for the next-generation displays is introduced.

1.2. Solution Process

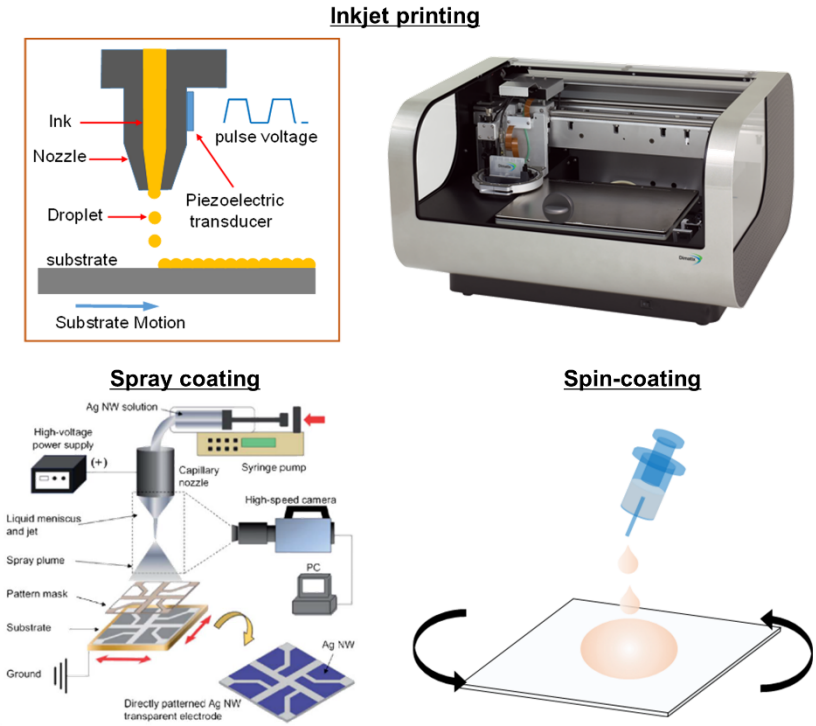

Figure 1.2 Solution-based deposition methods (Source: HZB, Dimatix, [21]).

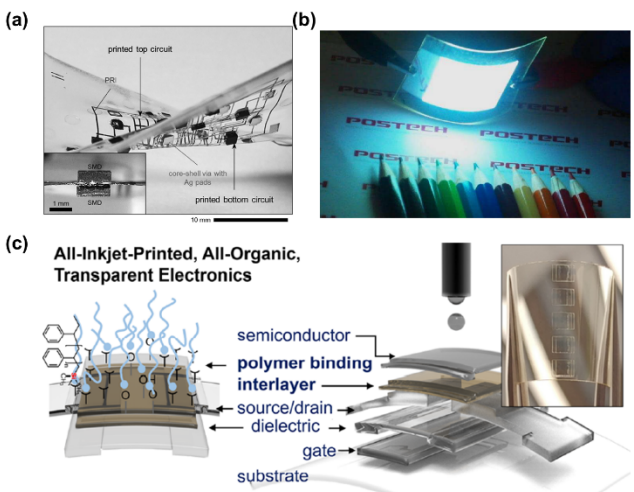

Figure 1.3 Solution-processed (a) stretchable electronic circuits, (b) flexible OLEDs, (c) organic thin-film transistors [23-25].

For facile fabrication of electronic devices on the flexible/stretchable platform, the conventional deposition methods, which have been conducted on a rigid surface, should be replaced. A solution-based process can be a possible candidate for a deposition technique of thin films on arbitrary substrates, based on the deposition of the ink composed of electronic materials and the subsequent curing process to evaporate the unnecessary solvent. Unlike conventional deposition processes such as chemical vapor deposition, atomic layer deposition, and epitaxy, the solution process was conducted under normal pressure, which indicates that high-vacuum equipment is not needed [11, 12]. The production of the devices by non-vacuum facilities dramatically decreases fabrication costs [13], and the solution process can expand its applications to large-area devices by introducing roll-to-roll manufacturing and multi-nozzle printing [14-16]. Furthermore, the solution-based fabrication approaches progressed under room temperature, and the low temperature of the annealing sequence for obtaining thin film prevents the flexible/stretchable substrates from being damaged [17, 18]. Based on these advantages, various deposition techniques of material inks have been developed according to the requirements of the electronic devices (**Figure 1.2**). First, a drop-on-demand inkjet-printing method has been established for the facile patterning of thin films without a patterning mask or extra lithography process [19, 20]. On the other hand, the large-area coating process can be implemented by spray-coating or spin-coating methods, and the thickness of the layer can be easily controlled by the volume of spraying and spin-coating rpm, respectively [21, 22]. The solution-process techniques have been utilized to the future display components on a plastic or elastomeric platform, such as stretchable electronic circuits [23], flexible OLEDs [24], and organic thin-film transistors [25] (**Figure 1.3**). In this Ph.D. dissertation, I focused on the solution-

process-based patterning techniques of the three display components: transparent electrodes on a flexible platform, conductive electrodes on a flexible/stretchable platform, and photo-curable polymer/Quantum dot (QD) composite on an arbitrary surface. And I will explain the necessity of the high-resolution patterning process for future display applications and suggest a novel solution-processed patterning technique that can achieve elaborate patterns with a micrometer scale.

1.3. High-resolution Patterning Techniques

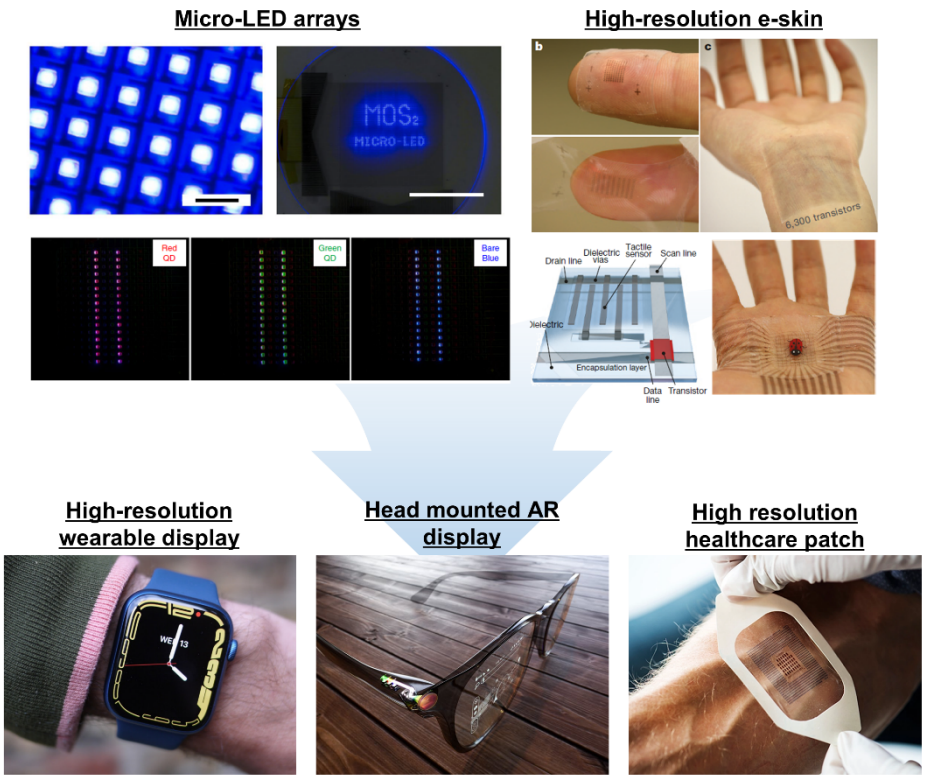

Figure 1.4 High-resolution display components (up) and future applications with high resolution electronics (down) (Source: [28, 29], Apple, Laser Focus World, Encompasshealth).

As the improvement of solution processing technology is essential for commercializing next-generation displays with curved surfaces and deformable platforms, a resolution enhancement of the electronic devices is another critical factor for advanced display performance (**Figure 1.4**). If the light-emitting elements are adopted to display devices with a limited area, such as a wearable watch or an augmented reality/virtual reality (AR/VR) devices, the size of a single light-emitting pixel and the pitch between the pixels should be reduced for expression of

complicated image and satisfying the human eye. For describing the same amount of information on the smaller area, the resolution of the display needs to be enhanced. Furthermore, when human eyes see two light sources, they cannot perceive two lights and recognize them as a single light source if the gap between them is narrower than a certain length. This gap is determined by the angle between the lights from each light source to human eyes, and the limit of the angles the human can recognize the gap is defined as angular resolution [26, 27]. In the case of the AR/VR device, the distance between the eye and the display is narrower than in conventional displays, and the pitch between the pixels should be narrower to satisfy the angular resolution. The resolution of the wearable healthcare system will also be increased for local measurement of the electrical signals. The display components with sizes under hundreds of micrometers have been investigated to demonstrate high-resolution electronic devices, such as micro-LEDs and high-resolution electronic skin [28-30]. For the integration of the various electronic elements into high-resolution applications, fine patterning of the interconnects and the electrodes should be preceded. Moreover, developing the high-resolution patterning technique based on the solution-processed approach is required for an embodiment of display applications on flexible/stretchable platforms.

Electrohydrodynamic (EHD) jet printing is a solution-processed printing technology that can provide high-resolution patterns with feature size down to submicron scale [31-33]. **Figure 1.5** represents the printing principle of EHD printing. The inner diameter of the nozzle can be manufactured in various diameters, from a few micrometers to several hundred micrometers. A high electric field must be applied between the electrode inside the nozzle and the target substrate to achieve stable ejection of the ink from the nozzle. As a result of the applied electric field, the

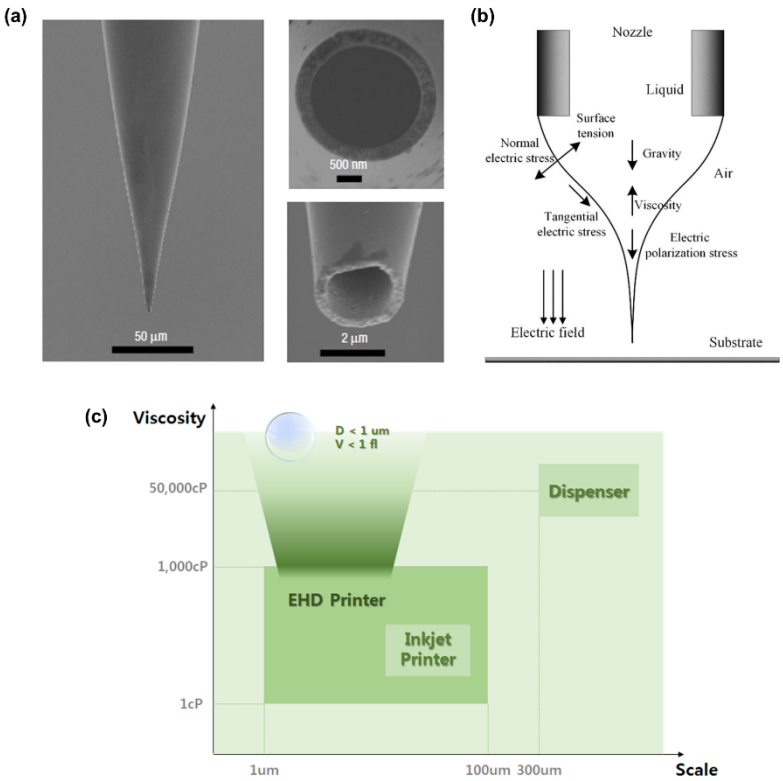

Figure 1.5 (a) Optical image of the nozzle tip, (b) printing principles of EHD printing, and (c) process window of the EHD printing (source: [34, 36], Enjet).

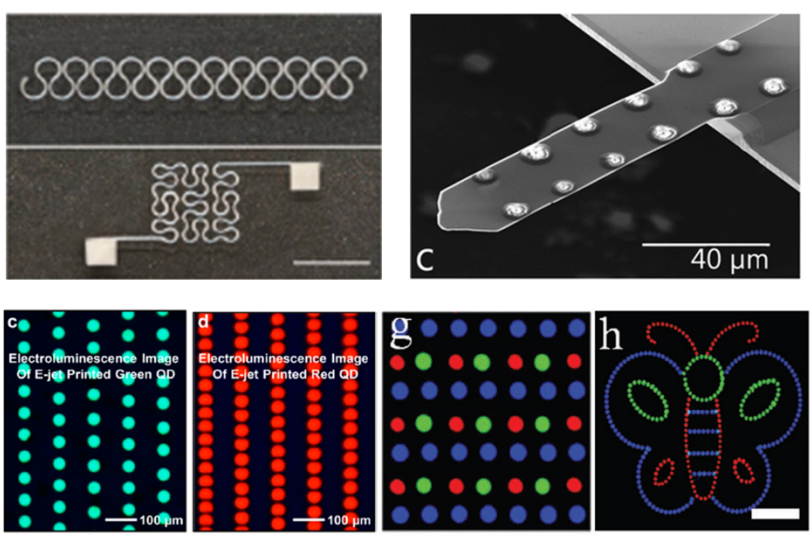

Figure 1.6 Various display components implemented by EHD printing process [37-40].

ink molecules are charged, and the cone-shaped meniscus of ink was formed at the end of the nozzle tip caused by the surface charge of ink [34-36]. The continuous droplets were ejected from the end of the nozzle when the sum of hydrodynamic force and electrostatic force overcomes the capillary force. Through the applied electric field with a high voltage of several kV, various material inks, even with high viscosity, can be printed on arbitrary substrates with a micrometer scale. Many researchers have been interested in EHD-printing of different materials on various surfaces, such as metallic nanowires on plastic and elastomeric substrate, polyethylene polymer on microcantilever surfaces, and QD ink and perovskite ink on glass [37-40] (**Figure 1.6**). In chapter 3 and chapter 4 of this dissertation, the conductive polymer, and the photocurable polymer are deposited on diverse surfaces by EHD printing to accomplish maskless patterning of the highly conductive electrodes and high-resolution patterning of color-conversion structures.

1.4 Organization of this dissertation

In this Ph.D. dissertation, I showed solution-based patterning techniques of various materials for fabricating high-resolution display elements. I focused on a patterning of three components without the requirement of a conventional patterning mask. I demonstrated a transparent electrode patterning with hundreds of micrometers for flexible electronics, highly conductive electrode patterning with tens of micrometers for flexible and stretchable electronics, and photocurable polymer/QD composite printing on various surfaces for uniform color conversion.

This dissertation contains five chapters, including **Introduction** and **Conclusion**.

Chapter 1 introduces a fabrication strategy for next-generation display applications in terms of form factor and device resolution. The requirement of the solution-based patterning process is also emphasized for achieving both high-resolution and low-cost patterning.

Chapter 2 presents a simple patterning method of the silver nanowire (AgNW) transparent electrodes (TEs) accomplished by the inkjet printing of the adhesive pattern templates and the transfer process of the AgNWs on the surface of the adhesive. As a result, precise patterns of AgNW TEs with hundreds of micrometers were formed on the plastic substrates for the flexible electronic devices.

Chapter 3 describes a high-resolution patterning method of the AgNW conductive electrodes on the flexible and stretchable substrates without a conventional patterning mask by inkjet and EHD printing of the conductive polymer on the spray-coated AgNW surface. The spin-coated adhesive layer before the

coating of AgNWs enhances the adhesion of the printed conductive polymer and the AgNWs covered by the polymer and adhesive layer.

Chapter 4 depicts the EHD printing method of a photocurable polymer/QD composite with high viscosity. Prior to the printing process, the optimization of mixing QDs with the polymer is required to prevent the aggregation of QDs in the polymer matrix and achieve uniform color-conversion structures.

Chapter 5 concludes the results and significant accomplishments of this dissertation. Besides, the vulnerable points that should be improved are also suggested for future study.

Chapter 2 Transfer-assisted Patterning Process of Transparent Electrodes

2.1. Introduction

This chapter suggests a straightforward deposition technique of the AgNW transparent electrodes based on inkjet-printing of adhesive templates and selective transfer of the AgNWs on them. Academic investigations focused on the possible alternatives of ITO TEs have been continuously implemented for next-generation flexible electronics [41-51]. Due to the fragility of the ITO and low flexibility [52, 53], the ITO TEs are not suitable for flexible electronics, and diverse conductive materials such as metallic nanowires, conductive polymer, graphene, and carbon nanotubes (CNTs) have been attracting severe attentions [54-62]. Among the several applicants, the interest in AgNW networks as future TEs have risen due to the formation of 1-dimensional (1-D) conductive paths with complex structures that both ensure high conductivity and transmittance [48, 49, 61, 63-66]. Moreover, the flexibility of the AgNW electrodes on plastic substrates and the stretchability of the elastomer-embedded AgNWs also expand their implementations to deformable electronics [67, 68]. Various efforts have been addressed for the commercialization of the AgNWs to resolve the several drawbacks of the AgNWs. First, multiple papers have reported the fabrication methods of optoelectronic devices with AgNWs,

including the embedding process, which compensates for the rough surface of AgNWs [69-71]. Besides, appropriate patterning methods of AgNWs should also be developed because electrodes with desired patterns at precise locations are needed in various high-resolution flexible electronics. Major patterning approaches have been focused on mask-assisted fabrication, such as photolithography [72-75], surface energy-controlled patterning [76, 77], and spray-coating on the mask-covered substrate [21, 78, 79]. Mask-assisted patterning is a promising way to block unnecessary deposition onto the non-patterned area. However, there is a drawback that the patterning mask should be manufactured whenever the pattern shape is changed. And as the resolution of the patterns develops, the fabrication cost of the photomask also increases because anisotropic etching of patterning masks with high resolution is complicated [80]. The transfer process of the pre-patterned AgNWs is another precise patterning technique that can resolve the solvent orthogonality issue during the deposition process [59, 77, 81-83]. However, these transfer methods require pre-structured stamps formed by photolithography or additional patterning processes. Although the selective patterning method of the AgNW networks was also suggested by transfer from the AgNWs on a hydrophobic surface onto the toner-printed copy paper [82], deposition of the high-quality AgNW on the hydrophobic stamp by the conventional solution process is complicated. Recently, various kinds of research have been focused on the patterning processes of AgNWs, which do not require a patterning mask. Direct printing methods of AgNW ink have been reported as promising techniques for fabricating AgNW layers with desired shapes, including inkjet printing [84-86] and EHD jet printing [37, 87-89]. However, the 1-D structure of AgNWs and aggregation inside the nozzle cause the nozzle clogging to disturb the stable formation of printed layers.

In this chapter, I fabricated facile-patterned AgNW networks by a combination of inkjet-printing of adhesive-blended conductive polymer pattern and selective transfer of the AgNW layers on the pre-pattened template.[1] For lamination of the PEDOT:PSS and the attached AgNWs, D-sorbitol was selected as an adhesive because D-sorbitol has been widely adopted as an electrical glue that achieves great mechanical and electrical contact [90-92]. After the attachment and peeling off of the AgNW stamp from the inkjet-printed PEDOT:PSS transfer template, the AgNW networks attached to the PEDOT:PSS template was only moved onto the region of the transfer template [93]. Employing the facile patterning method, my AgNW-transferred PEDOT:PSS TEs were formed on various substrates, showing not only highly tunable optoelectronic properties but also fine lines with widths down to 30 micrometers. In addition, unlike the brittle ITO TEs, the AgNW-transferred PEDOT:PSS TEs showed superior mechanical flexibility during the flexibility test with a bending radius down to 2 mm. The AgNW-transferred PEDOT:PSS TEs were applied to various flexible electronics to decrease the applied voltage and power consumption, such as flexible LED arrays, touch panels, and all-solution-processed polymer light-emitting diodes (PLEDs).

[1] Figures and contents included in this chapter are based on a published paper [93]. The conduct of this study is equally contributed by J. Park and G. Kim. Some materials in this chapter were also used in Dr. J. Park's Ph. D. dissertation.

2.2. Patterning of AgNW Transparent Electrodes Based on Inkjet-printing of Adhesive PEDOT:PSS Templates

2.2.1. Main Concept

Figure 2.1 shows a facile patterning process of AgNW networks by integrating the inkjet printing of the PEDOT:PSS patterns and selective transfer of the AgNW networks only onto the region of the transfer template. First, the modified PEDOT:PSS pattern was inkjet-printed as the transfer template. To enhance the adhesive force of the PEDOT:PSS film, D-sorbitol material was selected as an adhesive which was mixed with the PEDOT:PSS materials. Various papers have been reported about the lamination process conducted by the PEDOT:PSS interlayers mixed with D-sorbitol [94, 95]. The adhesive property of D-sorbitol provides mechanical contact during attachment between two divided parts of the devices, while conductive PEDOT:PSS enables electrical contact between adjacent layers. In addition, Park et al. previously suggested the patterning method of PEDOT:PSS on various substrates without any damage, which can be achieved by the dry transfer of PEDOT:PSS mixed with D-sorbitol [96]. Based on these mechanisms, I introduced PEDOT:PSS mixed with D-sorbitol (from now on, I will call it D-PEDOT:PSS) as a transfer template of AgNWs. The adhesive property of D-sorbitol helps the AgNWs easily transfer from the PDMS stamp to the transfer template. In addition, the decent conductivity of PEDOT:PSS layer not only enables the slight improvement of sheet resistance but also helps the uniform distribution of current because the vacancies of

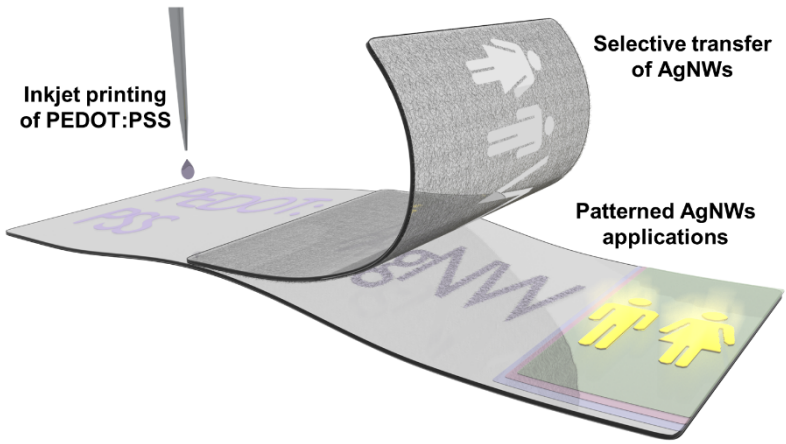

Figure 2.1 Illustration of a patterning method of AgNWs by integration of the inkjet-printing of the PEDOT:PSS and selective transfer of AgNWs.

AgNW layers are filled with conductive PEDOT:PSS [97]. Second, the fabrication of the AgNW-coated PDMS stamp was conducted without the implementation of any pre-patterned structure on the elastomeric PDMS. To acquire the uniform AgNW networks and the optimized optoelectronic characteristics for the use of TEs, the treatment time of plasma on PDMS, the concentration of AgNWs, coating numbers, and the extra conductivity-enhanced treatment were optimized. During the annealing process, the AgNWs and the PEDOT:PSS transfer template were merged into one composite film because the D-sorbitol contained in the PEDOT:PSS template partially melted at the temperature of 100 ℃ and for achieving the conformal lamination between AgNWs and PEDOT:PSS. At the same time, the adhesive force of the AgNW/PEDOT:PSS film with the PDMS stamp decreased, and the mismatch of the adhesion force occurred. The Adhesion mismatch enables the selective transfer of the AgNW networks to the surface of the PEDOT:PSS transfer template. The conducted TEs by my patterning method can be demonstrated on glass, plastic, and

PDMS substrates, showing applicability to flexible or stretchable electrodes.

2.2.2. Experimental Section

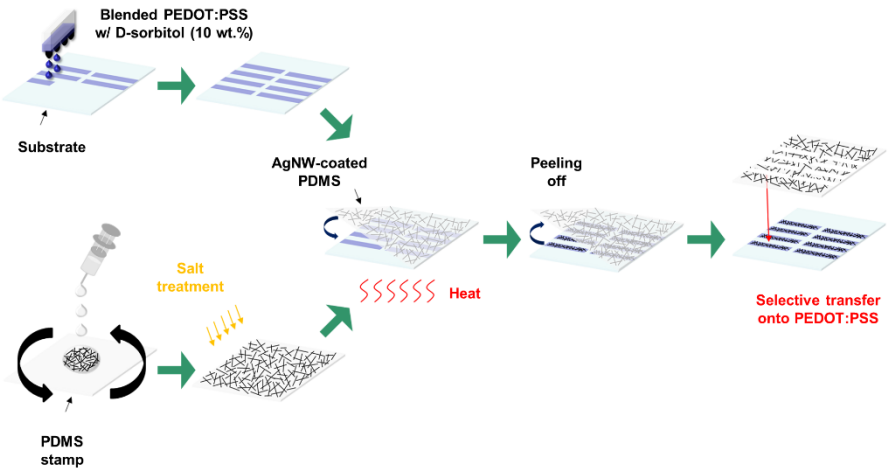

Figure 2.2 Schematic of patterning process of the AgNWs

Figure 2.2 represents the selective patterning process of the AgNWs on the inkjet-printed PEDOT:PSS template. First, the AgNW-coated PDMS stamp was prepared. PDMS substrate was conducted by mixing a PDMS elastomer base and curing agent (Sylgard 184, Dow Corning) at a weight ratio of 10:1 and then pouring it onto a petri dish. The planarization and thermal curing process were followed for the PDMS stamp with a thickness of 1200 μm. The AgNW solution (1 wt.% in IPA with a diameter of 32 nm and length of 25 μm, Nanopyxis) diluted with IPA at a volume ratio of 1:3 for enhancement of uniformity of AgNW layers after the spin-coating of the AgNW solutions on the PDMS stamp. Prior to the spin-coating of the AgNWs, an air plasma treatment (CUTE-1MP, Femto Science) at 15 W for 15 s was implemented on the surface of the PDMS stamp to form hydroxyl groups on the surface and hence enhance wettability. The diluted AgNW solution was spin-coated on the plasma-treated PDMS stamp at 2000 rpm, and the coating number of the AgNWs was optimized for the demonstration of the tunability of optoelectronic

properties. After drying at room temperature to remove solvents without any cracks possibly induced by a thermal expansion of the PDMS stamp, the conductivity improvement process progressed with sodium chloride (NaCl) [61, 98]. The AgNW networks on PDMS stamps were immersed in 1 wt.% NaCl solution dispersed in DI water and then washed in the DI water for 9 min to improve the conductivity of the AgNW networks while maintaining the transmittance. During the fabrication of the AgNW stamps, PEDOT:PSS patterns were simultaneously prepared on the target substrate. The D-sorbitol (Sigma-Aldrich) aqueous solution was prepared by dissolving the D-sorbitol in DI water with a concentration of 2.35 g/g. At the same time, the conductive PEDOT:PSS (HIL-1005, Orgacon) was mixed with fluorosurfactant (Capstone FS-30, Chemours) with 2 wt.% to reduce the surface tension and improve jettability during the inkjet-printing process. The fluorosurfactant-blended PEDOT:PSS was mixed with a D-sorbitol (Sigma-Aldrich) aqueous solution at a weight ratio of 9:1, and the stirring process was followed to achieve D-PEDOT:PSS solution. After that, the pre-patterned D-PEDOT:PSS transfer template was obtained using a piezoelectric inkjet printer (DMP-2831, Dimatix Corp.) on the various substrates. The volume of the D-PEDOT:PSS droplet was 10 pL in normal fabrication, and it was optimized to 1 pL for achieving micro-patterning of the blended PEDOT:PSS line in a width of 30 μm. In the case of PEN (Q65H, Teijin Dupont Films) substrates, they were treated with an ultraviolet (UV)-ozone cleaner (AH1700, Ahtech LTS) for 5 min to enhance the wetting property. In the case of PDMS substrates, they were treated with air plasma at 15 W for 4 min as the surface treatment. After the inkjet printing with the desired pattern, the samples were annealed at 120 ℃ for 1 h, except for the PDMS. The transfer template with the pre-patterned PEDOT:PSS film and the AgNW-coated PDMS stamp were

attached while applying mild pressure. Subsequently, the attached sample was placed on the hot plate set to 100 ℃ for 10 min to enable the effective AgNW transfer from the PDMS stamp onto the transfer template. After cooling at room temperature for 5 min, the PDMS stamp was peeled off, and the AgNW networks were selectively transferred only onto the PEDOT:PSS transfer template. I manufactured various display applications to apply the flexible AgNW-transferred PEDOT:PSS TEs to flexible electronics. First, two types of light-emitting diode (LED) arrays were fabricated. Red LEDs (SML-P11UT, Rohm Semiconductor) were placed on the AgNW-transferred PEDOT:PSS TEs using a chip placement machine (TM220A, NeoDen Tech) to achieve the LED arrays with desired patterns. For conformal bonding between the LED and electrode, silver epoxy (Ablebond 84-1LMISR4, Henkel) was dispensed using an automatic dispenser (SHOTmini 200Sx, Musashi Engineering). Second, the touch screen panels (TSPs) were demonstrated with the AgNW-transferred PEDOT:PSS TE on PEN substrate as the bottom electrode and ITO on polyethylene terephthalate (PET) substrate as the top electrode. The copper tape was attached to both sides of the top and bottom electrodes to connect them with a touch panel module (NJY-0141-TP4RES, NJY TOUCH). Afterward, the scotch tape spacer and top electrodes were placed on the bottom electrodes. Finally, all solution-processed polymer light-emitting diodes (PLEDs) that operate under low-operation voltage were fabricated by conducting the AgNW transfer on the previously transferred PEDOT:PSS top anodes of devices [96]. Due to the weak adhesion between the PEDOT:PSS anode and active layers of the devices, the plasma treatment time of the PDMS stamp was optimized to 10 s. The completed devices were encapsulated using a cover glass and UV-curable resin (XNR5570, Nagase ChemteX Corp.). The sheet resistance of the electrodes was measured by a four-point

probe (FPP-5000, Changmin), and their optical property was obtained using a UV/VIS spectrometer (Lambda 35, Perkin Elmer). The images were taken with an optical microscope (DSX-HRSU, OLYMPUS Corp.) and a field emission scanning electron microscope (FE-SEM, Hitachi S-4800). The surface roughness and thickness were examined by a non-contact mode atomic force microscopy (NC-AFM) system (XE-100, Park system). The adhesion with the substrate was explored by the test using the 3M scotch tape, and the resistance of each electrode was measured by a semiconductor parameter analyzer (4155C, Agilent). The bending test was carried out using a custom-made bending machine, and their resistance was measured by a sourcemeter (Keithley 2400, Keithley) during the bending stress. For the application to PLEDs, their electrical and optical characteristics of PLEDs with a pixel size of 1.4×1.6 mm^2 were measured by a digital multimeter (Keithley 2000, Keithley) and a source-meter unit (Keithley 237, Keithley) by sweeping the bias voltage with an interval of 0.1 V and a spectrometer (CS-1000A, Konica Minolta), respectively.

2.2.3. Results and Discussion

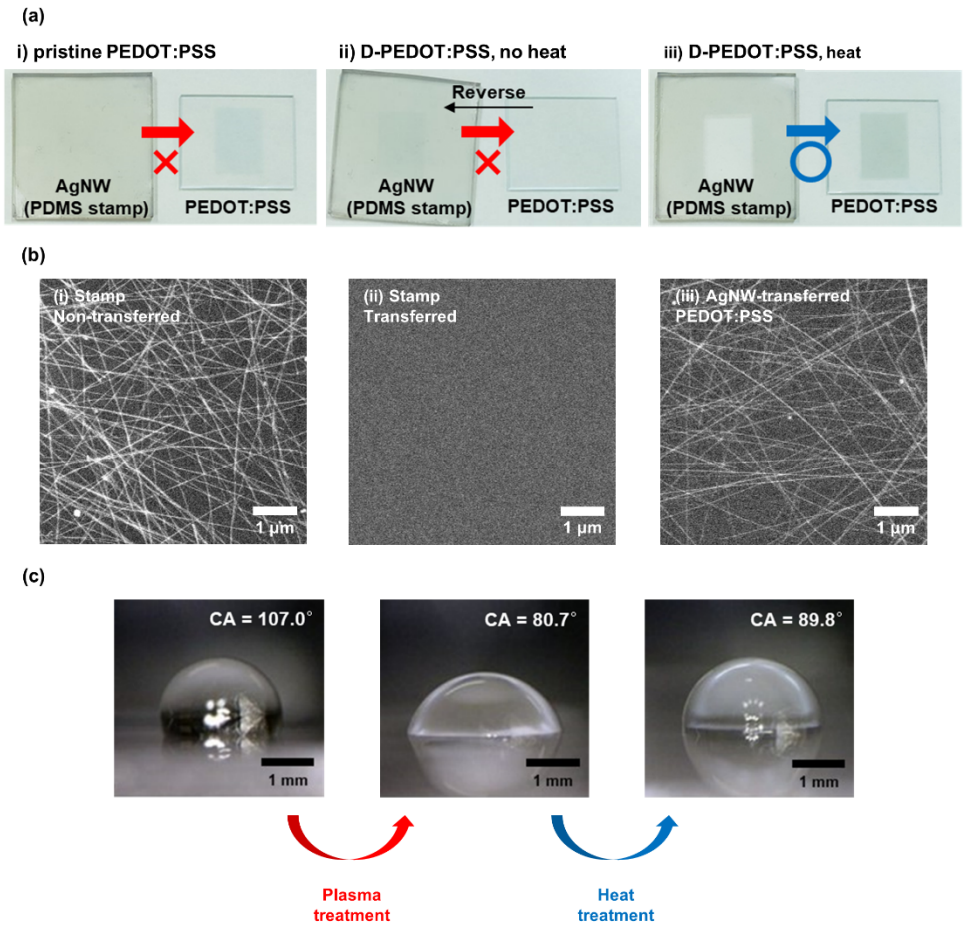

Figure 2.3 (a) Optical images of AgNW transfer according to the various conditions, (b) SEM images of the AgNW-coated PDMS stamp at (i) non-transferred area, (ii) transferred area, and (iii) AgNW-transferred PEDOT:PSS, and (c) optical images of contact angle of DI water on the PDMS stamp according to the transfer process.

Figure 2.3 shows the optimization of facile patterning of AgNW networks with a combination of optimized PEDOT:PSS ink and transfer of the AgNWs on the PEDOT:PSS surface. First, a D-sorbitol aqueous solution was blended with the PEDOT:PSS ink to increase the adhesion of the PEDOT:PSS surface. The adhesive

property of the D-sorbitol easily provides mechanical attachment between two interfaces of devices. At the same time, the conductive PEDOT:PSS makes it possible to ensure electrical contact between them. The previous research demonstrated the patterning process of PEDOT:PSS TEs by transfer-printing of PEDOT:PSS onto the target substrates [96]. In this publication, the sheet resistance change and feasibility of the transfer process were investigated according to a concentration of D-sorbitol. And the PEDOT:PSS pattern in blended PEDOT:PSS was successfully transferred onto PDMS with a D-sorbitol concentration of above 10 wt.%, while the conductivity decreased as the concentration of D-sorbitol increased. Therefore, the blended PEDOT:PSS with 10 wt.% D-sorbitol solution was selected for AgNWs transfer templates for both the conformal transfer of AgNWs and the reliable conductivity of PEDOT:PSS. According to **Fig. 2.3(a)**, the transfer of the AgNWs on the pristine PEDOT:PSS was not observed because the adhesion of the pristine PEDOT:PSS is not enough to attach the AgNWs on the PEDOT:PSS. On the other hand, the AgNWs and the PEDOT:PSS were laminated and formed as one composite layer in the case of the inkjet printing of the D-PEDOT:PSS. Heat treatment is another crucial factor for the successful transfer process of AgNWs. When the AgNW-coated PDMS stamp was attached to the PEDOT:PSS-printed target substrate, AgNWs and D-PEDOT:PSS merged into one film, as I mentioned before. For the implementation of the transfer of the AgNWs from the PDMS stamp to the PEDOT:PSS surface, the adhesion force between the PDMS stamp and the AgNWs is a critical factor for the transfer process. During the heat treatment, the adhesion force between the PDMS stamp and the AgNWs decreases. Cracks occur on the plasma-treated surface due to the thermal expansion of the PDMS, and the adhesion force of the PDMS decreases [96, 99, 100]. I confirmed the change of the

adhesion force through the contact angle measurement because the adhesion force is closely related to the contact angle [77]. According to **Fig 2.3(c)**, the contact angle of the DI water on PDMS decreases after plasma treatment, and the contact angle reduction proves the possibility of the deposition of AgNWs on the PDMS stamp. Furthermore, the increase of the contact angle after the heat treatment demonstrates the degradation of the adhesion force of the PDMS. Since the AgNWs and the D-PEDOT:PSS were laminated and became a single composite, the AgNWs were detached from the PDMS stamp only after the thermal annealing process. As shown in the SEM images in **Fig. 2.3(b)**, the AgNW networks were fully transferred onto the PEDOT:PSS transfer template without any AgNW residues on the transferred part of the PDMS stamp. However, when the transfer process during the attachment was conducted without the heat treatment, the PEDOT:PSS transfer template was reversely transferred to the PDMS stamp. I fabricated a several AgNW-transferred PEDOT:PSS TEs patterned by an inkjet-printing with various patterns on different substrates, including glass, PEN, and PDMS substrates, showing applicability to flexible or stretchable electrodes (**Figure 2.4**). According to the enlarged images of the AgNW-transferred PEDOT:PSS templates on various substrate, the AgNWs was precisely transferred even at the edge of the PEDOT:PSS templates. The AgNWs also can be transferred onto the PEDOT:PSS transfer template fabricated on organic layers. **Figure 2.5** indicates transferred AgNW networks on AI 4083, one of the most widely used materials in organic light-emitting diodes. The PEDOT:PSS transfer template was deposited by the transfer process to prevent damage to underlying organic layers. Patternability of AgNWs on the PEDOT:PSS layers ensures the processability of top electrodes even on hydrophobic layers such as light-emitting layers by spin-coating of the PEDOT:PSS hole-injection layers (HIL) (**Figure 2.5(c)**).

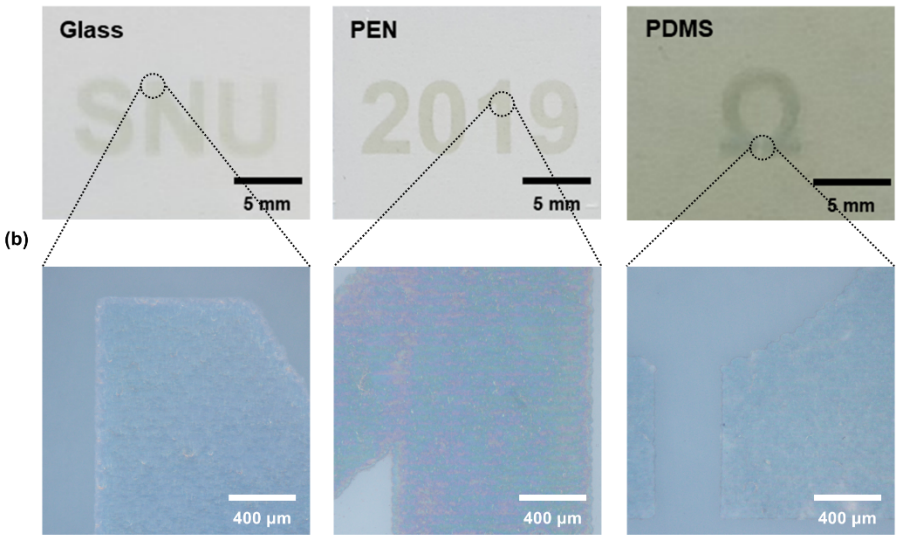

Figure 2.4 (a) Optical images of the AgNW-transferred PEDOT:PSS patterns on various substrates, and (b) enlarged image of the patterns.

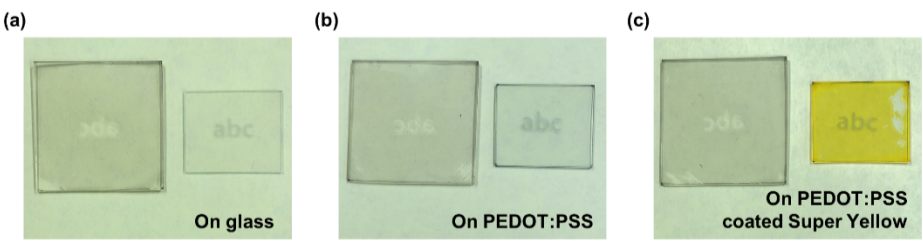

Figure 2.5 Optical images of the AgNW-transferred PEDOT:PSS on a) glass substrate, b) PEDOT:PSS HIL, and c) on PEDOT:PSS-coated SY.

Optoelectronic properties of AgNW-transferred PEDOT:PSS TEs are exhibited in **Fig. 2.6** and **Table 2.1**. The transmittance was compared at a wavelength of 550 nm, and a figure of merit (FOM) was derived through Haacke's method [101]. The AgNW-transferred PEDOT:PSS TEs were fabricated on various substrates, including glass, PEN, and PDMS. In the case of the glass substrate, the AgNW-transferred PEDOT: PSS exhibited a sheet resistance (R_{sh}) of 8.2 Ω/sq and a transmittance (T) of 87.4 %. In case of the PEN substrate, the AgNW-transferred

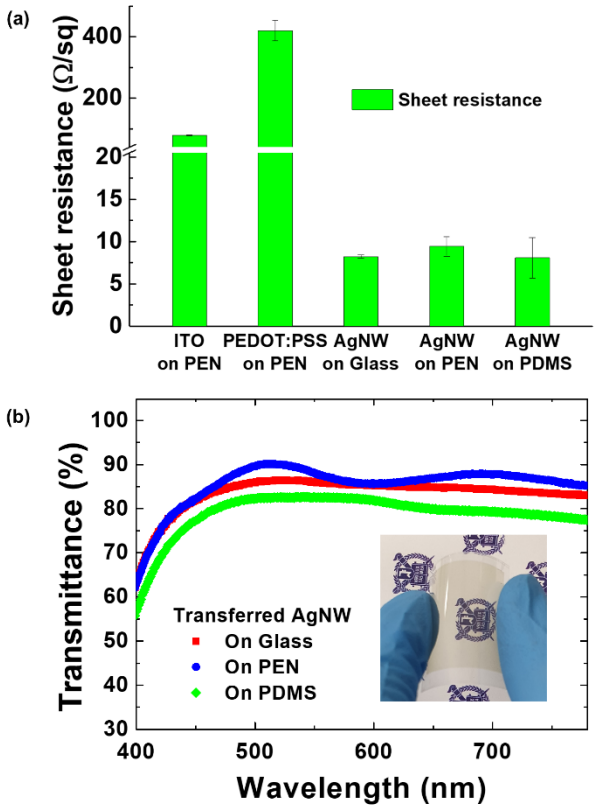

Figure 2.6 (a) Sheet resistance of the ITO, PEDOT:PSS, and AgNW-transferred PEDOT:PSS patterns on various substrates, and (b) Transmittance in the wavelength range from 400 nm to 780 nm. The inset image of the (b) shows the AgNW-transferred PEDOT:PSS on PEN substrate.

	Sheet resistance (Ω/sq)	Transmittance (%)	FOM (Figure of Merit) ($10^{-3}\Omega^{-1}$)
ITO on PEN	78.8	86.1	2.8
PEDOT:PSS on PEN	419.7	99.8	2.4
Transferred AgNW On Glass	8.2	86.1	27.3
Transferred AgNW On PEN	9.4	88.1	29.9
Transferred AgNW On PDMS	8.1	82.6	18.4

Table 2.1 Optoelectronic properties of ITO, PEDOT:PSS, and AgNW-transferred PEDOT:PSS

PEDOT:PSS showed R_{sh} of 9.4 Ω/sq and T of 88.1 %, respectively. I compared the optoelectronic properties of the three TEs on the PEN: ITO, PEDOT:PSS, and AgNW-transferred PEDOT:PSS. The measured R_{sh} of the ITO TEs on the PEN was 78.8 Ω/sq at a T of 86.1 %. The low conductivity of ITO compared to that on the glass originated from the low heat resistance of the PEN substrate. The process-capable temperature of the PEN substrate is 150 ℃ [102], but the ITO films need a much higher temperature for the crystallization of the deposited ITO [103]. In addition, the PEDOT:PSS on the PEN also showed poor conductivity with excellent transmittance. As a result, the FOM value of the ITO was 2.8 $m\Omega^{-1}$ and that of PEDOT:PSS was 2.4 $m\Omega^{-1}$, while the AgNW-transferred PEDOT:PSS achieved a great FOM of 29.9 $m\Omega^{-1}$ which was caused by maintaining outstanding conductivity of the patterned AgNWs. And the optoelectronic property of AgNW-transferred PEDOT:PSS on the PDMS substrate was also measured, and the AgNW TEs on the PDMS showed R_{sh} of 8.1 Ω/sq and T of 82.6 %, respectively. In conclusion, the AgNW-transferred PEDOT:PSS can be a proper candidate for the flexible TEs to replace the ITO at the flexible electronics. And the patterned AgNWs maintained their properties even on the PDMS substrates. In addition, the optoelectronic properties of the AgNW-transferred PEDOT:PSS can be easily controlled by the change of the AgNW-coating conditions, such as the number of coatings and concentration of the AgNW (**Figure 2.7**). The AgNW TEs can be tuned from semi-transparent electrodes with high conductivity (R_{sh}: 1.9 Ω/sq and T: 24.0 %) to highly transparent electrodes with moderate conductivity (R_{sh}: 38.6 Ω/sq and T: 93.5 %). Therefore, the AgNW-transferred PEDOT:PSS TEs can be straightforwardly tuned according to the demand of the display applications.

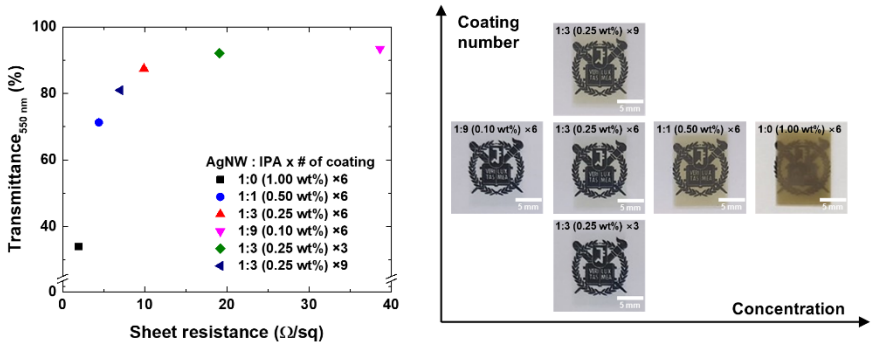

Figure 2.7 Optoelectronic properties of the AgNW-transferred PEDOT:PSS TEs with various spin-coating conditions and concentrations of AgNW solution.

In addition to the easy tunability of the electrode properties, there are two more advantages when the AgNWs are patterned by the selective transfer method. First, the resolution of the AgNW TEs can be enhanced by inkjet printing of the PEDOT:PSS templates with a width of tens of micrometers. **Figure 2.8(a)** shows the AgNW-transferred PEDOT:PSS lines with widths from 200 μm to 30 μm on the glass substrates. In case of the 30 μm width, the inkjet-printing droplet was reduced from 10 pl to 1 pl to achieve a precise pattern. Patternability of the AgNWs with my selective transfer method in a width of 30 μm was comparable with conventional patterning methods [60, 77]. According to **Fig. 2.8(c)**, AgNWs also can be transferred to the PEDOT:PSS template on a PEN substrate as narrow as the width of 100 μm, expanding their applications to flexible electronics in the microscale. When the LED was connected with TEs with a width of 50 μm, the LED connected to the AgNW-transferred PEDOT:PSS emitted green light with higher intensity compared to the PEDOT:PSS only electrode (**Figure 2.8(b)**), And that phenomenon proves that the transferred AgNWs on the PEDOT:PSS dramatically reduce the current level.

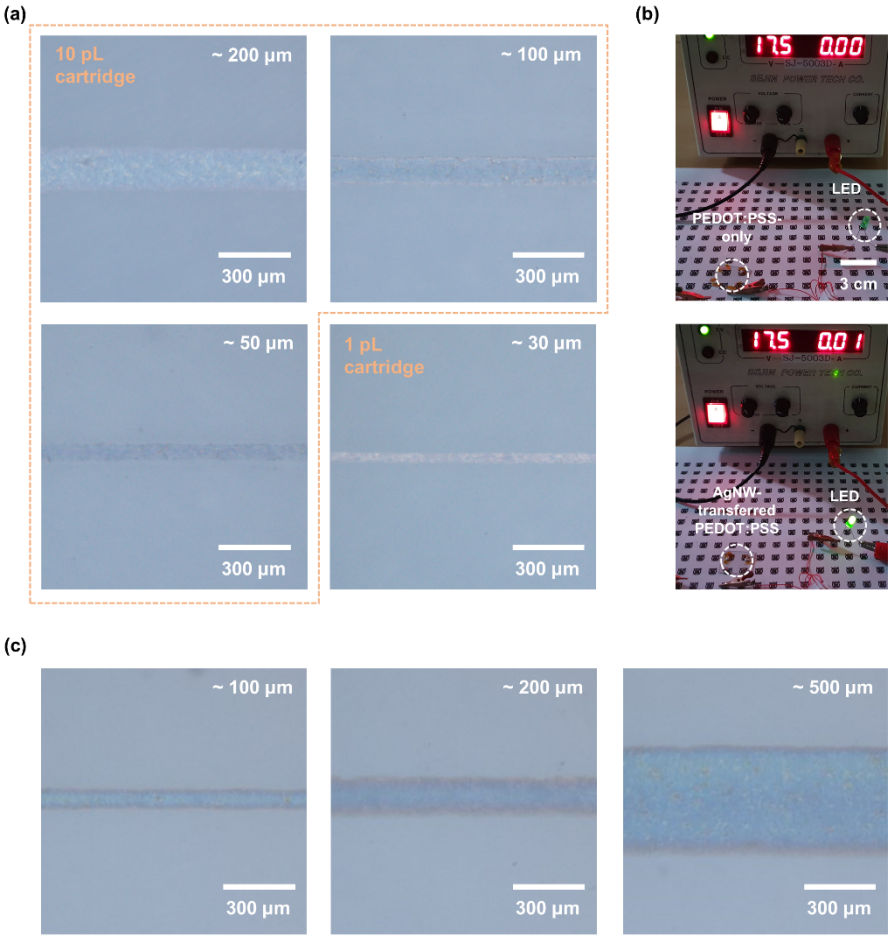

Figure 2.8 Optical images of the (a) AgNW-transferred PEDOT:PSS line on the glass substrates with width 200 μm, 100 μm, 50 μm, and 30 μm, (b) light emission of LEDs connected with PEDOT:PSS-only (top) and AgNW-transferred PEDOT:PSS TEs (bottom) with width of 50 μm, and the (c) AgNW-transferred PEDOT:PSS patterned on PEN substrates with width of the 500 μm, 200 μm, and 100 μm.

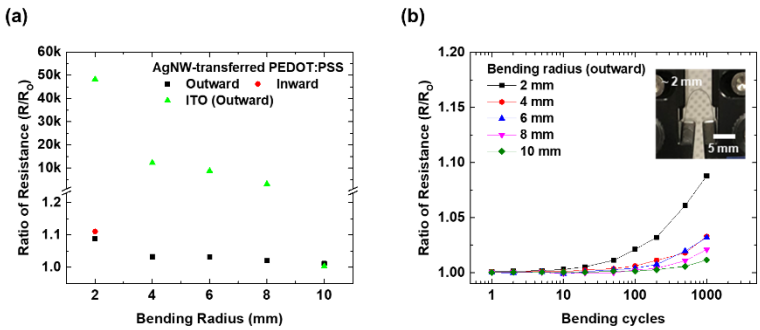

Figure 2.9 (a) Resistance change of AgNW-transferred PEDOT:PSS and ITO TEs after 1000 cycles of bending test according to the change of bending radius, and (b) resistance change of the TEs according to the number of bending cycles.

And another superiority of the selective transfer patterning of the AgNW is mechanical flexibility. I conducted the patterning process of the AgNWs on the PEN substrate with a thickness of 125 μm, and the flexibility of the ITO TEs and AgNW-transferred PEOD:PSS TEs on PEN were measured by a custom-made bending test machine. The mechanical flexibility was investigated using a bending test under various bending radii of 2, 4, 6, 8, and 10 mm (**Figure 2.9**). Unlike the ITO film with inherent brittleness, the AgNW-transferred PEDOT:PSS TEs on the PEN substrates maintained their resistance after 1000 bending cycles at all bending radii, exhibiting little resistance change of 1.09 even at the radius of 2 mm.

Based on these results, I applied the flexible AgNW-transferred PEDOT:PSS TEs to several flexible electronic devices, such as LED arrays, touch screen panels (TSPs), and all solution-processed polymer light-emitting diodes (PLEDs). In these various applications, my simple patterning method of the AgNW networks facilitates the circuit design with a high degree of freedom, unlike their conventional patterning.

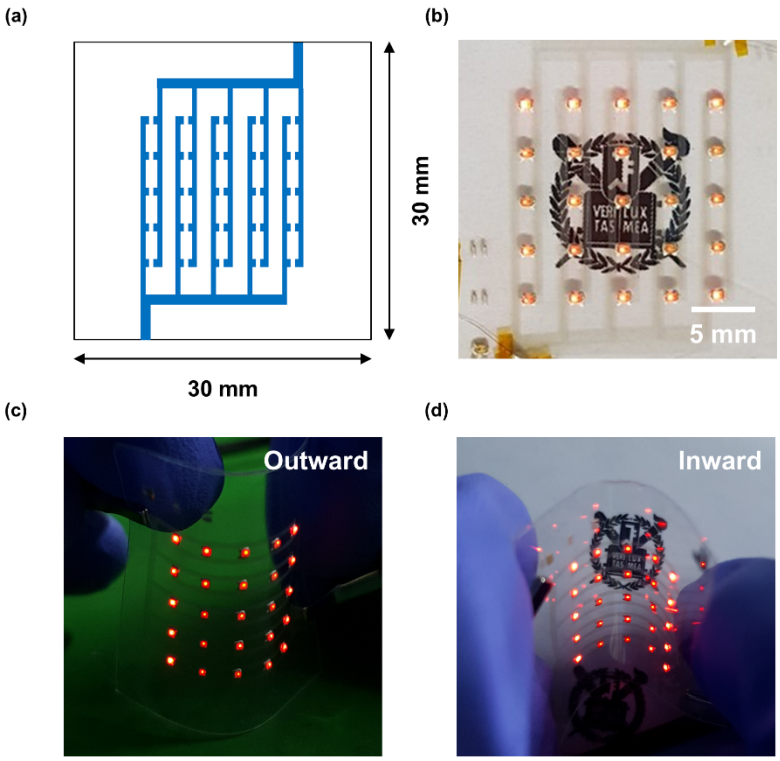

Figure 2.10 (a) Schematic design of 5x5 LED array, optical image of the operated LED arrays under (b) flat, (c) outward bending, and (d) inward bending state.

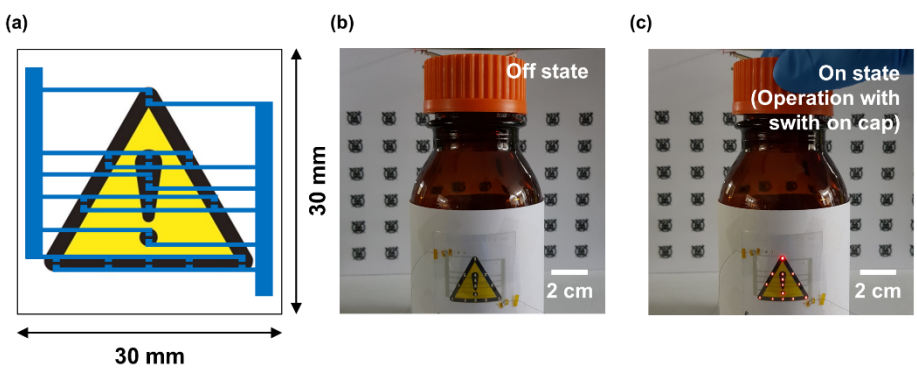

Figure 2.11 (a) Schematic design of warning-sign array, optical image of (b) off and (c) on state of warning-sign array which is operated by the ITO switch attached on the top of bottle cap.

First, I demonstrated the flexible LED arrays with the AgNW-transferred PEDOT:PSS TEs as the interconnects of the LEDs. Two types of LED arrays were

fabricated: a 5 x 5 array and a warning-sign array. The schematic circuit diagrams of two arrays are shown in **Fig. 2.10(a)** and **Fig. 2.11(a)**. Each LED segment was placed on the designed location, which was determined by patterns of the AgNW-transferred PEDOT:PSS TEs on the PEN substrate. When the bias was applied to the 5 x 5 LED array, all LEDs of the array emitted light brightly and operated normally, exhibiting a clear background image, unlike the previous report using the opaque electrodes (**Figure 2.10(b)**) [56]. In addition, the stable LED operation was achieved due to the remarkable mechanical flexibility of the AgNW-transferred PEDOT:PSS TEs under the bending state with an inward and outward bending state, according to **Fig. 2.10(c) and (d)**. In addition, the warning-sign array was also constructed as one of the other practical examples to demonstrate highly customizable LED arrays with my TEs. A switch composed of two ITO-coated PEN substrates was attached to a bottle cap, enabling the warning-sign LED array to turn on only when operators touch the bottle cap. The warning sign LED array attached on a curved surface of the bottle exhibited on/off operation at both opening and closing situations (**Figure 2.11(b) and (c)**).

Second, the TSPs were fabricated using the AgNW-transferred PEDOT:PSS TEs as the bottom electrodes with a rectangular mesh pattern composed of 500 μm width and 700 μm pitch on the PEN substrate (**Figure 2.12(a) and (b)**). For a demonstration of the TSPs, the spacer and ITO top electrodes were placed on the bottom AgNW-transferred PEDOT:PSS mesh pattern. My TSP responds to the resistance change through the touch panel module by sensing the pressure in the active area and the resulting physical and electrical contact between the bottom and top electrodes. As a result, my TSPs demonstrated great sensitivity without distortion or crosstalk and repeatability, showing clear characters on the laptop screen corresponding to the pressure I applied on their active region (**Figure 2.12(c)**).

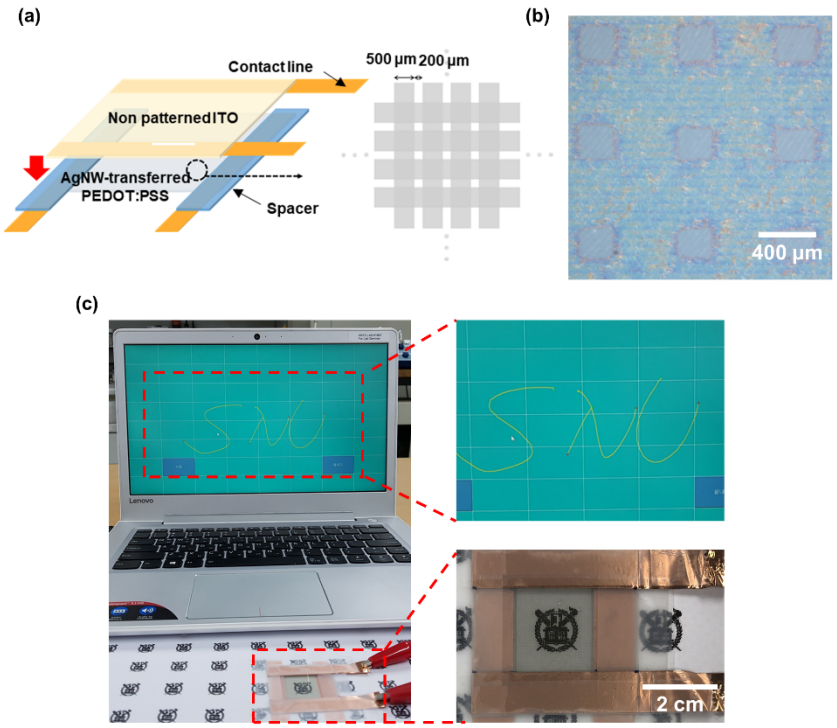

Figure 2.12 (a) Schematic design of the TSP with ITO top electrodes and AgNW-transferred PEDOT:PSS bottom TE, (b) optical image of the patterned AgNW-transferred PEDOT:PSS for TSP panel, and (c) image of TSP operation.

In addition to the AgNW patterning on directly inkjet-printed PEDOT:PSS films, the AgNW networks can be selectively transferred onto indirectly deposited PEDOT:PSS films such as transfer printing, as I previously mentioned in **Fig. 2.5**. According to the patternability of the AgNWs on the organic layers, I applied AgNW-transferred PEDOT:PSS TEs to anodes of all solution-processed PLEDs [96]. I used the D-PEDOT:PSS TEs transferred onto the active layers of the PLEDs as the transfer template. The AgNW networks were selectively transferred to fabricate transparent anodes of the PLEDs, to compensate low conductivity of the D-PEDOT:PSS TEs (**Figure 2.13**). For successful transfer of the AgNW networks onto

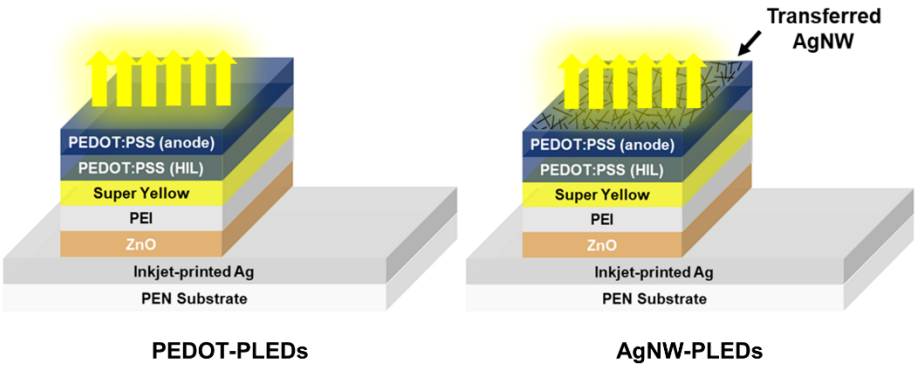

Figure 2.13 Schematic of the all-solution-processed PLEDs with PEDOT:PSS-only (left) and AgNW-transferred PEDOT:PSS (right) top anode.

	Sheet resistance (Ω/sq)	Transmittance at 550 nm (%)	Figure of Merit ($m\Omega^{-1}$)
Optimized [a)]	8.2	86.1	27.3
PLED application	8.1	82.3	17.5

a) Reference TE in this work except for PLED application

Table 2.2 Optoelectronic properties of AgNW-transferred TEs under different fabrication condition.

the transferred PEDOT:PSS TEs and stable operation of PLEDs, I modified the plasma treatment time to PDMS stamp and thickness of the blended PEDOT:PSS TEs for successful transfer of AgNWs onto the transferred PEDOT:PSS (**Table 2.2**). The fabricated AgNW-transferred showed 8.4 Ω/sq and 8.1 Ω/sq of sheet resistance and 85.7 % and 82.3 % of transparency for each case, respectively. **Figure 2.14(a) and 14(b)** shows device characteristics and light emission images of the PLEDs on PEN substrates with different anodes; the blended PEDOT:PSS (PEDOT-PLEDs) and the AgNW-transferred PEDOT:PSS TEs (AgNW-PLEDs). According to current density-voltage-luminance (J-V-L) characteristics, the AgNW-PLEDs exhibited a

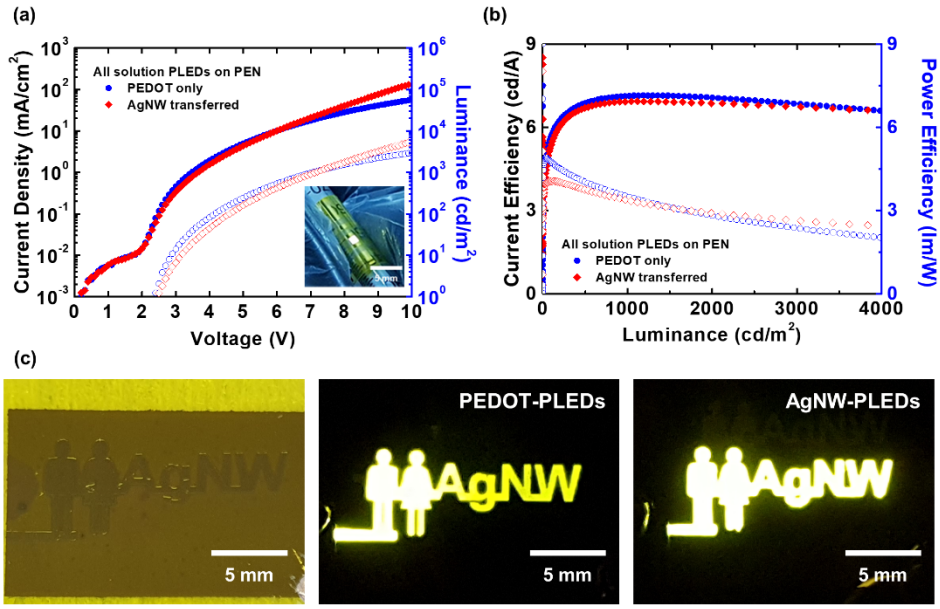

Figure 2.14 (a) J-V-L characteristics and (b) efficiencies of the PEDOT-PLEDs and AgNW-PLEDs, and optical images of (c) off-state of PLEDs (left), on-state of PEDOT-PLEDs (middle), and on-state of AgNW-PLEDs (right).

On PEN	Turn-on voltage (V)	Voltage at 1 mA(V)	C.E. at 1000 cd/m² (cd/A)	P.E. at 1000 cd/m² (cd/A)
PEDOT only	2.4	9.3	7.1	3.5
AgNW transferred	2.5	8.1	6.9	3.4

♣ A turn-on voltage is defined as the voltage at 1 cd/m²
♣ A CE and PE mean a current efficiency and power efficiency, respectively

Table 2.3 Device characteristics of the PEDOT-PLEDs and AgNW-PLEDs in terms of turn-on voltage, operating voltage at current of 1 mA, current efficiency and power efficiency.

higher current density than the PEDOT-PLEDs at the high voltage range without changing the turn-on voltage. In addition, the AgNW-PLEDs demonstrated a similar current efficiency of 6.92 cd/A and a higher power efficiency of 3.37 lm/W at luminance of 1000 cd/m^2 compared to those of the PEDOT-PLEDs (**Table 2.3**). The

increased power efficiency of the AgNW-PLEDs originated from the reduced sheet resistance caused by the enhanced conductivity of the anodes after the selective transfer of the AgNWs on the PEDOT:PSS transfer template. Furthermore, the AgNW-PLEDs showed stable light emission even under bending stress with a bending radius of 3.5 mm (an inset image of the J-V-L graph). The light emission images of two types of PLEDs with large-scale pixels were also compared to investigate the lower voltage drop and uniform luminous emission of the AgNW-PLEDs. Unlike the PEDOT:PSS PLEDs, the AgNW PLEDs emitted uniformly through the whole pixels, even at the edge of the large pixel pattern far from the contact pad (**Figure 2.14(c)**). Therefore, it is evident that my all-solution-processed PLEDs with the AgNW-transferred PEDOT:PSS anodes can achieve significant improvement in operating voltage and power consumption with maintaining their optoelectronic properties of the PLEDs.

2.3. Conclusion

In summary, I demonstrated the facile patterning method of the AgNW networks by conducting the inkjet-printing of the PEDOT:PSS transfer template and selective transfer of the AgNW networks onto it. The AgNW-transferred PEDOT:PSS TE on the PEN substrate showed not only superior optoelectronic properties but also more outstanding mechanical stability compared to the ITO. Various electrodes with different optoelectronic properties were also fabricated by adjusting the AgNW coating conditions. In addition, it exhibited the fine-line electrodes, which have a minimum width of 30 μm while consuming less power due to their high conductivity and thus reduced voltage drop. Furthermore, the previous issues of the AgNWs, such as the rough surface and weak adhesion with the substrate, were overcome by the partially embedded AgNWs in the PEDOT:PSS matrix, allowing a smoother surface and stronger adhesion with the substrate. Finally, employing the AgNW-transferred PEDOT:PSS TEs, several applications were demonstrated to explore highly customizable AgNW-transferred PEDOT:PSS TEs with excellent optoelectronic properties. The formation of high-performance flexible TEs and their facile patterning pave the way for realizing highly customizable flexible electronics in cost-effective and large-area fabrication. In the future, the application areas using my electrodes will be further expanded, including the bottom electrodes of the optoelectronic devices and stretchable electronics.

Chapter 3 High-resolution Patterning of Conductive Electrodes

3.1. Introduction

This chapter introduces a maskless patterning method of AgNW electrodes on various next-generation display platforms with high resolution. Although the AgNWs can be easily deposited on various substrates via a solution process [104-107], a patterning process is one of the remaining hurdles for applying the AgNW networks to future display applications. In addition, the importance of patterning deformable conductive electrodes with high resolution has grown as the resolution of deformable electronics has increased with the development of wearable electronic devices with micro-meter scales such as micro-LEDs [108-111], wearable sensors [112, 113], and stretchable integrated circuits [114, 115]. Therefore, a lot of studies have suggested various AgNWs patterning techniques. In Chapter 2, I previously introduced a maskless patterning method based on inkjet-printing of PEDOT:PSS ink blended with D-sorbitol and selective transfer of AgNWs only on the blended PEDOT:PSS patterns. When the AgNW-coated stamp was attached to PEDOT:PSS and the AgNW-attached PEDOT:PSS template was annealed above the melting temperature of adhesive, AgNWs were combined with PEDOT:PSS template and easily transferred from the elastomer stamp to target substrate.

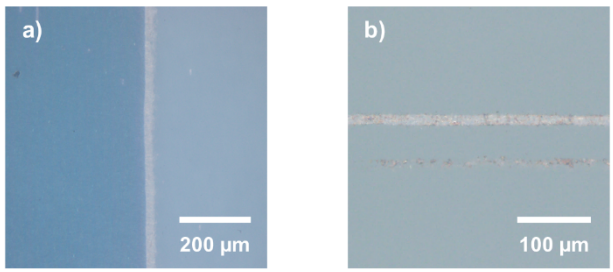

Figure 3.1 Optical images of the transfer failure at (a) pattern edge of large-scale electrodes and (b) patterns with micrometer scale width.

Although this approach ensured facile AgNW patterns on flexible substrates, there were several limitations on the fabrication of high-resolution electrodes and stretchable applications. First, mechanical stress during the lamination of the AgNW-coated PDMS stamp causes a decrease in patterning accuracy in the case of the micrometer scale. When the heat was applied to the AgNW stamp attached to the PEDOT:PSS-patterned substrate, the AgNWs were laminated on the PEDOT:PSS surface and formed a single electrode layer. When the AgNW stamp was detached from the PEDOT:PSS surface, the AgNWs on the side of patterns were ripped from the PDMS stamp because the AgNWs attached to the PEDOT:PSS template was only transferred from the PDMS stamp (**Figure 3.1(a)**). The lack of uniformity of the AgNW pattern edge is a serious drawback in patterns with a micrometer scale. In addition, an external force was applied to the PDMS stamp during the attachment process for uniform lamination between the AgNWs and the PEDOT:PSS surface. Unlike the PEDOT:PSS patterns with a large area, the AgNW-PEDOTPSS patterns with a micrometer scale showed low transfer yield because the mechanical force easily causes critical damage on the microscale patterns with a small contact area (**Figure 3.1(b)**).

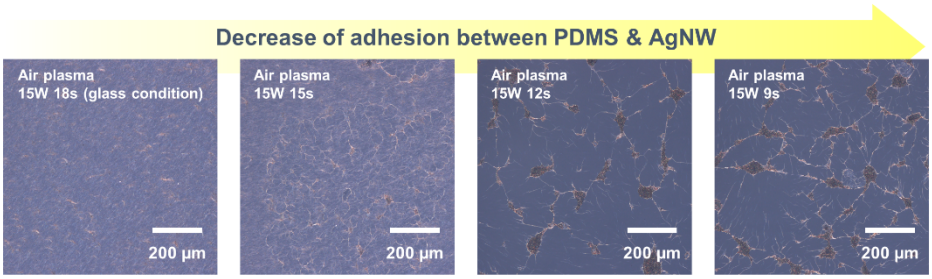

Figure 3.2 Optical images of the spin-coated AgNW on the PDMS stamp with different adhesion.

The selective transfer method of AgNWs also showed weakness in stretchable electronics. During the transfer process, the adhesion force between the PDMS stamp and the AgNWs (F_a) and the adhesion force between the substrate and the PEDOT:PSS template (F_b) were involved in the selective patterning of the AgNWs. If F_a is smaller than F_b, the AgNW networks attached to the PEDOT:PSS were successfully transferred onto the desired substrate [116]. While the F_b is sufficient to achieve facile patterning in the case of the glass and plastic substrate, a process window of the selective transfer of AgNWs on the PDMS substrate is narrow because the stamp and the substrate are composed of the same material. In order to obtain successful delamination of the AgNWs from the stamp surface, F_a should be optimized by reducing the surface treatment time. **Figure 3.2** shows the AgNW-coated PDMS stamp surface with various surface treatment conditions. An air-plasma treatment time was controlled to optimize the adhesion between PDMS and stamp. However, the reduced F_a obtained by lowering the plasma treatment time diminished the uniformity of the AgNW layers, and thus the electrical properties of the patterned AgNWs deteriorated. In conclusion, an improved patterning technique of the AgNWs should be required for high-resolution patterning on the elastomeric

substrate.

Previously, several patterning approaches based on the printing of a protective layer have been reported. For example, Li et al. suggested a printing-based patterning method based on printing poly(methyl methacrylate) (PMMA) on pre-coated AgNWs [117]. The printed PMMA layer covered the AgNWs and protected them from the removal process of uncovered AgNWs. Although the PMMA-assisted patterning showed high patterning freedom according to the inkjet-printed PMMA patterns, the droplet size of the inkjet-printing disturbed the resolution improvement. In addition, PMMA covered on AgNW patterns should be dissolved after the patterning process because the insulating property of PMMA hinders electrical contact with adjacent layers. In addition to the PMMA-assisted patterning, Wan et al. achieved high-resolution patterning of AgNW lines by a selective covering of PMMA on pre-patterned AgNWs, which were previously fabricated with the same patterning method [118]. However, the complicated design of patterns and repeated patterning process were necessary for high-resolution AgNW lines and therefore interrupted the freedom of patterning.

In this chapter, I suggested an adhesive-assisted patterning method of AgNWs based on enhanced adhesion between the patterned PEDOT:PSS covering layer and the underlying adhesive layer. Poly(vinyl alcohol) (PVA) was reported as an adhesive layer between substrates and PEDOT:PSS polymer by forming an interpenetrating polymer network with PEDOT:PSS polymer chain [119]. So I printed PEDOT:PSS on the AgNW-coated PVA surface to hold the AgNW patterns by placing the AgNWs between the PEDOT:PSS and PVA. Unlike the previous patterning approaches based on the protective layer, PEDOT:PSS was patterned even on the elastomeric substrates with high resolution in my patterning strategy. After

spin-coating of PVA adhesive on the amine-functionalized substrate, spray-coating of AgNW on the PVA underlying layer was followed. When the PEDOT:PSS was printed on AgNW/PVA surface, PEDOT:PSS covered the AgNWs and penetrated AgNW networks. AgNWs covered by adhesion-enhanced PEDOT:PSS were protected during removal and formed reliable electrode patterns without damaging the patterned area. Combination of conductive PEDOT:PSS and AgNWs showed reliable electrical contact without the extra dissolving process of PEDOT:PSS and demonstrated superior adhesion with substrates due to the presence of underlying PVA. Strong bonding between PEDOT:PSS and PVA enabled precise patterning of AgNWs onto various substrates, even on PVA-coated plastic substrates and pre-stretched elastomers with reliable mechanical stability. Electrical properties of patterned AgNWs with PEDOT:PSS can be easily controlled by optimization of spray-coating conditions of AgNWs. For patterning AgNWs with high resolution, PEDOT:PSS was also printed on AgNWs by EHD printing. Under the EHD printing process, high voltage is applied between the substrate and nozzle, and ions are accumulated at the ink surface. Accumulated ions at the PEDOT:PSS ink surface forms a conic surface at the end of the nozzle, and the ink is continuously dropped from the cone. Through EHD printing of PEDOT:PSS on AgNW, the AgNW lines can be patterned with a width under 20 μm and a pitch of 40 μm. The AgNW patterned by inkjet and EHD printing can be applied to various electronic devices, including stretchable LED arrays and heaters with mesh structures. And the reliable conductive property of patterned AgNWs expands their applicability to various high-resolution deformable electronics.

3.2. High-resolution Maskless Patterning of AgNWs Based on Adhesion Enhancement of PEDOT:PSS

3.2.1. Main Concept

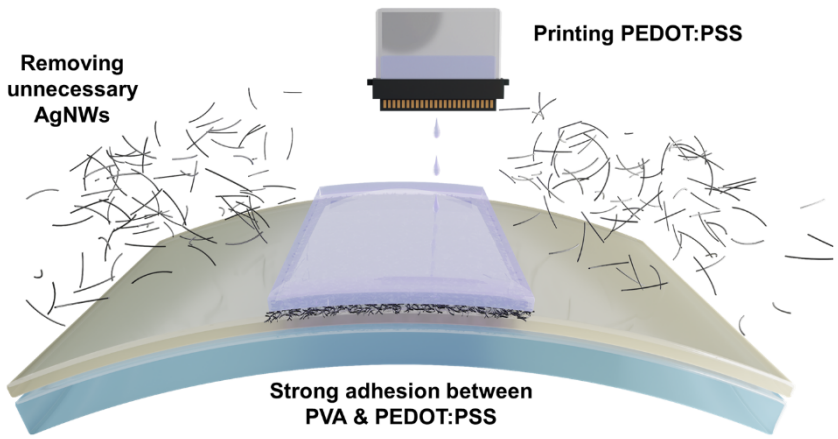

Figure 3.3 Schematic image of the principles of PVA-assisted patterning method.

The importance of the patterning method of the AgNWs has grown to apply the AgNWs to high-resolution deformable electronics, as I mentioned in chapter 3.1. An alternative patterning approach should be introduced to achieve both resolution improvement of the electrode patterns and stable fabrication on substrates with poor heat resistance. **Figure 3.3** shows the maskless patterning concept of the AgNW electrodes with a PVA-assisted method. Inoue et al. previously reported a promising method of developing the adhesion of PEDOT:PSS by introducing adhesive layers between the PEDOT:PSS and the substrates [119]. According to the reported approach, the conductive polymers such as PEDOT:PSS, polypyrrole, and polyaniline were coated on the polymer adhesive layer previously coated on the

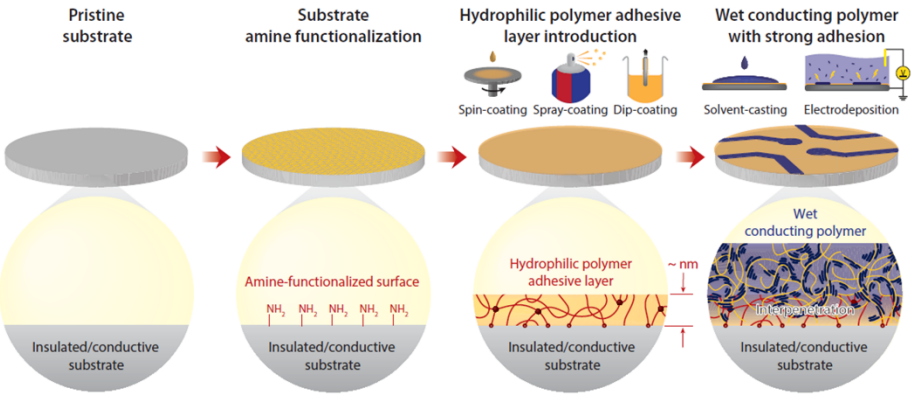

Figure 3.4 Schematic image of the deposition of PEDOT:PSS with enhanced adhesion by underlying adhesive layer [119].

amine-functionalized substrate. Interpenetration between the conductive polymer and the adhesive layer, like PVA or polyurethane, improves the adhesion of the conductive polymer and prevents the polymer layers from detachment (**Figure 3.4**).

In my work, the PEDOT:PSS is patterned on the AgNW-coated PVA substrates for preserving the underlying AgNWs during the patterning process. The PVA layer is previously deposited on the target substrate by a spin-coating method to create an adhesive surface under the AgNW layers. The PVA layer can be fabricated on arbitrary substrates, including elastomeric materials, by producing amine groups on the target surface. After spin-coating of the PVA adhesive layer, AgNWs are deposited on underlying PVA layers by spray-coating. Although the conventional patterning method needs masks for patterning the AgNW electrodes, the AgNWs are spray-coated on the whole region in my patterning method without the requirement of patterning masks to enhance the patterning freedom of AgNWs and decrease fabrication cost. To define the AgNW electrode patterns without a prevailing patterning mask, the PEDOT:PSS is selected as a protective layer owing to the

enhanced adhesive property of the PEDOT:PSS on the PVA layer. PEDOT:PSS shielding layer patterns are deposited on the AgNWs according to desired patterns by various printing techniques. The printed PEDOT:PSS patterns are covered on the AgNW surface, and the PEDOT:PSS penetrates through the voids between the AgNW networks and successfully combines with the PVA layer underneath the AgNW. As a result, the improved adhesion of the PEDOT:PSS after heat treatment protects the AgNWs from external mechanical stress and prevents the AgNW networks from detachment during the removal process of unnecessary AgNWs outside the pattern region.

3.2.2. Experimental Section

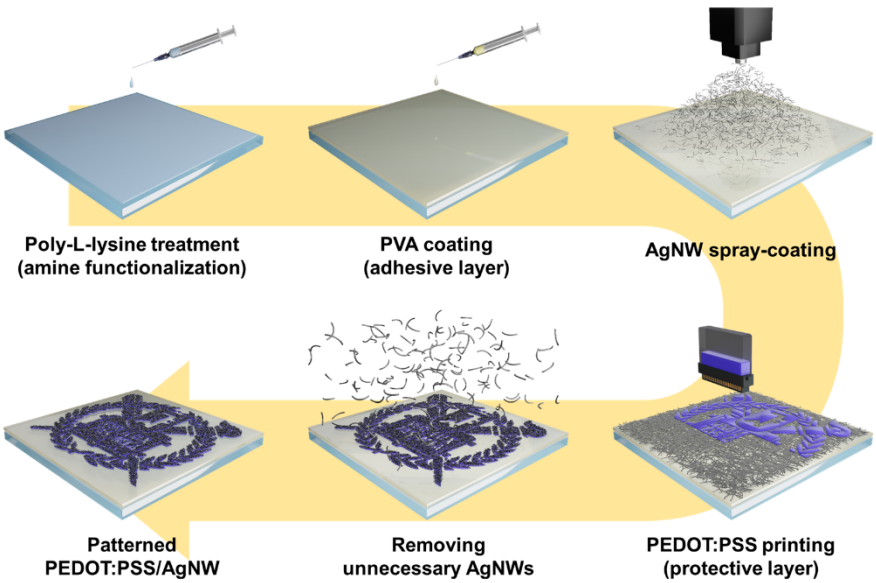

Figure 3.5 Schematic image of patterning sequence of AgNWs based on PVA-assisted method.

Figure 3.5 represents a patterning sequence of AgNW electrodes based on the PVA-assisted method. First, an aqueous poly-l-lysine (PLL) solution (0.1 % w/v, Sigma-Aldrich) was prepared for the amine-functionalization of an applied substrate. Both eagle glass and PEN (Q65H, Teijin Dupont Films) were cleaned using an ultra-sonication bath in acetone, IPA, and DI water, respectively. For fabrication on an elastomeric substrate, the PDMS elastomer base was mixed with a curing agent (Sylgard 184, Dow Corning) with a weight ratio of 15:1, and mixed PDMS was spin-coated on glass at 300 rpm. After curing PDMS with a temperature of 120 ℃ for 1 hour, the PDMS was peeled off from the glass substrate and attached to the stretching jig for applying strain before patterning the AgNWs. After preparation of the

substrates, ultraviolet-O_3 treatment (AH1700, Ahtech LTS) was conducted on the substrate for 10 minutes to create a hydroxyl group on the glass and PEN surface, and air plasma treatment (CUTE-1MP, Femto Science) was implemented with the power of 30 W for 20 s in case of pre-stretched PDMS substrate. For the fabrication of an amine-functionalized PLL layer on a UV-treated substrate, the PLL solution was drop-casted for 10 minutes, and a rinsing process with DI was followed. After amine-functionalization, 5 wt.% PVA (Sigma-Aldrich) solution dissolved in DI was spin-coated on a PLL-treated surface at 2000 rpm to increase the adhesion between the substrate and the electrodes, and the annealing process on 80 ℃ a hotplate was followed. AgNW (Yurui Chemical Co., Ltd) solution was subsequently deposited on PVA layers by a spray-coating method. Two types of AgNW inks were prepared. For the fabrication of transparent electrodes, AgNW solution (10 g/L in IPA, diameter of 100 nm and length of 35 μm) was diluted with IPA at a volume ratio of 1:3 to achieve uniform conductivity of fabricated transparent electrodes. Secondly, for highly conductive micro-patterned electrodes, AgNW solution (5 g/L in IPA, diameter of 30 nm and length of 25 μm) was sonicated by tip-sonicator (VCS 130, Sonics & Materials Inc.) at 60 % amplitude (78 W) for 10 min, to reduce the length of AgNWs and consequently to improve patternability at a micrometer scale. Prepared AgNWs were deposited on a PVA-coated substrate by spray-coater (eNano, Enjet Corp.) with a stage temperature of 80 ℃, air pressure of 3 kPa, and a flow rate of 3 ml/min. After deposition of AgNWs, PEDOT:PSS (0.8 wt.% in DI, IJ-1005, Orgacon) layer was printed on the AgNW surface according to designed patterns. Two types of printing methods were adopted: inkjet printing and EHD printing. In the case of large patterns with a minimum feature size of 50 μm, PEDOT:PSS pattern was printed by an inkjet printer (DMP-2831, Dimatix Corp.) with optimized PEDOT:PSS ink. PEDOT:PSS

ink used at inkjet-printing was prepared by diluting PEDOT:PSS with DI at a weight ratio of 1:1 and then dissolving 1 wt.% of fluorosurfactant (Capstone FS-30, Chemours). For patterns with a width of less than 40 μm, PEDOT:PSS was deposited by an EHD printer (SIJ-S050, SIJ Technology Inc.) with an inner nozzle diameter of 30 μm. In this case, PEDOT:PSS diluted with DI was dissolved with 0.3 wt.% of Triton X-100 (Sigma-Aldrich). In both cases, the deposited PEDOT:PSS pattern was annealed on a 130 ℃ hotplate for 1 hour to enhance the adhesion between PEDOT:PSS and PVA layer. After the annealing process, the surface of the substrate was wiped with IPA to remove non-patterned AgNWs. After the removal process, sonication was performed with a bath sonicator to remove AgNW residues that were not part of AgNW patterns. A transmittance of the AgNW TEs was measured by UV/VIS spectrometer (Lambda 35, Perkin Elmer), and the sheet resistance was observed by a custom-made four-point probe. The optical images of the patterned AgNWs were taken by two types of optical microscopes (DSX-HRSU, OLYMPUS Corp., and RX-100, Hirox). The resistance changes of the AgNWs during a bending or stretching test were measured by a sourcemeter (Keithley 2400, Keithley). Cs-corrected transmission electron microscope (Cs-TEM, JEM-ARM200F, JEOL Ltd.), FE-SEM (JSM-7401F, JEOL Ltd.), and energy-dispersive X-ray (EDS) Spectrometer (Aztec Energy, Oxford) were used to capture the image of patterned electrodes and analyze the electrode components. NC-AFM (XE-100, Park Systems Corp.) was performed to measure the surface morphology and thickness of the micro-patterned AgNW lines. The resistance of AgNWs during the 3M tape test and the resistance of patterned AgNWs with EHD printing was measured by a semiconductor parameter analyzer (4145B, Agilent Technologies) at room temperature in a dark box and air atmosphere. The temperature of the AgNW heaters

was measured by an infrared thermal imaging camera (T420, FLIR system).

3.2.3. Results and Discussion

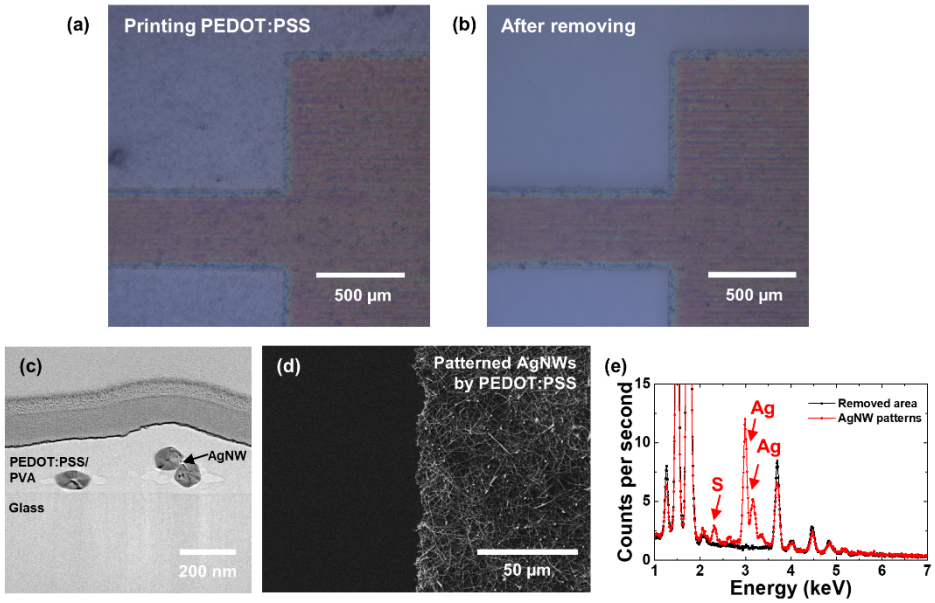

Figure 3.6 Optical image of the AgNW electrodes (a) before and (b) after removing process, (b) Cs-TEM image of the cross-section of patterned AgNWs, (d) SEM image of the edge of the AgNW patterns, and (e) EDS spectrum of the AgNW-removed region and AgNW patterns region.

Figure 3.6 explains the fabrication process sequence with PVA-assisted patterning of AgNW electrodes. Before the spin-coating of an adhesive layer, PLL solution was deposited on prepared substrates to form amine groups [120]. Created PLL layer improved the adhesion between the PVA adhesive layer and the target substrates. After spray-coating the AgNWs on the PVA, uniform PEDOT:PSS patterns can be printed on the AgNW surface without extra surface treatment (**Figure 3.6(a)**). The cross-section image of the AgNW electrodes was captured by the Cs-TEM after the printing process of the PEDOT:PSS (**Figure 3.6(c)**). According to the Cs-TEM image, PEDOT:PSS successfully filled the gaps in AgNW networks, and

the composite electrode layer, which consists of PEDOT:PSS, PVA, and AgNWs, was formed. After the annealing process of the printed PEDOT:PSS, the removal process, including wiping with a wiper soaked in IPA and bath sonication in DI water, was followed. After the removal process, the AgNWs covered by the PEDOT:PSS layer remained stable on the substrates without damage due to the improved adhesion of the PEDOT:PSS, while the AgNW networks on the PVA layer were removed clearly (**Figure 3.6(b)**). For evaluation of the patterning accuracy of the PVA-assisted patterning method, the FE-SEM image of the edge of the AgNW pattern was captured, and EDS analysis was also progressed, as shown in **Fig. 3.6(d) and (e)**. According to the SEM results, AgNWs were only observed on the PEDOT:PSS-printed area, while the AgNWs were removed clearly on the non-patterned area. Furthermore, EDS analysis also confirmed the patterning accuracy because the sulfur peak originated from the PEDOT:PSS polymer chains, and the Ag peak from the AgNW networks was only observed at the patterned area. For precise patterning of the AgNWs, an annealing condition of the electrode layers after the PEDOT:PSS inkjet-printing process was optimized. According to **Fig. 3.7(a)**, the annealing temperature conditions were controlled from 80 ℃ to 150 ℃. With the annealing temperature below 100 ℃, the AgNW patterns took damage from external force and vanished during the removal process. In addition, the AgNWs uncovered by PEDOT:PSS remained on PVA underlying layer in case of the annealing temperature of 150 ℃. As a result, the possible temperature range for enhancing the PEDOT:PSS adhesion and successfully removing AgNWs from the non-patterned area was from 100 ℃ to 140 ℃. I also measured the resistance of the dogbone-shaped AgNW patterns with various annealing temperatures suitable for precise patterning (**Figure 3.7(b)**), and the proper range of the annealing temperature for achieving both precise

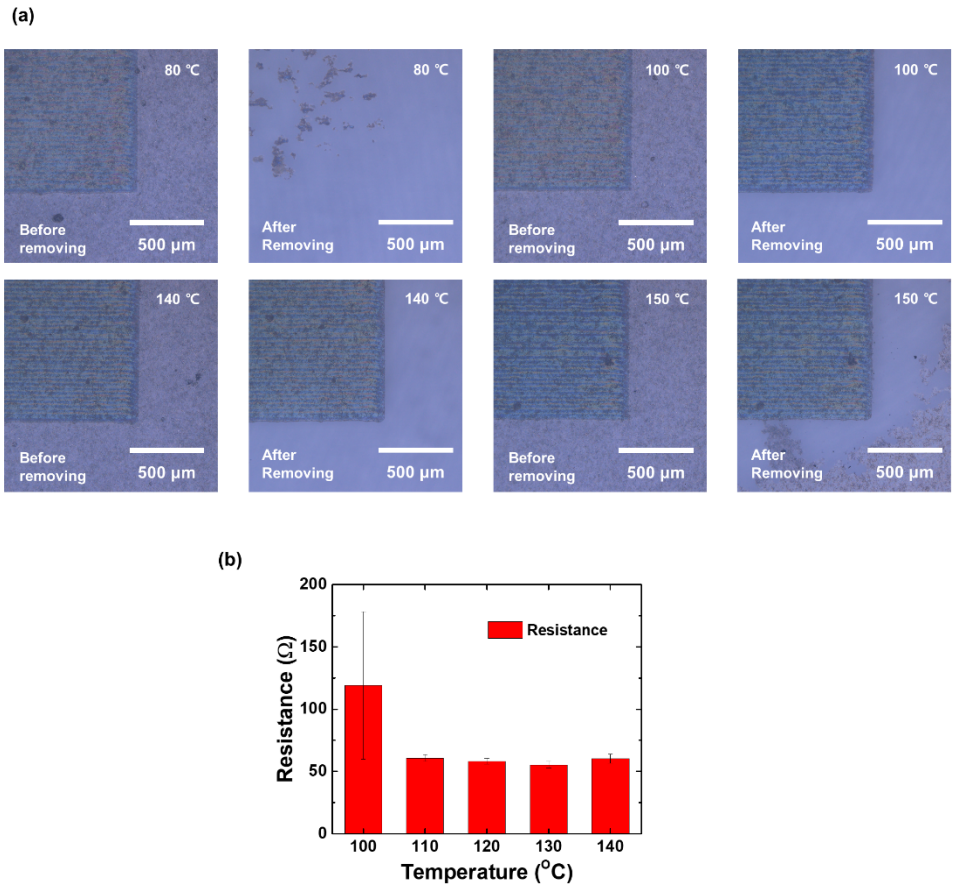

Figure 3.7 (a) Optical images and (b) resistance of the patterned-AgNWs according to the annealing temperature of the PEDOT:PSS electrodes.

patterning and conductivity enhancement was selected from 110 ℃ to 140 ℃.

The AgNW layers were patterned with high patterning freedom on various substrates, as shown in **Fig. 3.8**. First, the AgNW layers can be fabricated on a glass substrate with different precisely designed patterns, from large-scale symbols with a length of 4 millimeters to English characters with a width of hundreds of micrometers. The patterning process of AgNWs can also be conducted on a plastic substrate by spin-coating of PVA adhesive on PLL-treated PEN (**Figure 3.8(c)**). A series of numbers was patterned on the plastic substrates without a scratch or crack.

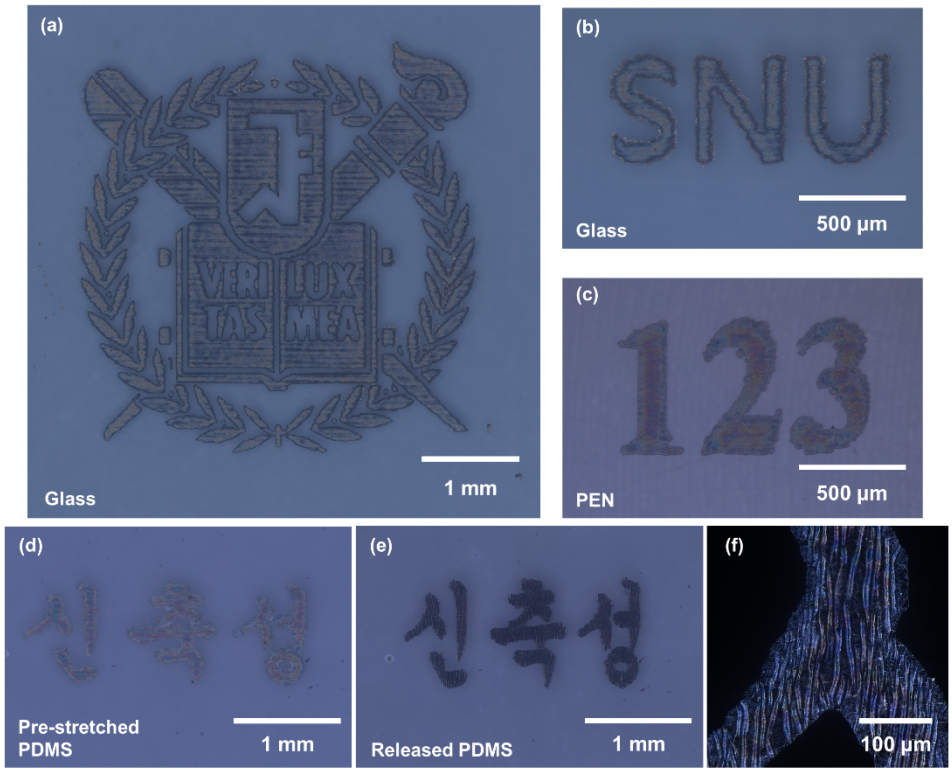

Figure 3.8 Optical images of various AgNW electrodes on diverse substrates patterned by inkjet-printing of PEDOT:PSS. (a) The large-scale logo patterns and (b) characters with a width of hundreds of micrometers on a glass substrate. (c) The AgNW patterns on the PEN substrate. The AgNW patterns on the (d) pre-stretched PDMS, (e) the patterns after releasing pre-strain, and (f) enlarged image of the patterns after releasing.

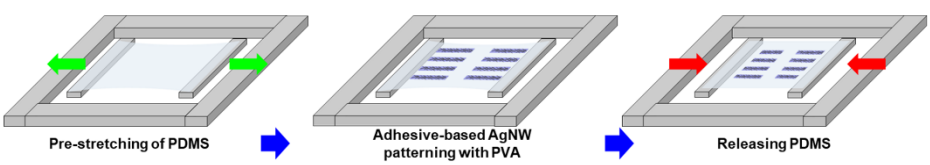

Figure 3.9 Schematic image of patterning sequence of the AgNWs on pre-stretched PDMS substrate.

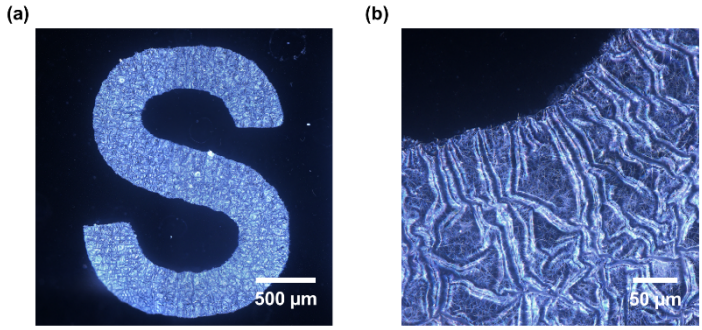

Figure 3.10 Optical images of (a) PVA-assisted-patterned AgNWs on 2-D pre-stretched PDMS substrate, and (b) enlarged image of the patterned AgNWs.

In addition, the AgNWs were patterned on elastomeric substrates to achieve stretchable electronics with the maskless patterning process. Unlike the patterning on a rigid and plastic platform, a cured PDMS substrate was attached to a stretching jig to fabricate the AgNW patterns on a pre-stretched PDMS surface with a 1-D strain of 20 % (**Figure 3.9**). The underlying PVA layer and AgNW layer were successfully coated on pre-stretched PDMS due to the amine-functionalized PLL layer on PDMS, and AgNWs can be patterned precisely on pre-stretched PDMS without damage (**Figure 3.8(d)**). After releasing the strain of AgNW-patterned PDMS, micro-wrinkled structures were exhibited on the surface of patterned AgNWs with a peak-to-peak length of 11 μm, and there was no significant distortion of the patterns after releasing process (**Figure 3.8(e) and (f)**). The PDMS could also be stretched with the biaxial strain, and the AgNW electrodes can be deposited with the desired pattern onto the 2-D stretched PDMS with the PVA-assisted patterning method. After releasing process, wrinkles with arbitrary shapes were formed on the patterns (**Figure 3.10**).

The PVA-assisted maskless patterning process of the AgNW was focused on

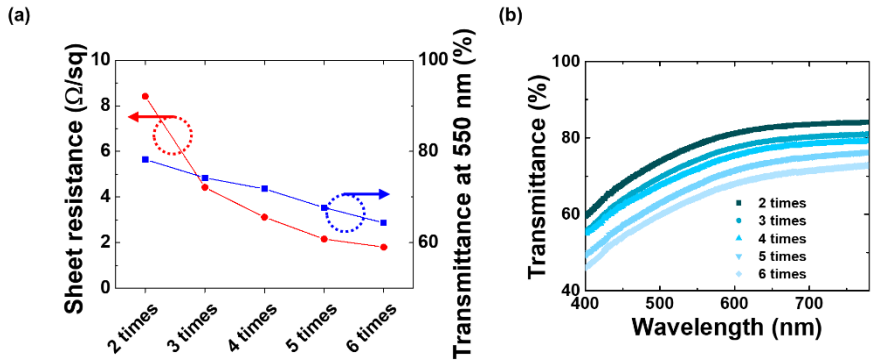

Figure 3.11 (a) Sheet resistance and optical transmittance at 550 nm of the AgNWs with various spray-coating conditions, and (b) optical transmittance of the AgNWs with various spray-coating conditions according to the wavelength.

	Sheet resistance (Ω/sq)	Transmittance (%)	FOM(Ω^{-1})
Condition 1	8.4	78.2	171.6
Condition 2	4.4	74.2	265.0
Condition 3	3.1	71.9	335.8
Condition 4	2.1	67.7	405.4
Condition 5	1.8	64.3	423.7

Table 3.1 The electrode properties of the AgNW transparent electrodes patterned with inkjet-printing of PEDOT:PSS.

two types of conductive electrodes: large-scale transparent electrodes and micro-meter scale highly conductive electrodes. For patterning the large-scale transparent AgNW electrodes, I conducted inkjet printing for the PEDOT:PSS covering layer deposition. **Figure 3.11** and **Table 3.1** represent the electrode property of transparent AgNW electrodes. Spray-coating counts of the AgNWs defined fabrication conditions of AgNW electrodes. The patterned AgNW electrode showed sheet resistance of 8.4 Ω/sq and transmittance of 78.2 %, which can be applied to transparent electrodes. The sheet resistance can be tuned from 8.4 Ω/sq to 1.8 Ω/sq, while the transmittance of electrodes was changed from 78.2 % to 64.3 %, and the

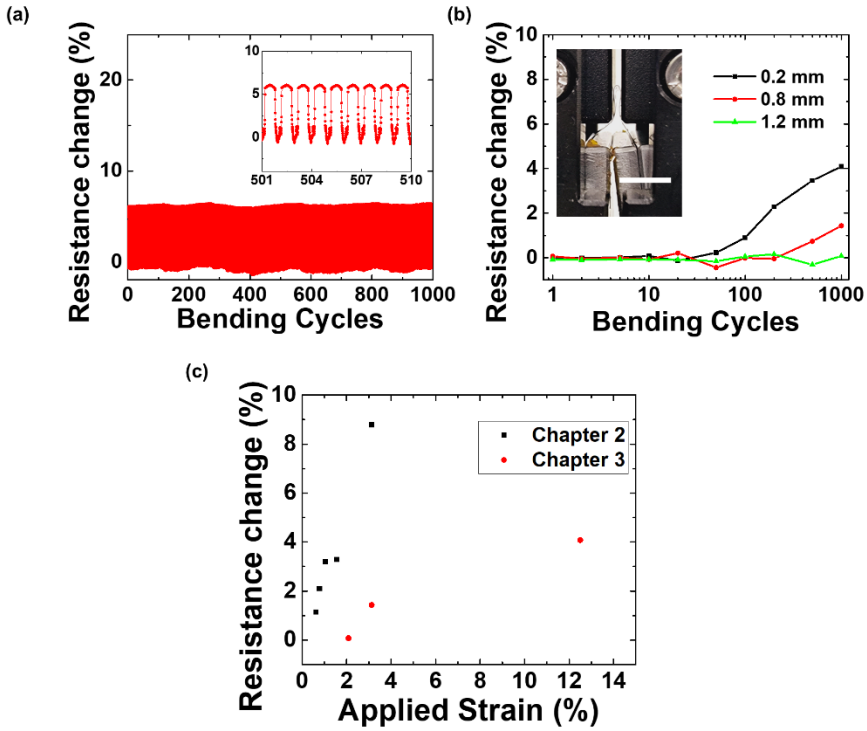

Figure 3.12 (a) Resistance change of the patterned AgNWs during the flexibility test with a bending radius of 1.2 mm, (b) Resistance change of the patterned AgNWs with different bending radii (inset of (b) shows the bending status of the AgNW electrodes with a bending radius of 0.2 mm (the length of the scale bar is 5 mm)), and (c) resistance change according to the calculated strain applied to the transferred AgNW TEs during the bending test.

Bending radius (mm)	2	4	6	8	10
Calculated strain (%)	3.1	1.6	1.0	0.8	0.6

Table 3.2 Calculated bending strain in chapter 2.

Bending radius (mm)	0.2	1.8	1.2
Calculated strain (%)	12.5	3.1	2.1

Table 3.3 Calculated bending strain in chapter 3.

figure of merit was also calculated by the electrical to optical conductivity ratio method [121]. The easy tunability of electrode properties with the same maskless patterning method paves the way for adjusting the electrode characteristics according to the various needs of display applications.

Figure 3.12(a) and (b) show the flexibility of maskless patterned AgNW electrodes. The PVA-assisted patterning process of the AgNWs was conducted on a PEN substrate with a thickness of 50 μm for applying harsh conditions with a bending radius of under 1 μm. The fabricated AgNW electrodes showed superior flexibility during 1,000 times of bending cycles under a bending radius of 1.2 mm. Resistance of the PVA-assisted patterned AgNWs was changed to 6 % at a single bending cycle, and it showed negligible resistance change under flat conditions after 1000 cycles (**Figure 3.12(a)**). In addition, the resistance of the patterned AgNWs showed a change of only 4.1 % after 1000 bending cycles under a bending radius of 0.2 mm, which was a folding condition of the plastic substrate (**Figure 3.12(b)**). To prove the flexibility enhancement of PVA-assisted patterning, I calculated an applied strain at the surface of the transferred AgNW electrodes in chapters 2 and 3 (**Figure 3.12(c) and Tables 3.2 and 3.3**) [122]. In the case of chapter 2, the AgNW was transferred on the PEN with a thickness of 125 μm. The maximum applied strain at the bending part of AgNWs was calculated as 3.1 % under the bending radius of 2 mm. In contrast, the applied strain was increased at the AgNWs fabricated by PVA-assisted patterning due to reduced PEN thickness (50 μm) and harsh bending conditions. Although the higher strain was applied to the AgNWs TEs patterned by the PVA-assisted method, the reduced resistance change was observed, and those results demonstrated that the flexibility of the patterned AgNWs was enhanced by replacing the transfer-based patterning technique to the PVA-assisted patterning.

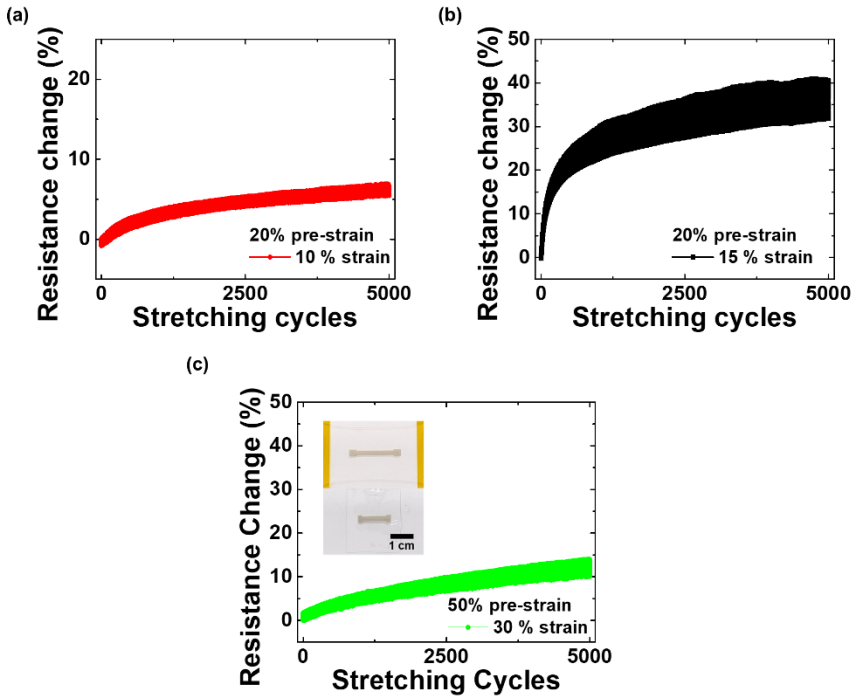

Figure 3.13 (a) Resistance change of the 20% pre-stretched AgNWs during the stretchability test with a strain of 10 %, (b) resistance change of the 20 % pre-stretched AgNWs during the stretchability test with strain of 15 %, and (c) resistance change of the 50% pre-stretched AgNWs during the stretchability test with a strain of 30 %.

The mechanical robustness of the AgNW electrodes fabricated by the PVA-assisted patterning method was also demonstrated with a stretching test (**Figure 3.13)**). After patterning AgNWs on the pre-stretched PDMS with a 1-D strain of 20 %, the released electrodes showed mechanical durability under 10 % and 15 % strain, as shown in **Fig. 3.13(a) and (b)**. The resistance of the AgNW electrodes only increased by 6 % after 5000 times of stretching with 10 % strain. In addition, the patterned AgNWs also demonstrated their stretchability under 15 % strain, with 20 % and 32 % after 1000 times and 5000 times of stretching. In addition, through the

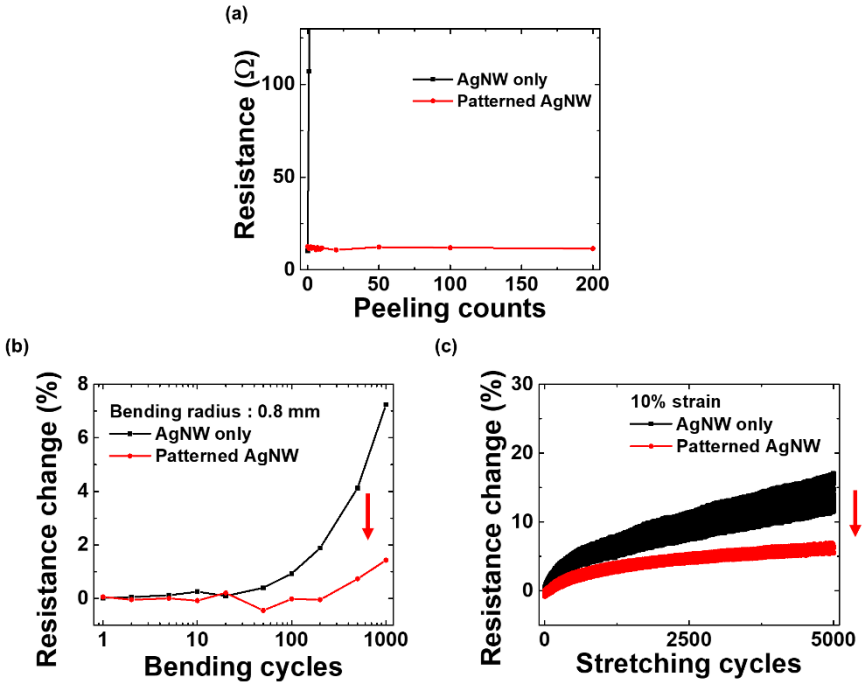

Figure 3.14 (a) Resistance change of the AgNW-only electrodes and patterned AgNW electrodes after 3M tape test, (b) resistance change of the AgNW-only electrodes and patterned AgNW electrodes during the flexibility test with a bending radius of 0.8 mm, and (c) resistance change of the AgNW-only electrodes and patterned AgNW electrodes during the stretchability test with a strain of 10 %.

increase of pre-strain to 50 %, the AgNWs can be successfully patterned on the PDMS and showed superior stretchability under the strain of 30 % with a resistance change of 10 % after 5000 stretching cycles (**Figure 3.13(c)**). Those results indicated that the stretching performance of the patterned AgNWs can be further enhanced by the optimization of substrate materials and pre-stretching technique.

The additional strength of the PVA-assisted patterning is the enhanced adhesion of the AgNWs originating from sandwiched structure between PEDOT:PSS and PVA layers. The improved adhesion of the patterned AgNW electrode was demonstrated

by the tape test with 3M tape (**Figure 3.14(a)**). The tape test was conducted by iteration of attachment and detachment of the 3M tape on the surface of electrodes. Unlike the AgNW-only electrodes, the AgNWs inserted between PVA adhesive and PEDOT:PSS pattern showed negligible resistance change, even after 200 times of peel-off sequence. Enhanced adhesion prevented the damage and loss of AgNWs, which occurred on the AgNW-only electrodes after the tape test. The comparison of the mechanical stability between the AgNW-only electrodes and the PVA-assisted-patterned AgNWs was also evaluated to determine the effect of the enhanced adhesion between the AgNWs and substrate. After the 5000 times of bending cycles under the bending radius of 0.8 mm, the resistance change of the PVA-assisted-patterned AgNWs was much smaller than the AgNW-only electrode, which showed a resistance increase of 7.2 % (**Figure 3.14(b)**). The stretchability test result also demonstrated an improvement in mechanical stability after the PVA-assisted patterning process, as shown in **Fig. 3.14(c)**. The AgNW electrodes fabricated by my patterning technique can be applied to various deformable applications with advanced mechanical stability.

Although the inkjet-printing process is an effective deposition method of elaborate PEDOT:PSS patterns on AgNW, it has limitations in decreasing the minimum feature size and enhancing the resolution of patterns with a micrometer scale. To enhance the patterning resolution of the AgNW electrodes, the PEDOT:PSS was printed by the EHD printing process (**Figure 3.15(a)**). For the fabrication of a jettable PEDOT:PSS ink, Triton X-100 was selected as a surfactant material. The Triton X-100 has been reported as a surfactant that reduces the surface tension of PEDOT:PSS and therefore reduces the applied voltage during EHD printing [123].

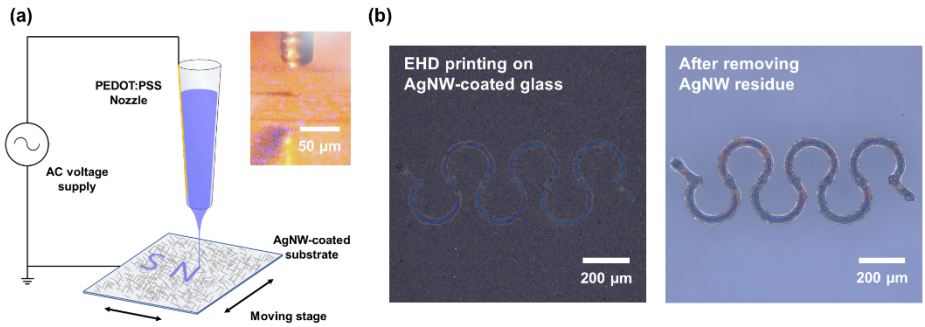

Figure 3.15 (a) Schematic image and optical image of the EHD printing process of PEDOT:PSS on the AgNW substrates, and (b) optical images of the EHD-printed PEDOT:PSS on the AgNW-coated PVA surface (left), and patterned AgNWs after removing process (right).

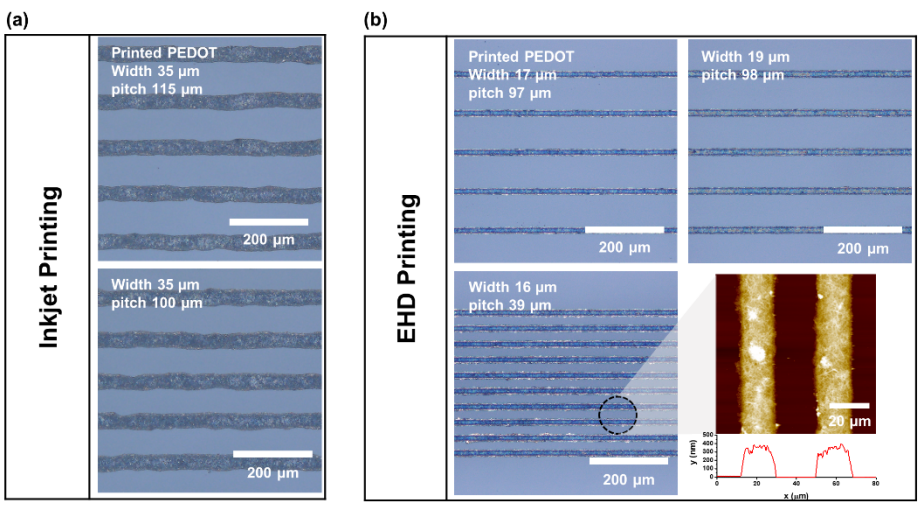

Figure 3.16 Optical images of the AgNW patterned with horizontal lines by (a) inkjet printing, and (b) EHD printing of PEDOT:PSS with various pitches and widths.

For stable EHD printing, Triton X-100 was mixed with PEDOT:PSS with a ratio of 0.3 wt.%. As a result, the meniscus of the PEDOT:PSS ink successfully appeared at the end of the nozzle with a cone shape, and the PEDOT:PSS ink was continuously ejected from the end of the meniscus. According to **Fig. 3.15(b)**, the PEDOT:PSS

was successfully printed on AgNW by EHD printing with a linewidth less than 30 μm. In addition, the EHD-patterned area maintained its shape without deformation after the removal process in the same way as patterning by inkjet printing. To confirm the fabrication limit of the inkjet-printing process and measure the conductivity of AgNWs patterned by EHD printing, I printed PEDOT:PSS horizontal lines on AgNWs by both inkjet printing and EHD printing. In the case of inkjet printing, the line was composed of a series of droplets with a 15 μm drop spacing. After removing residual AgNWs, the width of the AgNWs line was measured to be 35 μm (**Figure 3.16(a)**). On the other hand, the continuous flow of PEDOT:PSS was implemented with the EHD-printing process. Therefore, I successfully demonstrated stable AgNW line patterns with a width of under 20 μm on glass substrates (**Figure 3.16(b)**). The thickness of the PEDOT:PSS was also optimized for patterning high-conductive AgNW patterns, as shown in the AFM image of **Fig. 3.16b**. In addition, the pitch between adjacent AgNWs was reduced to 39 μm with the EHD-printed pattern. The reduced scale of AgNW patterns with the PVA-assisted method enables the fabrication of complicated circuits, and it thus will extend the applicability of the patterning approach to various high-resolution display applications. Through those precise patterning results on the glass, I fabricated various AgNW patterns through EHD-printing of PEDOT:PSS on diverse substrates. First, the English characters were patterned by the EHD printing with a linewidth of under 15 μm (**Figure 3.17(a)**) and 20 μm (**Figure 3.17(b)**). A serpentine structure was also patterned on polyimide (PI) substrates attached to pre-stretched PDMS with siloxane bonding originating from (3-aminopropyl)triethoxysilane treatment on PI [124]. After releasing the strain of PDMS, a wrinkled structure was created on the PI surface, as shown in **Fig. 3.17(c)**. In addition, a coiled structure with a pitch of 150 μm was exhibited on

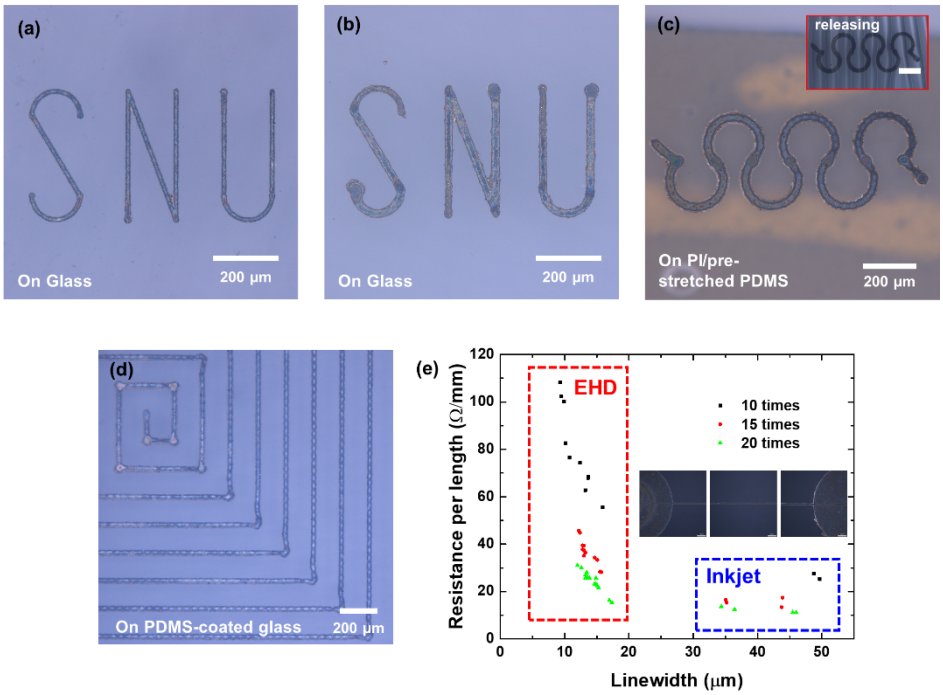

Figure 3.17 Optical images of the AgNW electrodes patterned with EHD printing. (a), (b) English characters on glass, (c) serpentine pattern on PI attached on pre-stretched PDMS, (inset image shows releasing state), (d) coiled structure on PDMS-coated glass. (e) Resistance of the AgNW electrodes patterned by EHD printing, with different width and AgNW coating counts.

PDMS coated on the glass substrate (**Figure 3.17(d)**). The EHD-printing-based patterning process showed a high degree of patterning freedom on various substrates, including plastic and elastomer. In addition, for measuring the conductivity of the EHD-patterned AgNW electrodes, I printed a single line with two contact pads at both ends and fabricated multiple samples by controlling linewidth. The conductivity of lines was also varied by adjustment of spray-coating counts of the AgNWs before EHD printing. Through optimization of the printing condition, the linewidth of the EHD-patterned AgNW lines could be reduced to 10 μm with resistance per length of

100 Ω/mm, in the case of the AgNWs with spray-coating 10 times (**inset of Figure 3.17(e)**). In the case of 20 times coating of AgNWs, the resistance per length of AgNWs was 15.4 Ω/mm with a linewidth of 17 μm (**Figure 3.17(e)**). And resistance per length was 28.2 Ω/mm with a linewidth of 15.7 μm and 55.5 Ω/mm with a linewidth of 15.9 μm, in the case of spray-coating 15 times and 10 times of AgNWs, respectively. Compared to the lines with the inkjet-printing sample, the conductivity of the AgNWs was maintained even if the linewidth of the AgNW patterns was reduced with the use of EHD printing, and PVA-assisted patterning showed reliability at high-resolution electrode patterning.

For applying PVA-assisted-patterned AgNWs to various wearable applications, I fabricated two types of electronic devices that can be demonstrated on a deformable platform. First, 3x3 stretchable LED arrays were manufactured on pre-stretched PDMS with 2-D pre-strain of 20 % on each axis (**Figure 3.18(a)**). Each LED part was placed between adjacent AgNW electrodes patterned by inkjet-printing of PEDOT:PSS, and pure epoxy and conductive silver (Ag) epoxy was previously dispensed on the LED location before placement of LEDs [125]. The pure epoxy enabled the LEDs for stable attachment with PDMS, and the Ag epoxy dispensed on both sides of the pure epoxy made electrical contact between the LEDs and the AgNW electrodes. After curing, the epoxy under the LED served as a rigid island, while the micro-wrinkles occurred on AgNW electrodes (**Figure 3.18(b) and (c)**). The 3x3 LED array with patterned AgNWs showed stable light emission under the strain of 13% at both axes without the degradation of the performance, and the LED arrays could be operated even with the vertical deformation without damage to the circuit (**Figure 3.18(d) and (e)**). Through the operation of the 3x3 LED array on the PDMS substrate, it is expected that the AgNWs fabricated by maskless patterning

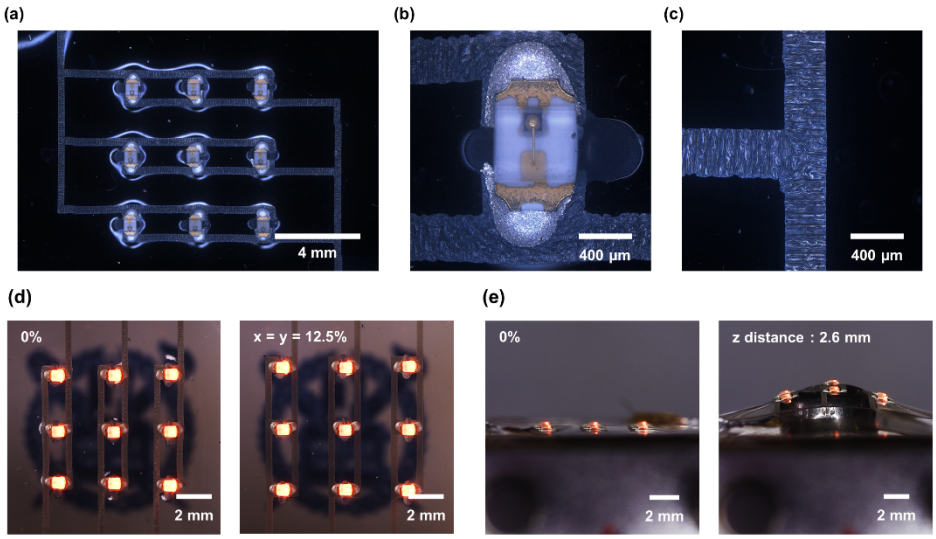

Figure 3.18 Optical images of the (a) 3x3 stretchable LED arrays on PDMS substrates, (b) enlarged image of a single LED attached on PDMS, and (c) patterned AgNWs with 2-D wrinkled structure, operation of the stretchable 3x3 LED arrays with the patterned AgNW electrodes at (d) 12.5 % of 2-D strain, and (e) vertical deformation of z-axis.

can show reliable operation on the stretchable platform. The second application was a wearable heater system with the AgNW mesh structure, which can be applied to various wearable heating components and automotive systems. The transparent mesh structure with a pitch of 200 μm and AgNW linewidth of 15 μm was successfully patterned with an area of 4 mm x 4 mm, implemented by PVA-assisted patterning process with EHD printing (**Figure 3.19(a) and (b)**). Ag paste achieved the electrical contact at the ends of the mesh structure, and the DC voltage was applied from 2 V to 4V. According to the infrared image shown in **Fig. 3.19(c)**, the thermal emission was detected at the entire surface of the mesh patterns. The maximum temperature was measured as 214 ℃ at the voltage of 4 V, 152 ℃ at 3 V, and 88 ℃ at 2 V (**Figure**

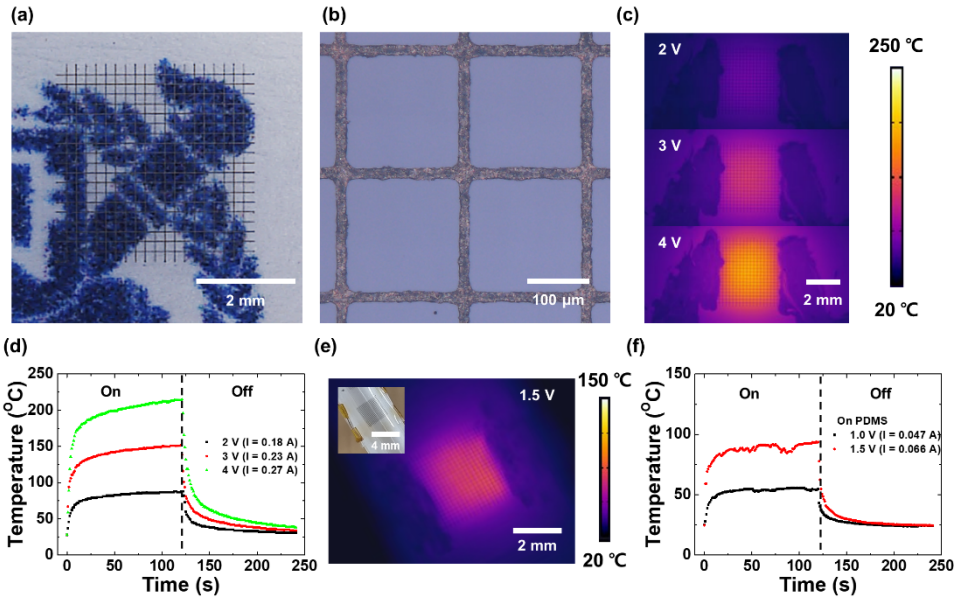

Figure 3.19 Optical images of the (a) EHD-patterned AgNW heater with mesh electrodes and (b) enlarged image of the AgNW heater. (c) Infrared thermal image of the voltage-applied AgNW heaters on a glass substrate. (d) Temperature change of the AgNW heaters with different voltages. (e) Thermal image of the AgNW heaters on PDMS substrates attached to a cylindrical structure. (f) Temperature change of the AgNW heaters on PDMS substrates with different voltages.

3.19(d)). The superior conductivity of the patterned AgNW mesh showed excellent heating characteristics. In addition, I fabricated AgNW mesh patterns on the pre-stretched PDMS substrate with a strain of 20 % on both axes. The mesh-patterned PDMS substrate was attached to a cylindrical needle cap with a diameter of 6.2 mm (**Figure 3.19(e)**). The AgNW heaters on the PDMS substrates showed stable heating performance on the cylindrical curvature. The maximum temperature of the heater surface was 94 ℃ at the voltage of 1.5 V and 58 ℃ at 1V, which is suitable for wearable applications. And the heater device on PDMS also exhibited stable

operation during the 4 minutes of on-off sequence (**Figure 3.19(f)**), which demonstrated reliability on the curved surface, such as the side view mirror of the automotive system and various wearable devices.

3.3. Conclusion

In conclusion, I suggested a maskless patterning process of AgNW conductive electrodes by interposing AgNWs between a PVA adhesive bottom layer and PEDOT:PSS conductive patterns. Enhanced adhesion between PVA and PEDOT:PSS patterns after annealing treatment preserved the loss or damage of AgNWs underlying the PEDOT:PSS, and the AgNWs were precisely patterned along the printed patterns of PEDOT:PSS. The AgNWs can be fabricated onto various platforms, including plastic substrates and elastomers, without distortion or damage to the desired pattern with superior mechanical stability through the PVA-assisted patterning method. In addition, by introducing EHD printing of PEDOT:PSS, it was possible to improve the resolution of AgNW patterns without degradation of conductivity. High-resolution patterning of the high-resolution AgNW conductive electrodes on both rigid and deformable substrates can enhance the performance of wearable electronic devices. In addition, demonstrating precise patterning without a patterning mask can increase patterning freedom and reduce fabrication costs. Furthermore, the reliable performance of the AgNWs display components patterned by the PVA-assisted method expands their applicability to high-resolution deformable electronics in the future.

Chapter 4 High-resolution EHD Printing of UV-curable Polymer for Color-conversion Structures

4.1. Introduction

This chapter explains the high-resolution patterning of the color-conversion structures, which compose of the QD and UV-curable resin. As the demand for high-resolution displays such as wearable and AR/VR devices has grown [126-128], the emission area of a single pixel needs to be reduced to achieve the resolution. The conventional organic-based OLEDs show the complexity of satisfying both high-resolution and pixel uniformity. Instead of the organic-based LEDs, various researchers and the display industry have been focused on the inorganic LEDs with sizes under 500 μm, which are called mini-LED (length from 100 μm to 500 μm) [129-131] and micro-LED (length under 100 μm) [28, 30, 110, 132-134]. The mini-LEDs and micro-LEDs contain the advantages of conventional inorganic LEDs, such as superior luminance, long lifetime, and applicability to high-resolution display and transparent display [135-138]. However, implementing the red-green-blue (RGB) full-color arrays with micro-LEDs is interrupted by the difficulty of the transfer process of the micro-LEDs on the pre-designed circuits. Three times iterative transfer process during the fabrication of full-color micro-LED arrays causes high production costs and low process yield due to the complicated alignment of RGB

arrays and repeated repair process of disconnected micro-LEDs [139-141]. On behalf of the fabrication of the full-color micro-LEDs, the alternative technique has gotten serious attention, based on combining monochromatic LED arrays and color conversion layers [142-144]. The transfer of the LEDs with single color dramatically shortens the fabrication time and simplifies the repair process of dead pixels. Among all the candidates for the color conversion materials, QDs have attracted numerous attention for materials of color filters. QDs are semiconducting materials with a few nanometers diameter, which radiate a specific wavelength of light by external light or electrical energy [145, 146]. The QDs are applied to various future displays and lighting applications due to their high quantum yield, narrow emission bandwidth, and size-dependent tunable wavelength [147-149]. Numerous studies have focused on the QDs as an emitting layer of the solution-processed light-emitting diodes with high color purity to replace the conventional organic emitting materials [150-152]. Besides, several researchers have reported that the QD was selected as a down-converting material in the color conversion filters [153-156]. When the QDs which emit green or red light (from now I call them green-QD and red-QD, respectively) are deposited on monochromatic blue LED arrays, the blue light from micro-LED pixels is converted to lights with an emission wavelength of the QD.

For the deposition of the QDs on arbitrary substrates, solution-based processes such as spin-coating or inkjet-printing have been adopted [157-160]. To increase the conversion rate and improve the color purity of the color filter, uniform QD layers with a sufficient thickness on the top of the LED surface are necessary. However, evaporating solvent during the annealing process causes the non-uniformity of the deposited layer, such as the coffee ring effect. Therefore, extra modification of the solvents should be needed [161-163]. In addition, the resolution of the inkjet-printing

of the QD solution is not suitable for a single pixel of micro-LED, and the photolithography of spin-coated QD layers needs high production costs [164, 165]. For both obtaining sufficient thickness of a color conversion layer and achieving uniform distribution of the QD films through the whole light-emitting area, drop-on-demand printing of color conversion composite materials composed of photocurable polymer and QD particles have been suggested [156, 166-169]. However, the high viscosity of polymer/QD composite and the development of high-resolution micro-LED arrays disturbed their patternability and commercialization. Therefore, I select EHD printing as an alternative patterning method for a high-resolution QD color conversion layer to overcome those severe issues. During the EHD printing process, high voltage is applied between the nozzle and substrate, and the applied electric field drives the stable jetting of ink materials from the end of the nozzle [34, 35]. EHD printing enables precise patterning of high-viscosity materials, and high-resolution patterns with submicrometer scales can be achieved because the droplet size of the ink material is much smaller than the nozzle diameter. Therefore, introducing the EHD printing technique to fabricate the QD color conversion layer is necessary for achieving high-resolution additive patterning of polymer/QD composite.

In this chapter, I demonstrate a facile patterning process of UV-curable polymer/QD composite patterns with a diameter of down to 30 μm. Green/red CdSe/ZnS QD solutions were mixed with a base polymer which can be cured by UV light. A Norland Optical Adhesive 61 (NOA 61) is selected as a UV-curable polymer material due to its high transparency and suitable viscosity for EHD printing [170, 171]. In the case of mixing QD with high concentration, the aggregation of the QDs in the polymer matrix hinders the stable jetting of the polymer/QD composites. In

order to resolve the aggregation issue, ligands of prepared QDs were optimized by blending butyl 3-mercaptopropionate (from now on, I will call it B3MP) during the mixing process of the QD-dispersed solution and NOA 61. The QDs maintained their photoluminescence (PL) property even after B3MP treatment. After the evaporation of the unnecessary solvent in the vacuum chamber, the homogeneous NOA 61/QD composite ink was achieved without aggregation of the QDs. The blended NOA 61/QD composite ink was successfully patterned by the EHD printing with a nozzle diameter of 30 μm. The color conversion structures with lens shape can be demonstrated through the proper surface treatment on the target substrate without the spread of the printed ink. The concentration of the QD in the NOA 61 was increased up to 150 mg/ml for better color purity of the light transmitted through the color-conversion structures. With my optimized polymer/QD ink, the printed arrays composed of 500 color conversion structures with a pitch of 100 μm were demonstrated without nozzle clogging. In addition, the color-conversion structures were precisely patterned on the designated area, such as a direct surface of the micro-LEDs, barrier-defined structures with narrow pitch, and PDMS hole array structures.

4.2. EHD-printing of Optimized UV-curable Polymer/QD Ink for Color Conversion Structures with High-resolution

4.2.1. Main Concept

NOA materials are mercapto-ester-based photocurable polymers that contain a mercapto-ester and acrylate monomers. Among the various NOA products, the NOA 61 was selected as an EHD-printed ink because the viscosity of the uncured NOA 61 is 300 cps which is possible for EHD printing. In addition, UV irradiation-based curing method facilitates the storage of the nozzle, and the high transparency is suitable for various optical applications. I previously implemented micro-island arrays on the elastomer by EHD printing of the NOA 61 on the PDMS surface (**Figure 4.1**). According to the datasheet of NOA 61, Young's modulus of the NOA 61 is 930 ~ 1103 MPa, which shows a significant difference compared to that of PDMS (3.7 MPa), and the NOA 61 is selected as a material for strain-engineering structures due to the large mismatch of the modulus. Although the formation of the plasma-induced silica layer should be preceded for stable jetting of EHD printing on PDMS, printed NOA 61 spreads and cannot form in a spreading shape on plasma-treated PDMS. In order to maintain the spherical shape of the printed droplet, a trichloro(1H,1H,2H,2H-perfluorooctyl)silane (FOTS) treatment was conducted on the plasma-treated PDMS surface. A FOTS treatment has been reported as a promising strategy for forming a self-assembled monolayer (SAM) on the target substrate for decreasing surface adhesion [172-174]. he EHD-printed NOA 61 structures maintained the shape of the lens on the PDMS substrates due to the

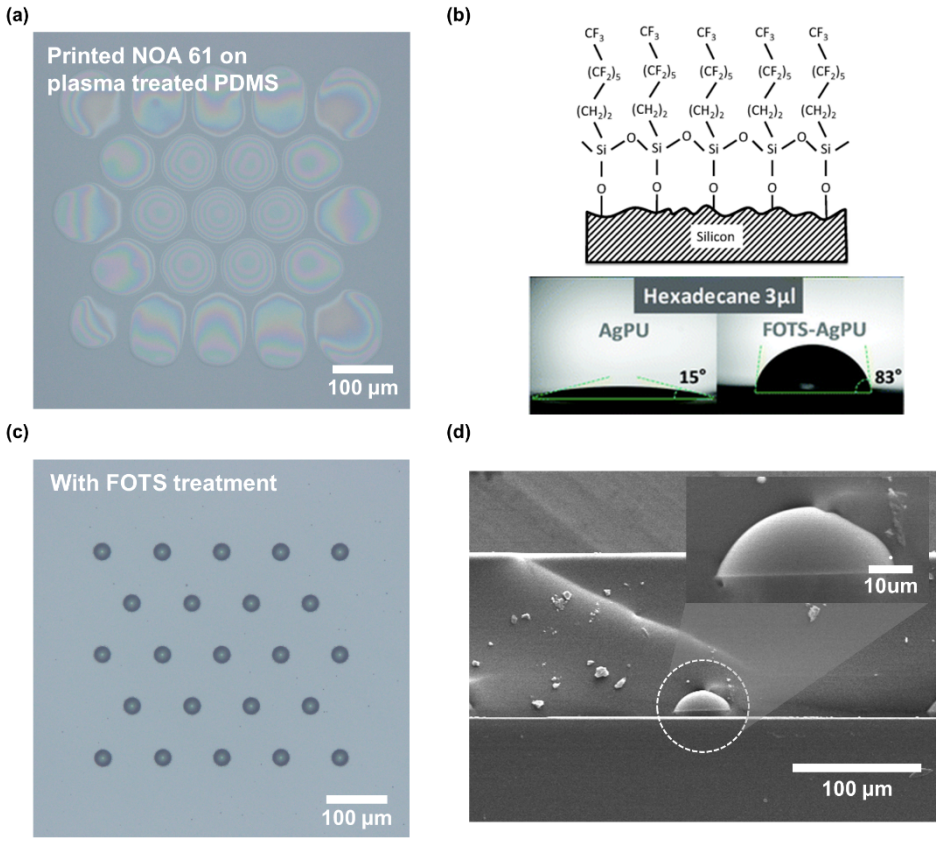

Figure 4.1 (a) Optical image of EHD-printed NOA 61 on plasma treated PDMS, (b) the effect of FOTS treatment [173, 174], (c) optical image of the EHD-printed NOA 61 on FOTS-treated PDMS, and (d) SEM image of the micro-island embedded in PDMS.

increased surface tension, and the thickness-controlled NOA 61 micro-islands were successfully embedded in the PDMS sheet with high resolution. Furthermore, the introduction of lens structure on the color filter surface enhances the out-coupling efficiency of the converted light [175], and the increasing conversion efficiency of the filters with microlens structure by longer path length of the incident light was also reported [176].

In addition to defining the structure of the EHD-printed NOA 61 ink, mixing

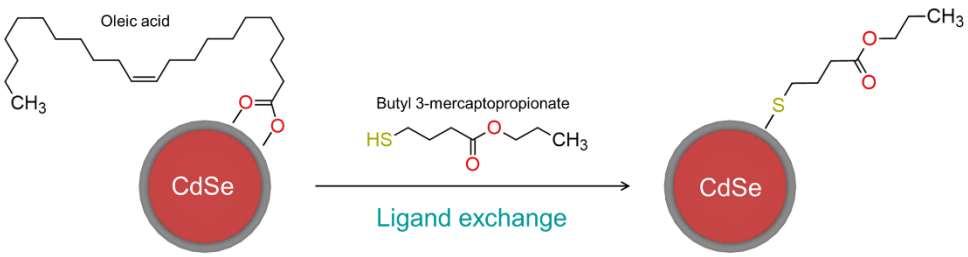

Figure 4.2 Schematic image of ligand exchange from OA to B3MP.

QDs with the UV-curable polymer is another challenge for fabricating the polymer/QD composite. Several papers have been reported about the mixture of NOA and QD [156, 166]. However, aggregation of the QDs during the mixing process with NOA material and accordingly disturbing the curing process of the NOA, which is based on the thiol-ene reaction concentration, hinder the uniformity of high-concentration QD [177]. Furthermore, the aggregated QDs cause clogging of the nozzle, which is also a limitation for increasing QD concentration and improving color-conversion properties. Therefore, several studies have focused on the ligand exchange of QDs from oleic acid (OA) to desired materials for reducing aggregation and improving the uniformity of polymer/QD composite [176-178]. In this chapter, I use B3MP material, which has a thiol group at the end of the molecular chain. The sulfur at the thiol group creates the bond with the surface of the QDs, and a shorter chain of the ligands enhances the thiol-ene reaction of NOA 61 without aggregations.

4.2.2. Experimental Section

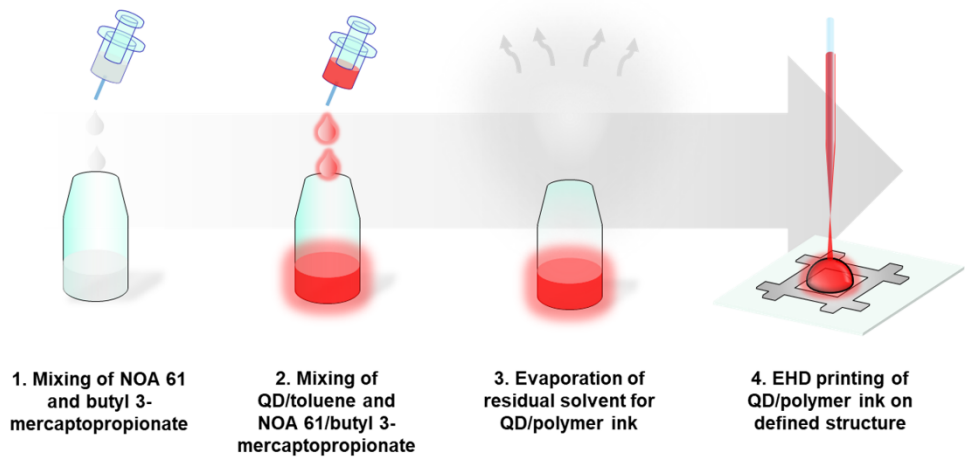

Figure 4.3 Schematic image of mixing process of NOA 61 and QDs

Figure 4.3 represents a mixing procedure of uniform UV-curable polymer/QD composite for EHD printing of color-conversion structure. First, NOA 61 (Norland Products) was diluted with B3MP (98 %, Sigma-Aldrich) at a volume ratio of 1:3 to produce sufficient B3MP molecules while mixing QDs. After 1 hour of stirring, QD solutions (CdSe/ZnS structure, 100 mg/ml in toluene, ligand: oleic acid, SJ Science) was mixed with NOA 61/B3MP composite, and the stirring on a hot plate with a temperature of 70 ℃ was followed. The concentration of NOA 61/QD composite was previously determined by the control of mixing QD solutions. After stirring overnight, the mixture was moved to the vacuum desiccator and placed on a hot plate. Under the low vapor pressure inside the desiccator, residual solvent composed of B3MP and toluene was evaporated to prepare NOA 61/QD composite ink with high concentration. I fabricated the composite ink with concentrations of 50 mg/ml, 100 mg/ml, and 150 mg/ml and conversion colors of red and green.

After the preparation of NOA 61/QD composite ink, the ink was deposited on

the target substrate by EHD printing. The NOA 61 and QD composite was deposited by an EHD printer (SIJ-S050, SIJ Technology Inc.) with an inner nozzle diameter of 30 μm. In order to create the hydrophobic surface for the lens-shaped surface, air plasma treatment (CUTE-1MP, Femto Science) was implemented with the power of 50 W for 30 s before the EHD printing process. After plasma treatment, the plasma-treated substrate and the bottle of FOTS were placed in the vacuum chamber for 30 minutes to conduct a vapor deposition of the FOTS molecules on the target substrate. During the EHD printing, applied voltage, nozzle height, and waveform shape were controlled to optimize the size of the color conversion structures. After fabrication of the color conversion structures with desired patterns, the curing process was conducted for 20 min under a UV light with a wavelength of 365 nm irradiated by a portable UV lamp (LF206LS, UVITEC Cambridge). In the case of the fabrication of the EHD printed barrier on colorless polyimide (cPI) substrate, cPI varnish was spin-coated with 1000 rpm on the glass substrate. And an imidization process, which consists of an annealing process in a furnace with a 320 ℃ for 1 hour, was followed. Pure NOA 61 barriers were also printed by EHD printing, with an inner nozzle diameter of 4 μm. In addition, the PDMS barrier was conducted by using the silicon mold fabricated by deep etching of hole patterns with the desired diameter on the Silicon mold.

The optical images and PL images of the EHD-printed color conversion structures were taken by two types of optical microscopes (DSX-HRSU, OLYMPUS Corp., and RX-100, Hirox). The absorbance of the QDs was measured by UV/VIS spectrometer (), and the PL properties of the reference QD and optimized QD were prepared with fluorescence spectrometers (Fluotime 300, PicoQuant). In order to prove the replacement of the ligand, nuclear magnetic resonance (NMR) analysis

(Avance III-500 and Avance III HD, Bruker) and Fourier Transform Infrared (FT-IR) analysis (Tensor 27, Bruker) were progressed. The color-conversion effect of the NOA 61/QD composite on the electroluminescent (EL) devices was measured by a spectroradiometer (CS-2000, Konica Minolta), and the operation of the EL devices was conducted by a source-measurement unit (Keithley 237, Keithley). The thickness of the NOA 61/QD composite film was measured by a surface profiler (DektakXT-A, Bruker).

4.2.3. Results and Discussion

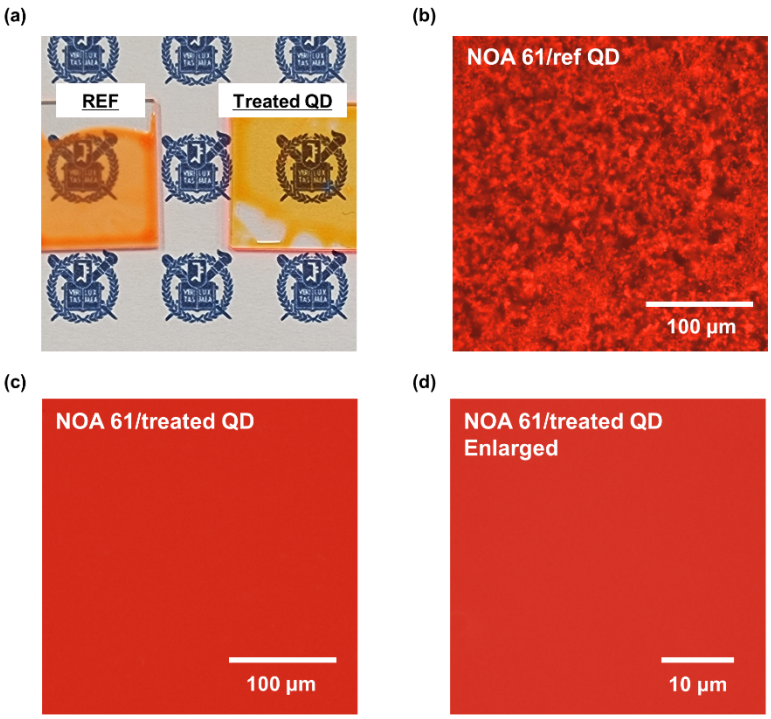

Figure 4.4 (a) Optical image of glass-coated ref QD and treated QD mixed with NOA 61, microscopic images of (b) NOA 61/ref QD, (c) NOA 61/treated QD, and (d) enlarged image of NOA 61/treated QD composite.

Figure 4.4 shows the spin-coated NOA 61/QD composite film on the glass substrate. In case of the reference QD (ref QD), the QD dispersed in toluene was mixed with NOA 61 without addition of the B3MP, and the solvent-evaporation process was followed. After evaporation process, the aggregations of the QDs were shown in NOA 61/ref QD ink. As a result, the light transmitted through the NOA 61/ref QD was scattered by the aggregated QD particles in the spin-coated NOA 61/QD composite, hence the images under the spin-coated layer appear blurry (**Figure 4.4(a)**). Unlike the ref QD, the NOA 61 with B3MP-treated QD (treated QD) showed clear image which was placed under the spin-coated NOA 61 layer.

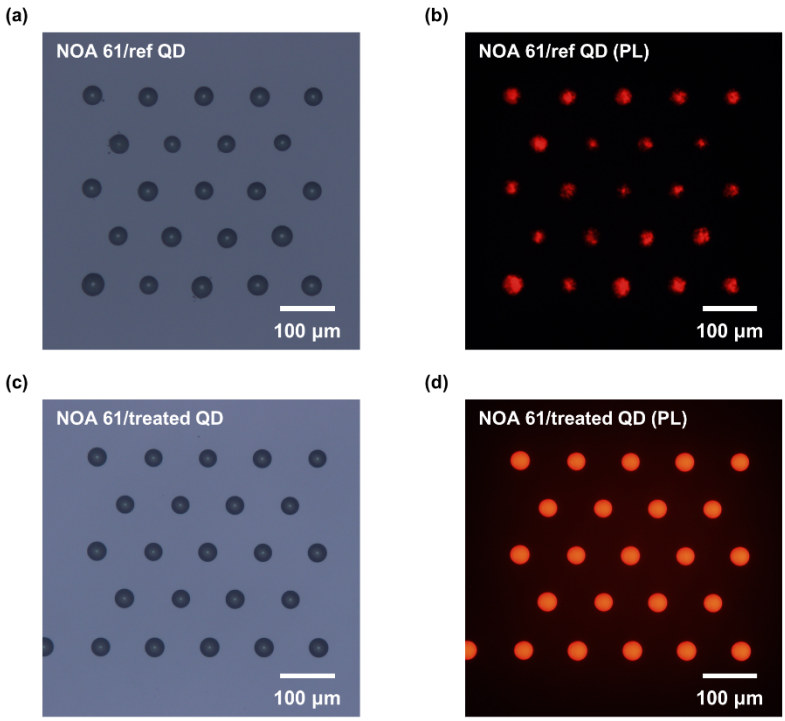

Figure 4.5 (a) Optical and (b) PL image of EHD-printed NOA 61/ref QD composite on the glass, and (c) optical and (d) PL image of EHD-printed NOA 61/treated QD composite on the glass.

According to the optical images of UV-irradiated NOA 61/ref QD layer in **Fig. 4.4(b)**, the multiple speckles with size of few micrometers were observed, due to the aggregation of the QDs in the NOA polymer. On the other hand, the NOA 61 layers mixed with B3MP treated QDs showed uniform emission of red light under the UV exposure without the large QD clusters (**Figure 4.4(c) and (d)**). The uniform ink treated by the B3MP enables the stable jetting during the EHD printing with nozzle diameter of 30 μm. I conducted the EHD printing of the both inks, on the FOTS-treated glass substrate. The PL images of the color conversion structures were captured at the same exposure, for comparing the degree of the color conversion

(**Figure 4.5**). The printed structure of ref QD composite showed irregular diameters and spreads of the ink droplets, because the ref QD ink exhibited unstable jetting morphology. In addition, according to the PL image, the QDs inside the nozzle were not ejected accurately because the aggregated QDs are blocked the tip of the nozzle, and then the printed structures showed nonhomogeneous color conversion. On the other hand, the treated QD ink was printed on the target substrate without nozzle clogging issue, so uniform color-conversion was observed with uniform jetting profile of the lens-shaped structures. Stable jetting of the QD composites also ensures the higher color-coversion rate compare to the aggregated QD composites.

To compare the optical characteristics of the reference QDs and B3MP-treated QDs, absorbance and PL intensity of the QDs were measured, as shown in Figure and Table. According to the graph of **Fig. 4.6(a)**, the QDs maintained their absorbance property even after B3MP treatment, and that result proves that the treated QDs can also be applied as color-conversion materials on the blue-color light sources. And the photoluminescence graph of **Fig. 4.6(b)** also demonstrates that the light emitted from the QDs maintains its peak wavelength and full width at half maximum (FWHM) after the B3MP-based treatment. In addition, the B3MP-treated QDs mixed with NOA 61 also retained their optical properties, in case of both red and green QDs (**Table 4.1**). Through those results, the composite of the NOA 61/treated QD confirms the applicability to the fabrication of the color-conversion structures.

For investigation of the molecular structure of the QDs after B3MP treatment especially, NMR and FTIR spectra of the both reference QD and B3MP-treated QD were measured. According to the graph of NMR spectra in **Fig. 4.7(a)** proves clearly of the presence of the B3MP. The NMR analysis of the QDs was conducted by

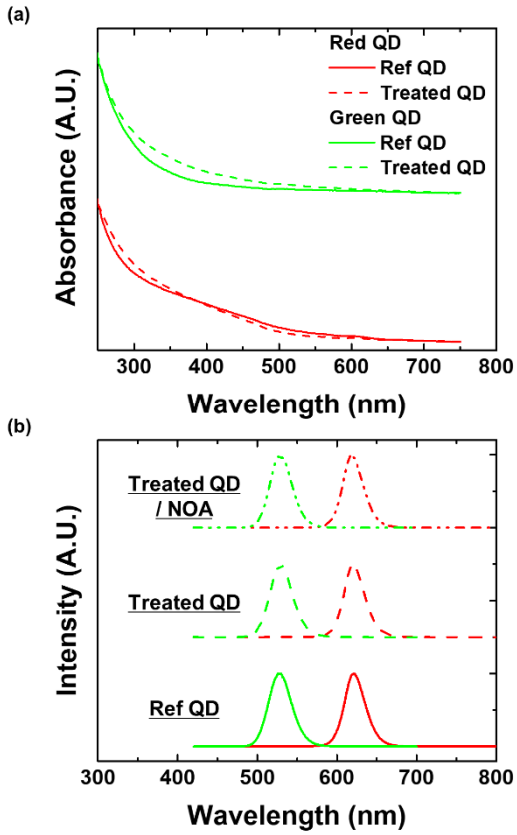

Figure 4.6 (a) absorbance and (b) PL spectrum of the red and green QDs.

		Emission wavelength (nm)	FWHM (nm)
Green QD	Ref QD	526	34
	Treated QD	530	32
	Treated QD/NOA	528	32
Red QD	Ref QD	621	31
	Treated QD	620	30
	Treated QD/NOA	619	30

Table 4.1 Optical properties of the QDs.

solid-state NMR method. The NMR peaks of the B3MPs were also measured in B3MP-treated QDs which was different from the reference QD. The appearance of the B3MP peaks at B3MP-treated QDs confirms the bonding of the B3MP molecules with the QD surfaces as a ligand, and therefore the B3MP treatment helps the QDs to be dispersed easily in the NOA 61. In addition, according to the graph of FT-IR

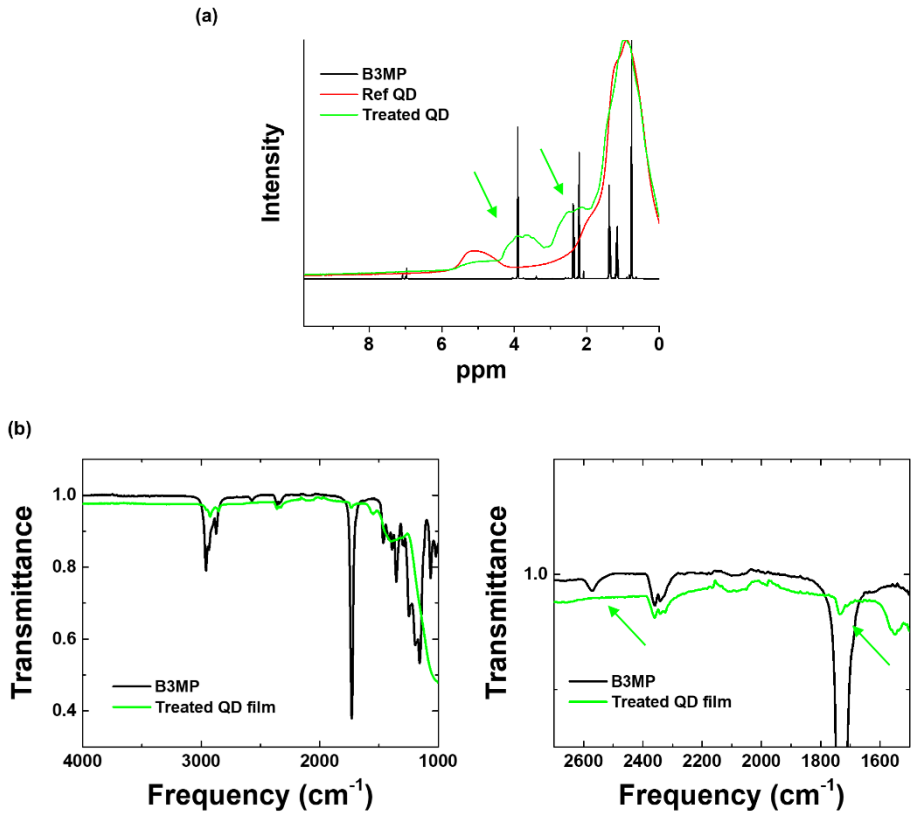

Figure 4.7 (a) 1H-NMR spectrum and (b) FT-IR spectrum of the B3MP, ref QD, and treated QD.

spectrum in **Fig. 4.7(b)**, I focused on the two absorbance peaks of the infrared light. First, the absorbed peak at the frequency of 2570 cm^{-1} was observed in case of the B3MP solvent. However, that peak was suppressed at the measurement of treated QD. The FT-IR peak at frequency around 2570 cm^{-1} shows the existence of the S-H stretching bond, which means that there is a thiol group in the molecular structure [177]. Second, the large absorption peak at frequency of 1730 cm^{-1} was measured in B3MP, and the peak at 1730 cm^{-1} can also be checked in case of B3MP-treated QD. The FT-IR peak at frequency around 1730 cm^{-1} represents C=O bond [179], which can be found in B3MP. Combining the two results according of NMR and FT-IR, it

is demonstrated that the B3MP molecules are bonded at the surface of the QDs after treatment, and the bond between the QD and the B3MP is activated by termination of hydrogen from the sulfur. Several papers report stability change of the QDs after the replacement of the ligands with other molecules [147, 180, 181]. However, the bonding between the QD surface and thiol group (S-H) is strong, and thiol group-based ligands enhance the stability of the QDs. In addition, the QDs with thiol group ligand also exhibited high thermal stability, showing no discoloration [181]. In conclusion, it is expected that the QDs with B3MP ligands also show enhanced stability compared to the OA-capped QDs.

Through the improved dispersion method of QDs in the UV-curable materials, I split the conditions of the QD concentration into 50 mg/ml, 100 mg/ml, 150 mg/ml. **Figure 4.8(a)** shows the rectangular patterns of the NOA 61/QD composites with area of 3 mm x 3 mm which was fabricated by bar-coating for obtaining same thickness and laser-cutting, for comparison of PL intensity according to the QD concentrations. According to Fig. 4.8(b), all conditions of the NOA 61/QD composites can be successfully printed on the target substrates, without a nozzle clogging or QD aggregation in the structures. In addition, the diameter of the color conversion structures can be controlled from 17 μm to 44 μm in case of the red QD composite with concentration of 100 mg/ml, by optimization of height of nozzle, jetting time, and applied voltage (**Figure 4.9(a)**). The green composite can also be printed with a diameter from 21 μm to 41 μm, showed the facile controllability of the size of the color-conversion structures (**Figure 4.9(b)**). According to the various demands, the performance of the color-conversion structures can be adjusted by change the concentration and the size.

For verifying applicability to the large-scale electronics, I printed English

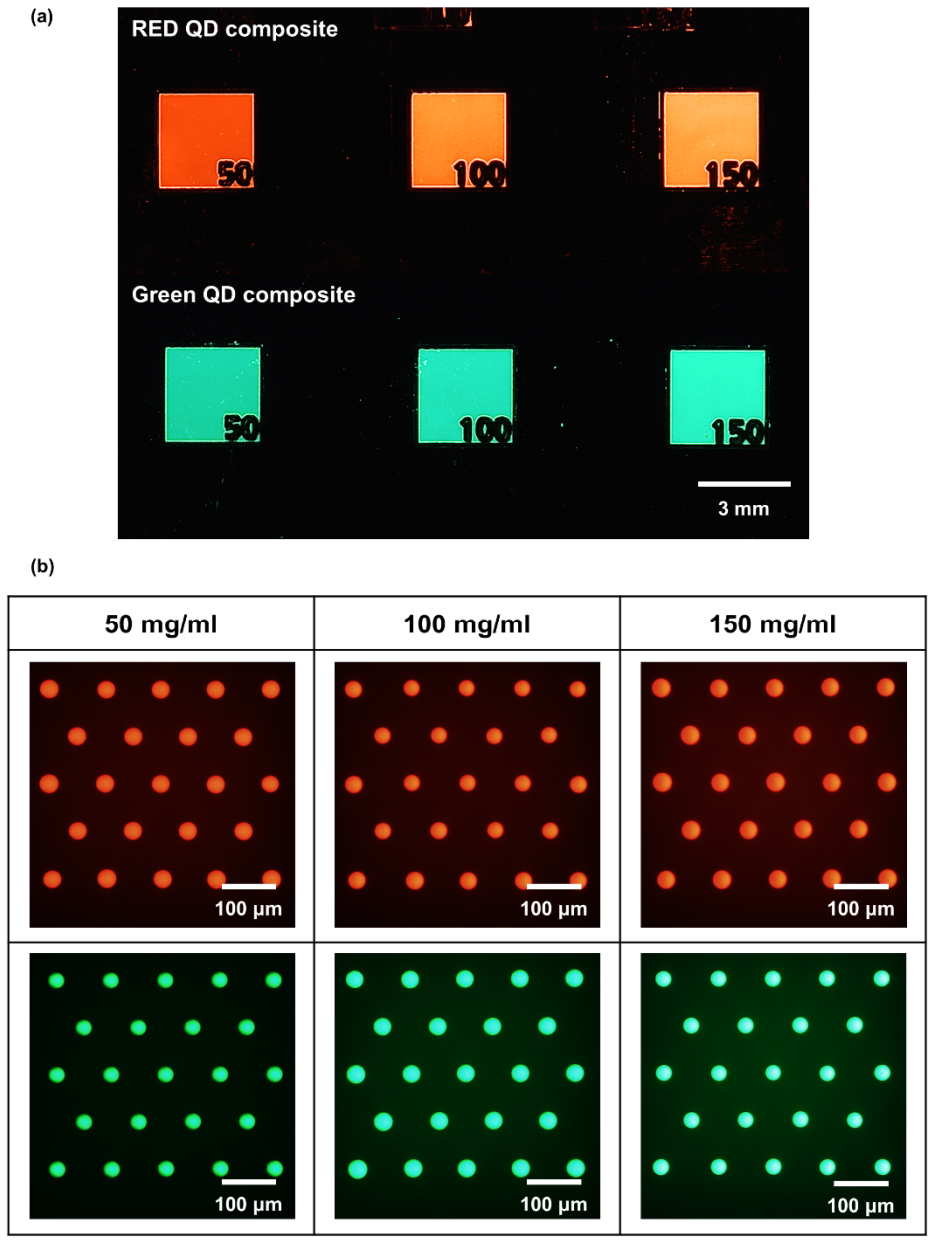

Figure 4.8 (a) PL images of the rectangular patterns of NOA 61/treated QD films, and (b) PL images of the EHD-printed NOA 61/treated QD composites on the glass with different color and concentration.

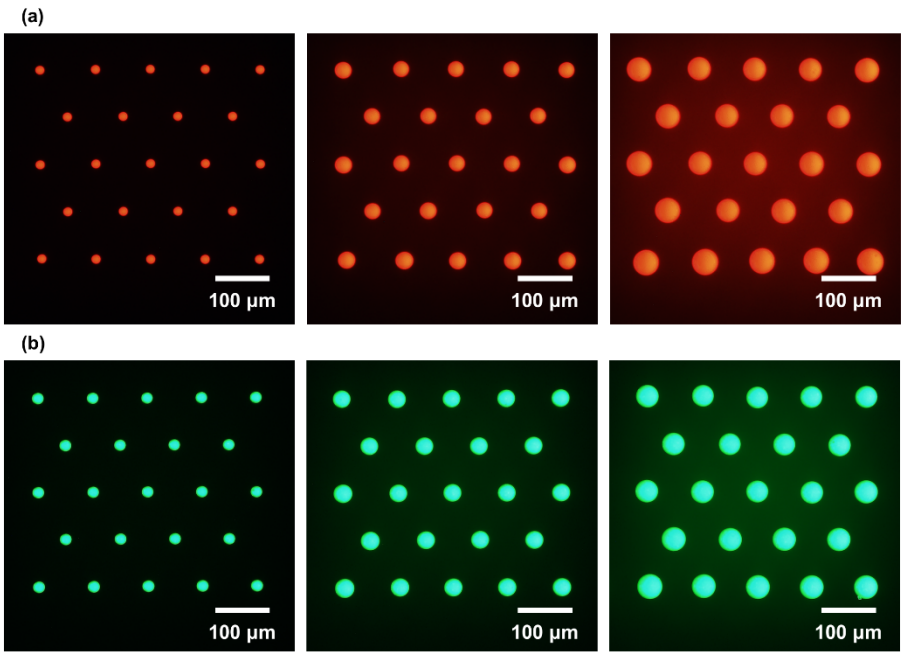

Figure 4.9 PL images of EHD-printed NOA 61/treated QD composite patterns of (a) red and (b) green with different diameters.

characters and traffic light patterns with size of few millimeters, which consist of lens arrays with a pitch of 100 μm. According to the PL image of **Fig. 4.10**, more than 400 red lenses with concentration of 100 mg/ml and 500 green lenses with concentration of 100 mg/ml were printed on a FOTS-treated substrate with stable lens size and uniform light emission. The printed structures with large areas extend their applications to large area full-color displays with microscale optoelectronic devices, and the drop-on-demand EHD printing enables the high degree of freedom of pixel patterning.

The color-conversion performance of the NOA 61/QD composite was evaluated by the deposition of the composite layers on the LED surface. **Figure 4.11** represents

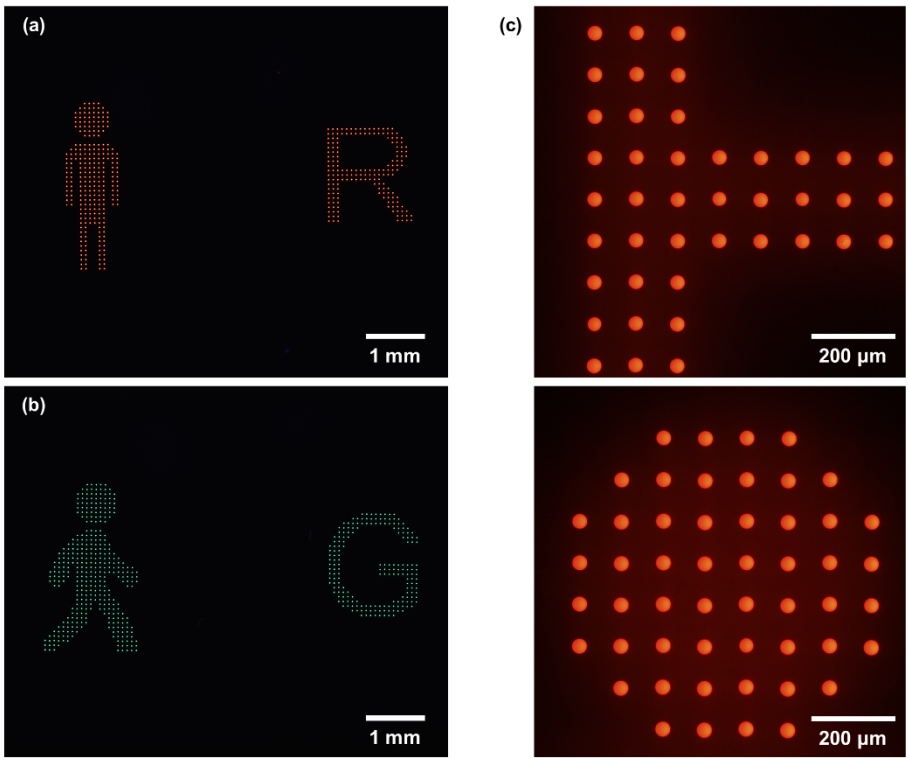

Figure 4.10 PL images of (a) red and (b) green NOA 61/QD color-conversion structures patterned by EHD-printing, and (c) enlarged view of (a).

the intensity of emitted light from the QD-composite-deposited LEDs, according to the wavelength and the concentrations of the QD composite. The graph in **Fig. 4.11(a) and (b)** shows the color-conversion properties of the red-QD composite and green-QD composites, and the results of the **Table 4.2** is the thickness of the NOA 61/QD composite measured by contact-based surface profiler. Despite the thickness of the composite layers were slightly thinner with increasing the QD concentrations, the blue wavelength peak which was not converted by QDs was effectively decreased and the color purity of the converted light was enhanced with the when the QD concentrations were increased, demonstrated with the CIE 1931 chromaticity diagram in **Fig. 4.11(d)**. With those results of emitted-light intensity, I calculated a

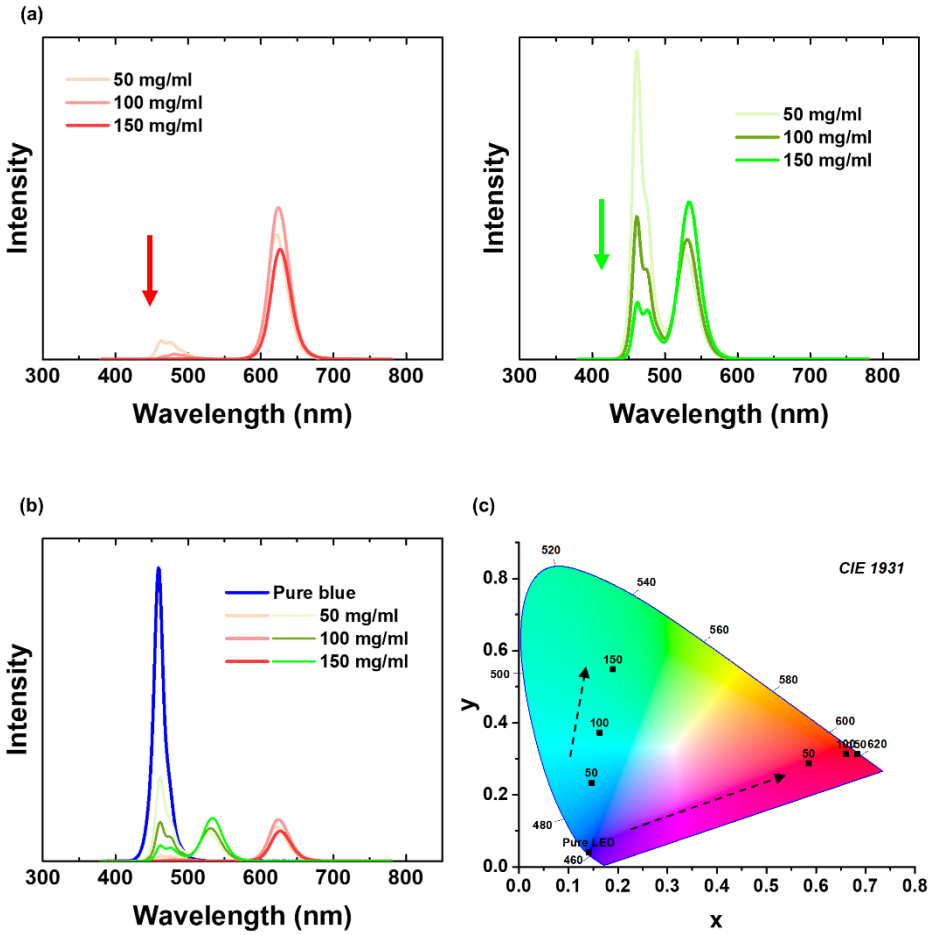

Figure 4.11 PL spectra of LEDs with (a) red and (b) green NOA 61/QD composite layer, (c) comparison with blue LED, and (c) Color gamut of the LEDs with NOA 61/QD composite.

Thickness (μm)	Red	Green
50 mg/ml	201	264
100 mg/ml	161	201
150 mg/ml	132	178

Table 4.2 Thickness of NOA/61 QD composite layers on the LED.

η_{CCE} (%)	Red	Green
50 mg/ml	13.5	15.1
100 mg/ml	15.0	16.0
150 mg/ml	12.6	18.8

Table 4.3 Color-conversion efficiency calculated by **Eq. (4.1)**.

color-conversion efficiency (η_{CCE}) of the QD composite layers (**Figure 4.11(c)**). The η_{CCE} is calculated by the ratio of emitted color-converted power to the absorbed light by QD, and the equation is derived as followed [182, 183]:

$$\eta_{CCE} = \frac{I_{CQD}}{I_B - I_{BQD}} \qquad (\mathbf{4.1})$$

where I_B is the intensity of the emitted blue light by the underlying LED, I_{BQD} is the intensity of the residual blue light which is not converted by the QDs, and I_{CQD} is the intensity of the light converted to desired color. According to **Eq. (4.1)**, the η_{CCE} of ~ 20 % was demonstrated in both case of red and green QD composite, which was exhibited in Table 4.3. Through the graph of the CIE Color System and derived conversion efficiency, I confirm a potential of the B3MP-treated QD composite as a color conversion layers for monochromatic LED devices. In addition, the color purity of the green-converted pixel will be enhanced by adjusting concentration of the QDs, thickening QD layers, and addition of conversion-improved materials, such as light-scattering particles. Furthermore, the color-conversion efficiency should be complemented for higher intensity of converted light, by applying optical structures for increasing outcoupling efficiency, and improving material property such as quantum yield.

For demonstration of the various color-conversion structures for display applications, I implemented three types of printed patterns on diverse surfaces: surface of the micro-LEDs, polyimide (PI), and PDMS. First, I directly printed NOA 61/QD composite on the surface of micro-LEDs with size of 100 μm × 250 μm. For reducing production time of the printed color conversion structures with relatively large area compared to the previously printed lens structure, the nozzle with inner diameter of 60 μm was selected, and the FOTS treatment was conducted for

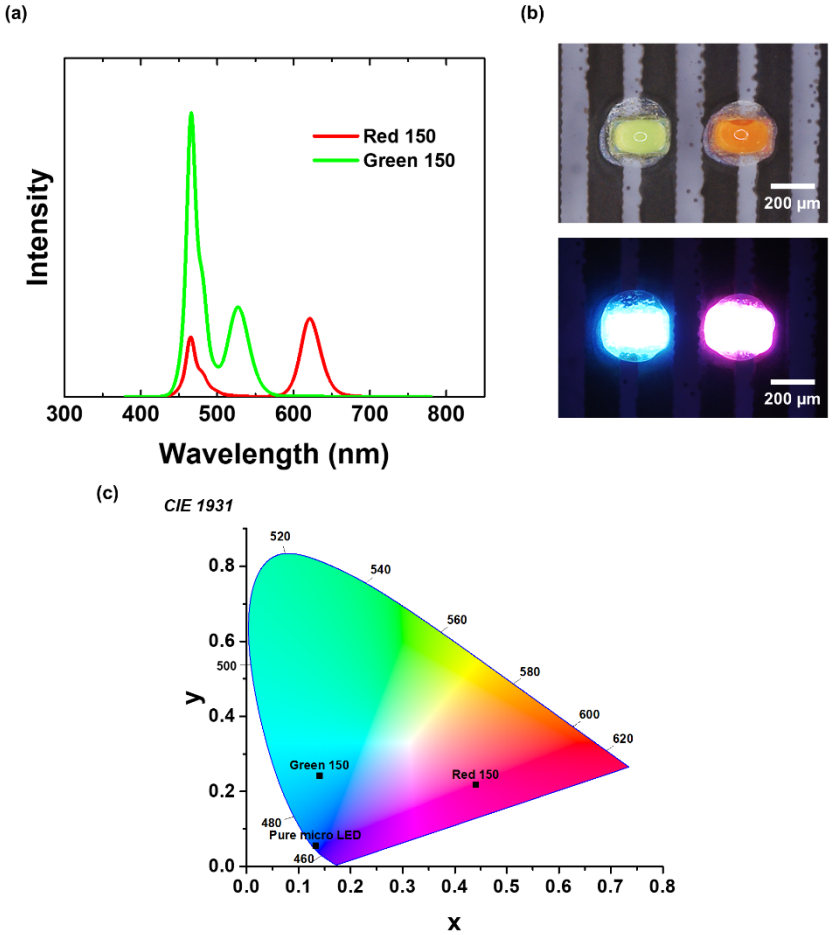

Figure 4.12 (a) PL spectrum of the NOA 61/QD composite-printed micro-LEDs, (b) optical image of off-state (top) and on-state (bottom) of micro-LEDs, and (c) Color gamut of color-converted micro LEDs.

η_{CCE} (%)	Red	Green
150 mg/ml	16.8	29.9

Table 4.4 Color-conversion efficiency of the NOA 61/QD composite-printed micro-LEDs.

Ref	This work (QD layer)	This work (printed QD)	[181]	[182]
η_{CCE} (%)	12.6 (Red) 18.8 (Green)	16.8 (Red) 29.9 (Green)	21	22

Table 4.5 Color-conversion efficiency of QD color filters.

increasing the height of the printed structures. **Figure 4.12** represents optical images of printed QD composites on the micro-LED surfaces and the device performance of the color-converted micro-LEDs. According to **Fig. 4.12(b)**, the QD composites were printed on the micro-LED surfaces without collapse of the composite inks at the LED boundary. In addition, the NOA 61/QD structures showed color-conversion effect during the operation of micro-LEDs (**Figure 4.12(a)**). The remaining peak of the blue wavelength were still observed at converted light, the color shift was demonstrated through the graph of CIE 1931 chromaticity diagram (**Figure 4.12(c)**). The η_{CCE} was also calculated with **Eq. (4.1)** (**Table 4.4**), and the calculated results were similar to the deposited QD layers on the macroscale LED surface as previously mentioned in **Table 4.3**. Through the comparison with calculated η_{CCE} to the previously reported results [183, 184] (**Table 4.5**), the NOA 61/QD composite showed acceptable performance, and optimization process should be needed for enhancement of η_{CCE} such as mixing of scattering materials. Those results show that the QD composite patterns can be used on the micro-LED arrays, After optimization and large-area fabrication.

For fabrication of the color-conversion structures on the light-emitting devices, the fill factor of the structure is a key factor for effective conversion, because the vacancy of the LED surfaces causes the leakage of emitted light and decrease the conversion efficiency. To maximize the fill factor of the NOA 61/QD composite and facile control of the pitch. Prior to the EHD printing of the NOA 61/QD composite ink, the parallel lines with width of under 10 μm was printed on the PI varnish coated glass substrate. The material of the barrier structures is pure NOA 61, and the barrier structures with micrometer scale was printed by EHD printing by a nozzle with inner diameter of 4 μm. After EHD printing of structures composed of parallel lines and

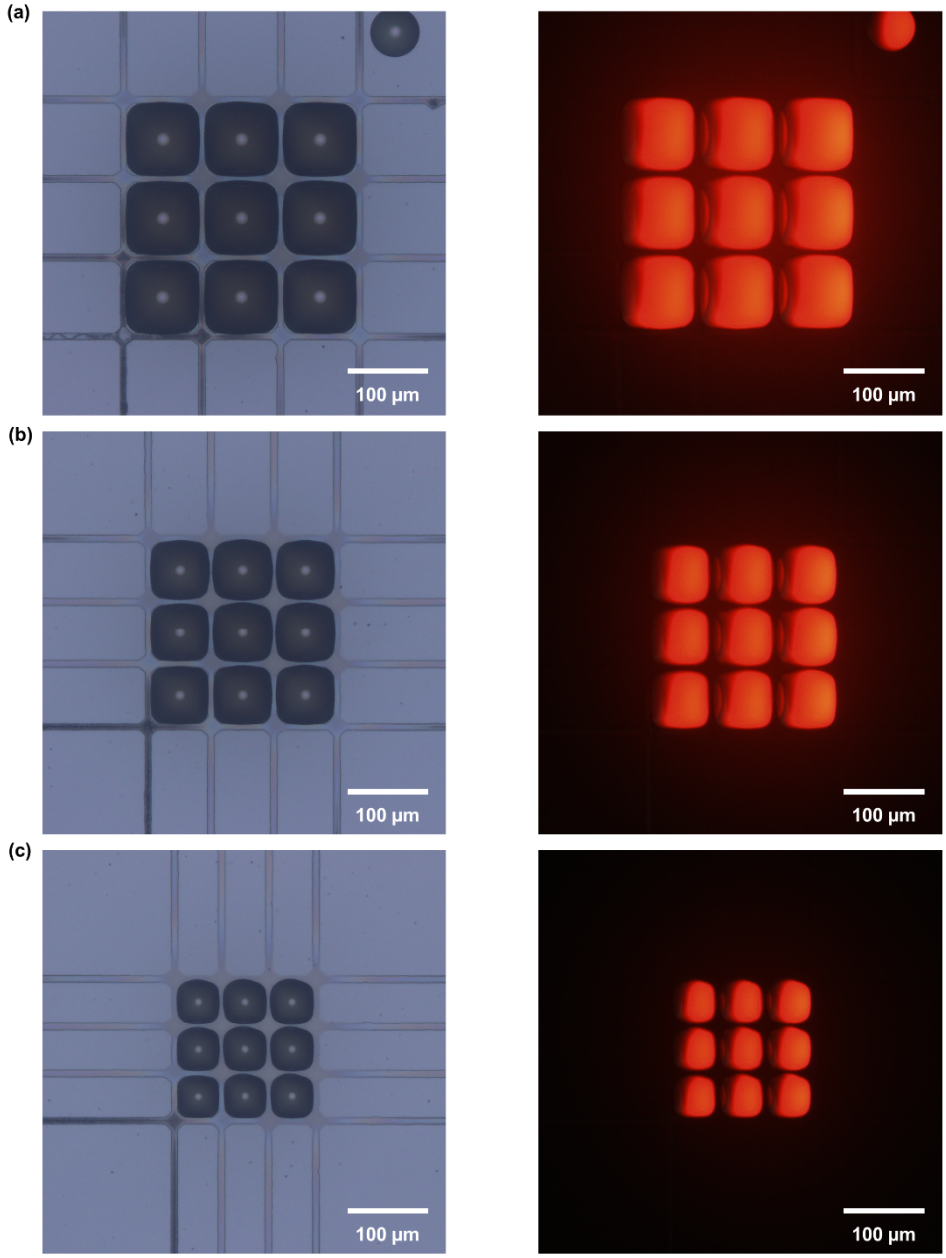

Figure 4.13 Optical (left) and PL (right) images of EHD-printed color-conversion structures defined by barrier lines with pitch of (a) 100 μm, (b) 80 μm, and (c) 60 μm.

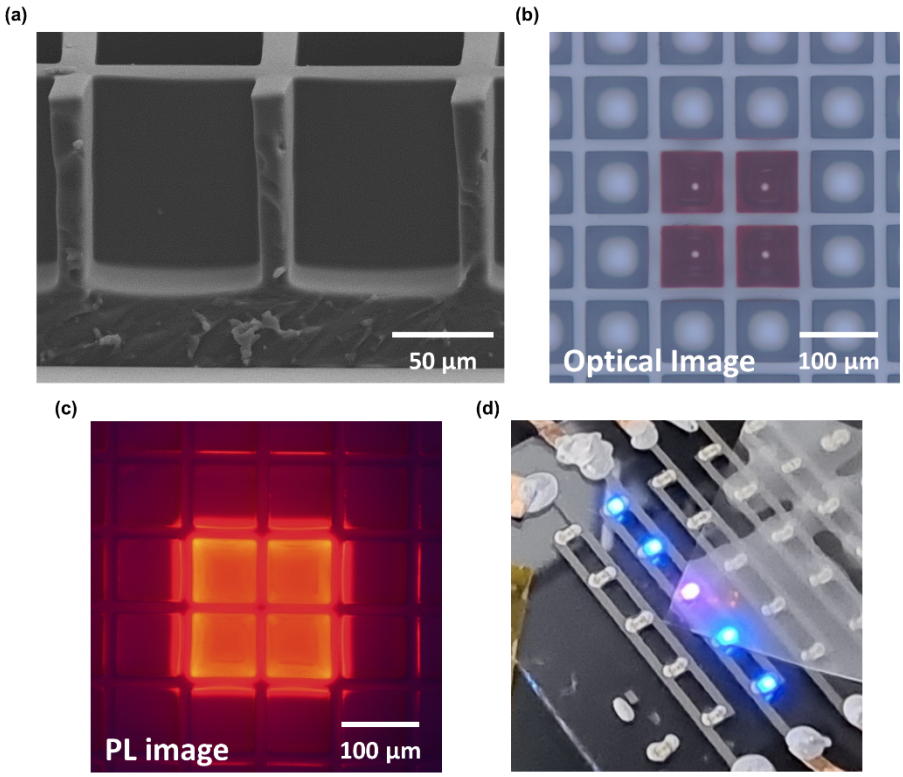

Figure 4.14 (a) SEM image of PDMS barriers fabricated by Si mold, (b)optical and (c) PL image of EHD-printed color conversion structure on PDMS substrate, (d) operation of LEDs with PDMS color-conversion sheet.

subsequent surface treatment, the QD composite ink was successfully printed on the vacancy surrounded by the printed lines. The previously printed NOA 61 lines prevent the spread of the printed QD composite ink, thus the printed barriers precisely define the size and the pitch of the printed color-conversion structure (**Figure 4.13**). The size of the NOA 61/QD structure was optimized down to 60 µm, and the pitch of the adjacent structure was 8 µm with minimized vacancy. Through the design of the EHD-printed barrier lines, the pitch and the size of the QD composite structures can be easily controlled with optimized fill factor. In addition,

after peel-off process of PI vanish from the glass, the printed structures can be attached to another surface which have light-emitting devices. The full-color displays with 211 pixels per inch (PPI) can be achieved by introducing barrier patterns with a pitch of 60 μm.

Printing process of the NOA 61/QD composites on the pre-defined structures can also be conducted on the stretchable substrates. For fabrication of the barriers on the PDMS elastomer, deep-etched Si is used as a mold structure for PDMS. After the etching process of the hole arrays with certain size and depth on the Si substrate, the PDMS was poured on the Si mold. When the cured PDMS was peeled off from the Si, the pillar structures which has the same size with the hole at Si were engraved on the surface of the PDMS. The uncured PDMS was spin-coated on the PDMS pillar structure for molding the pattern of pillar. Following the curing and detachment process, the PDMS hole arrays which have same area and depth with Si mold was achieved (**Figure 4.14(a)**). I fabricate the PDMS hole arrays with depth of 100 μm for efficient amounts of QDs, and the width of barrier is 20 μm and the pitch between adjacent holes is 100 μm. The NOA 61/QD composite was EHD-printed on the PDMS hole with desired location, and the color-conversion structures were demonstrated by filling the composite ink on the hole, according to **Fig.4.14(b)**. PL image confirms the color-conversion property of the printed composite on the PDMS hole, and the fabricated color-conversion PDMS sheet was firmly laminated with the LED arrays **(Fig.4.14(c) an (d)**). Because of the high transparency of the PDMS, the sheet-attached LED exhibited showed great color-conversion effect, and the QD-composite-printed PDMS sheet with designed patterns can be attached to the arbitrary surface, such as curved or wavy structures.

4.3. Conclusion

In summary, I suggested high-resolution patterning of the color-conversion structures by the EHD printing of the composite of photocurable polymer and QDs. For achieving both high concentrations of QDs and uniform mixture of QD and polymer without the aggregation, B3MP was selected for the ligand exchange of QDs. After bonding of B3MP molecules and QD surface, the QDs were uniformly mixed with NOA 61 polymer with high concentration up to 150 mg/ml, and the NOA 61/QD composite was stably ejected from the EHD nozzle tips without the nozzle clogging. Through the hydrophobic surface treatment on the target substrate, the EHD-printed NOA 61/QD composites formed a lens-shaped structure with diameter of tens of micrometers, and the uniform PL image was obtained under the UV exposure.The large area patterns of composites composed of lens-shaped structure arrays with pitch of 100 μm was obtained with steady printing. The color-conversion property of QDs were tested with measuring the PL intensity, and the optimized NOA 61/QD composite inks demonstrated a potential for commercialization as a color-conversion structures of monochromatic displays. Furthermore, the facile printability of the QD composites on the desired location and arbitrary surfaces by the EHD-printing device expands its application targets to flexible and stretchable electronics.

Chapter 5 Conclusion

5.1. Summary

In this dissertation, I suggest a solution-based maskless patterning process of various optoelectronic elements. The inkjet-printing of the conductive polymer and the EHD-printing of the conductive polymer and photocurable polymer enables the facile fabrication of the TEs, conductive electrodes, and color-conversion structures with micrometer scale. Furthermore, I demonstrate the deposition procedures of the ink materials on substrates with low thermal stability, such as plastic or elastomeric substrates. In other words, my patterning techniques listed in this dissertation can be applied to the manufacturing process of next-generation display products.

First, I explained the patterning method of the AgNW TEs by combining the inkjet printing of adhesive polymer patterns on the target substrate and the transfer process of the AgNWs from the flat PDMS stamp to the surface of the polymer patterns. Through the blending process of the adhesive materials and PEDOT:PSS conductive polymer, the printed PEDOT:PSS templates achieve improved lamination of the AgNWs on the template surface and enhanced uniformity of the bilayer electrode structures. The AgNW patterns conducted by the selective transfer technique can be deposited on diverse substrates without degradation of the electrode properties. Moreover, the patterned AgNW TEs on the plastic substrate showed superior flexibility, and the various flexible display applications with the patterned

AgNWs were demonstrated for the advanced current level.

Second, the drawbacks of the AgNW patterning based on the selective transfer, such as a narrow process window on the PDMS substrate and the damage by the external lamination force, were complimented. Prior to the spray-coating of AgNW, the PVA adhesive layer was coated on the target substrate. When the PEDOT:PSS was printed on the AgNW-coated PVA surface, the permeation of the PEDOT:PSS into the voids of AgNW networks and the formation of interpenetration network with PVA molecules enhanced the adhesion of PEDOT:PSS and protect the AgNWs which is placed under the printed PEDOT:PSS. The AgNWs were precisely patterned according to the printed patterns of the PEDOT:PSS, after the facile removing process of residual AgNWs. Therefore, I can implement PVA-assisted patterning techniques onto various substrates, including a pre-stretched elastomeric platform. In addition, the PEDOT:PSS ink was also printed by EHD printing to improve the resolution of the AgNW patterns. The width of the patterns was further reduced to 15 μm without damage or disconnection of the current. Through those advantages, the PVA-assisted patterning technique can be applied to various stretchable applications with high resolution.

Third, I focused on the facile patterning concept of the color-conversion structures for high-resolution display panels. To improve the uniformity of the QD color-conversion layer, I dispersed QDs into the photocurable polymer, which has high viscosity. In addition, ligand exchange of the QDs was optimized for improving the dispersion of QD. The optimized QD and NOA 61 polymer composite showed uniform PL without the aggregation of the QDs. Therefore, the composite inks can be deposited through the EHD nozzle with a diameter of 30 μm. By EHD printing the high viscosity QD composite, a single color-conversion structure can be

patterned with a minimum feature size of 20 μm, and the various QD composite patterns composed of structure arrays were demonstrated with a high degree of freedom.

5.2. Limitations and Suggestions for Future Researches

In this session, the limitations of my studies and suggestions for future research will be discussed. My suggestion is focused on the PVA-assisted patterning of the AgNWs and EHD printing of the QD composite.

(1) Fabrication of AgNWs by PVA-assisted patterning: The PVA-assisted patterning process of the AgNWs was proposed as an alternative in the case of the patterning of AgNWs with micrometer-scale. Although the AgNWs can be patterned onto the pre-stretched PDMS substrate, all of the substrates during the patterning process should be flat. However, the demand for electrode deposition on the curved surface with arbitrary curvature also has grown for microscale electronics, such as 3D waveguides, 3D-antenna, and smart contact lenses [185-187] (**Figure 5.1(a) and (b)**). By introducing direct patterning of the electrodes on the curved surface, the damage to the electronic circuits during the detachment, a drawback of the conventional lamination method, can be prevented [188]. Various studies have been reported about the EHD printing of inks on the curved surface because stable printing can be achieved by control of the electric field according to the height and angle of the nozzle [189, 190]. After coating the PVA adhesive layer and AgNWs sequentially, optimizing the EHD-printing condition of PEDOT:PSS ink should be studied. Furthermore, the simulation of the jetting of the EHD-printed ink on the uneven surface needs to be preceded for uniformity of the printed line (**Figure 5.1(c)**).

(2) EHD printing of polymer/QD composite: Although the color-conversion microstructure patterns with uniform light-conversion were demonstrated by the EHD printing of UV-curable polymer/QD composite, the color-conversion

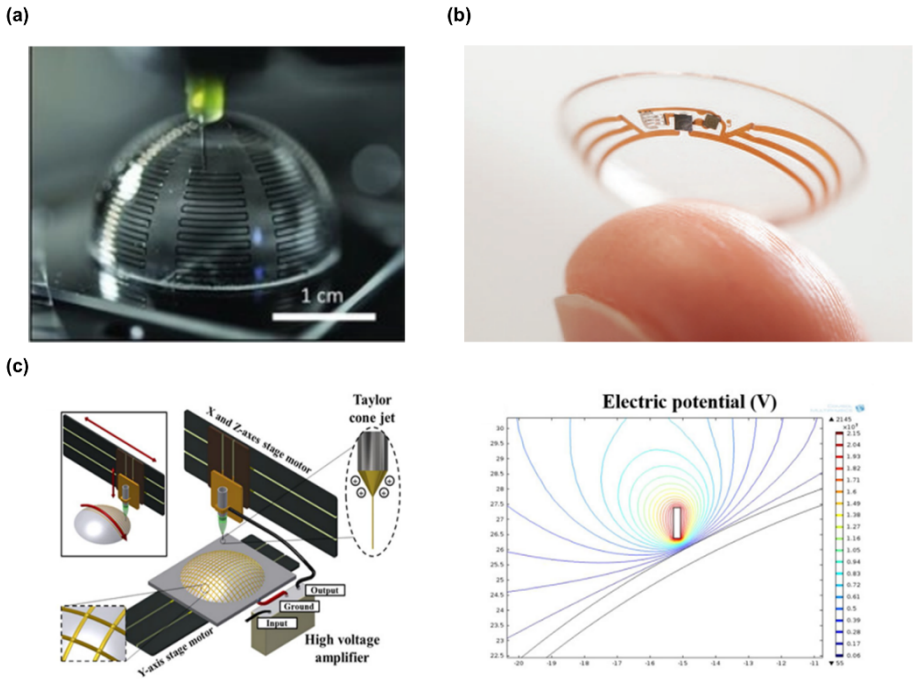

Figure 5.1 (a) Printing of the 3D antenna on convex surface, (b) smart lens, and (c) Simulation results of the EHD-printing on curved surface [186, 187, 189].

efficiency of the should be enhanced for commercialization. In addition to the quantum yield of the QDs through the material synthesis [191], a dispersion of the scattering materials with a high refractive index into polymer/QD composite is another crucial factor for improving the color purity [192-194]. For applying the composite ink to EHD printing, optimizing the uniform dispersion process will be challenging.

Reference

[1] Ohshima H 2014 Mobile display technologies: Past developments, present technologies, and future opportunities *Jpn. J. Appl. Phys.* **53** 03CA1

[2] Koo J H, Kim D C, Shim H J, Kim T H and Kim D H 2018 Flexible and stretchable smart display: materials, fabrication, device design, and system integration *Adv. Funct. Mater.* **28** 1801834

[3] Kwon S, Hwang Y H, Nam M, Chae H, Lee H S, Jeon Y, Lee S, Kim C Y, Choi S and Jeong E G 2020 Recent progress of fiber shaped lighting devices for smart display applications—a fibertronic perspective *Adv. Mater.* **32** 1903488

[4] Lee Y, Chung J W, Lee G H, Kang H, Kim J-Y, Bae C, Yoo H, Jeong S, Cho H and Kang S-G 2021 Standalone real-time health monitoring patch based on a stretchable organic optoelectronic system *Sci. Adv.* **7** eabg9180

[5] Yokota T, Zalar P, Kaltenbrunner M, Jinno H, Matsuhisa N, Kitanosako H, Tachibana Y, Yukita W, Koizumi M and Someya T 2016 Ultraflexible organic photonic skin *Sci. Adv.* **2** e1501856

[6] Ha M, Lim S and Ko H 2018 Wearable and flexible sensors for user-interactive health-monitoring devices *J. Mater. Chem. B* **6** 4043-64

[7] Kim H, Pique A, Horwitz J, Mattoussi H, Murata H, Kafafi Z and Chrisey D 1999 Indium tin oxide thin films for organic light-emitting devices *Appl. Phys. Lett.* **74** 3444-6

[8] Sierros K A, Morris N J, Ramji K and Cairns D R 2009 Stress–corrosion cracking of indium tin oxide coated polyethylene terephthalate for flexible optoelectronic devices *Thin Solid Films* **517** 2590-5

[9] Camino G, Lomakin S and Lazzari M 2001 Polydimethylsiloxane thermal degradation Part 1. Kinetic aspects *Polymer* **42** 2395-402

[10] Spechler J A, Koh T W, Herb J T, Rand B P and Arnold C B 2015 A transparent, smooth, thermally robust, conductive polyimide for flexible electronics *Adv. Funct. Mater.* **25** 7428-34

[11] Abbel R, Galagan Y and Groen P 2018 Roll-to-Roll Fabrication of Solution Processed Electronics *Adv. Eng. Mater.* **20** 1701190

[12] Lee P, Lee J, Lee H, Yeo J, Hong S, Nam K H, Lee D, Lee S S and Ko S H 2012 Highly stretchable and highly conductive metal electrode by very long metal nanowire percolation network *Adv. Mater.* **24** 3326-32

[13] Park J W, Kang B H and Kim H J 2020 A review of low-temperature solution-processed metal oxide thin-film transistors for flexible electronics *Adv. Funct. Mater.* **30** 1904632

[14] Hwang K, Jung Y S, Heo Y J, Scholes F H, Watkins S E, Subbiah J, Jones D J, Kim D Y and Vak D 2015 Toward large scale roll-to-roll production of fully printed perovskite solar cells *Adv. Mater.* **27** 1241-7

[15] Wang D, Hauptmann J, May C, Hofstetter Y J, Vaynzof Y and Müller T 2021 Roll-to-roll fabrication of highly transparent Ca: Ag top-electrode towards flexible large-area OLED lighting application *Flex. Print. Electron.* **6** 035001

[16] Cao X, Ye Y, Tang Q, Chen E, Jiang Z, Pan J and Guo T 2020 Numerical analysis of droplets from multinozzle inkjet printing *J. Phys. Chem. Lett.* **11** 8442-50

[17] Majee S, Karlsson M C, Wojcik P J, Sawatdee A, Mulla M Y, Dyreklev P, Beni V and Nilsson D 2021 Low temperature chemical sintering of inkjet-

printed Zn nanoparticles for highly conductive flexible electronic components *npj Flex. Electron.* **5** 1-8

[18] Rim Y S, Chen H, Liu Y, Bae S-H, Kim H J and Yang Y 2014 Direct light pattern integration of low-temperature solution-processed all-oxide flexible electronics *ACS Nano* **8** 9680-6

[19] Feng C, Zheng X, Xu R, Zhou Y, Hu H, Guo T, Ding J, Ying L and Li F 2020 Highly efficient inkjet printed flexible organic light-emitting diodes with hybrid hole injection layer *Org. Electron.* **85** 105822

[20] Chung S, Cho K and Lee T 2019 Recent progress in inkjet-printed thin-film transistors *Adv. Sci.* **6** 1801445

[21] Park S-E, Kim S, Lee D-Y, Kim E and Hwang J 2013 Fabrication of silver nanowire transparent electrodes using electrohydrodynamic spray deposition for flexible organic solar cells *J. Mater. Chem. A* **1** 14286-93

[22] Jang J and Hong Y 2020 Effects of lithium doping and ultraviolet photo-patterning on electrical properties of InGaZnO thin film transistors *Thin Solid Films* **707** 138098

[23] Byun J, Oh E, Lee B, Kim S, Lee S and Hong Y 2017 A Single Droplet-Printed Double-Side Universal Soft Electronic Platform for Highly Integrated Stretchable Hybrid Electronics *Adv. Funct. Mater.* **27** 1701912

[24] Han T-H, Choi M-R, Jeon C-W, Kim Y-H, Kwon S-K and Lee T-W 2016 Ultrahigh-efficiency solution-processed simplified small-molecule organic light-emitting diodes using universal host materials *Sci. Adv.* **2** e1601428

[25] Ha J, Chung S, Pei M, Cho K, Yang H and Hong Y 2017 One-step interface engineering for all-inkjet-printed, all-organic components in transparent, flexible transistors and inverters: polymer binding *ACS Appl. Mater.*

Interfaces **9** 8819-29

[26] Nayyar A, Mahapatra B, Le D and Suseendran G 2018 Virtual Reality (VR) & Augmented Reality (AR) technologies for tourism and hospitality industry *Int. J. Eng. Technol.* **7** 156-60

[27] Dunn D, Tippets C, Torell K, Kellnhofer P, Akşit K, Didyk P, Myszkowski K, Luebke D and Fuchs H 2017 Wide field of view varifocal near-eye display using see-through deformable membrane mirrors *IEEE Trans. Vis. Comput. Graph.* **23** 1322-31

[28] Hwangbo S, Hu L, Hoang A T, Choi J Y and Ahn J-H 2022 Wafer-scale monolithic integration of full-colour micro-LED display using MoS_2 transistor *Nat. Nanotechnol.* **17** 500-6

[29] Wang S, Xu J, Wang W, Wang G-J N, Rastak R, Molina-Lopez F, Chung J W, Niu S, Feig V R and Lopez J 2018 Skin electronics from scalable fabrication of an intrinsically stretchable transistor array *Nature* **555** 83-8

[30] Meng W, Xu F, Yu Z, Tao T, Shao L, Liu L, Li T, Wen K, Wang J and He L 2021 Three-dimensional monolithic micro-LED display driven by atomically thin transistor matrix *Nat. Nanotechnol.* **16** 1231-6

[31] Lee K-H, Lee S-S, Ahn D B, Lee J, Byun D and Lee S-Y 2020 Ultrahigh areal number density solid-state on-chip microsupercapacitors via electrohydrodynamic jet printing *Sci. Adv.* **6** eaaz1692

[32] Kang K, Yang D, Park J, Kim S, Cho I, Yang H-H, Cho M, Mousavi S, Choi K H and Park I 2017 Micropatterning of metal oxide nanofibers by electrohydrodynamic (EHD) printing towards highly integrated and multiplexed gas sensor applications *Sens. Actuators B: Chem.* **250** 574-83

[33] Han Y and Dong J 2018 Electrohydrodynamic (EHD) printing of molten

metal ink for flexible and stretchable conductor with self-healing capability *Adv. Mater. Technol.* **3** 1700268

[34] Park J-U, Hardy M, Kang S J, Barton K, Adair K, Lee C Y, Strano M S, Alleyne A G, Georgiadis J G, Ferreira P M and Rogers J A 2007 High-resolution electrohydrodynamic jet printing *Nat. Mater.* **6** 782-9

[35] Lee A, Jin H, Dang H-W, Choi K-H and Ahn K H 2013 Optimization of experimental parameters to determine the jetting regimes in electrohydrodynamic printing *Langmuir* **29** 13630-9

[36] Pan Y and Zeng L 2019 Simulation and validation of droplet generation process for revealing three design constraints in electrohydrodynamic jet printing *Micromachines* **10** 94

[37] Cui Z, Han Y, Huang Q, Dong J and Zhu Y 2018 Electrohydrodynamic printing of silver nanowires for flexible and stretchable electronics *Nanoscale* **10** 6806-11

[38] Pikul J H, Graf P, Mishra S, Barton K, Kim Y-K, Rogers J A, Alleyne A, Ferreira P M and King W P 2011 High precision electrohydrodynamic printing of polymer onto microcantilever sensors *IEEE Sens. J.* **11** 2246-53

[39] Kim B H, Onses M S, Lim J B, Nam S, Oh N, Kim H, Yu K J, Lee J W, Kim J-H and Kang S-K 2015 High-resolution patterns of quantum dots formed by electrohydrodynamic jet printing for light-emitting diodes *Nano Lett.* **15** 969-73

[40] Zhu M, Duan Y, Liu N, Li H, Li J, Du P, Tan Z, Niu G, Gao L and Huang Y 2019 Electrohydrodynamically printed high-resolution full-color hybrid perovskites *Adv. Funct. Mater.* **29** 1903294

[41] Sugimoto A, Ochi H, Fujimura S, Yoshida A, Miyadera T and Tsuchida M

2004 Flexible OLED displays using plastic substrates *IEEE J. Sel. Top. Quantum Electron.* **10** 107-14

[42] Kim S, Kwon H J, Lee S, Shim H, Chun Y, Choi W, Kwack J, Han D, Song M and Kim S 2011 Low-power flexible organic light-emitting diode display device *Adv. Mater.* **23** 3511-6

[43] Trung T Q and Lee N E 2016 Flexible and stretchable physical sensor integrated platforms for wearable human-activity monitoringand personal healthcare *Adv. Mater.* **28** 4338-72

[44] Lee S, Yeo J-S, Ji Y, Cho C, Kim D-Y, Na S-I, Lee B H and Lee T 2012 Flexible organic solar cells composed of P3HT: PCBM using chemically doped graphene electrodes *Nanotechnology* **23** 344013

[45] Da Silva W J, Kim H P, bin Mohd Yusoff A R and Jang J 2013 Transparent flexible organic solar cells with 6.87% efficiency manufactured by an all-solution process *Nanoscale* **5** 9324-9

[46] Jin D U, Lee J S, Kim T W, An S G, Straykhilev D, Pyo Y S, Kim H S, Lee D B, Mo Y G and Kim H D 2009 65.2: Distinguished Paper: World-Largest (6.5”) Flexible Full Color Top Emission AMOLED Display on Plastic Film and Its Bending Properties *SID Symp.Dig. Tech. Pap.* **40** 983-5

[47] Chung S, Jang M, Ji S B, Im H, Seong N, Ha J, Kwon S K, Kim Y H, Yang H and Hong Y 2013 Flexible High-Performance All-Inkjet-Printed Inverters: Organo-Compatible and Stable Interface Engineering *Adv. Mater.* **25** 4773-7

[48] Wang J, Liang M, Fang Y, Qiu T, Zhang J and Zhi L 2012 Rod-coating: towards large-area fabrication of uniform reduced graphene oxide films for flexible touch screens *Adv. Mater.* **24** 2874-8

[49] Lee J, Lee P, Lee H, Lee D, Lee S S and Ko S H 2012 Very long Ag nanowire synthesis and its application in a highly transparent, conductive and flexible metal electrode touch panel *Nanoscale* **4** 6408-14

[50] Lee J, Lee P, Lee H B, Hong S, Lee I, Yeo J, Lee S S, Kim T S, Lee D and Ko S H 2013 Room-temperature nanosoldering of a very long metal nanowire network by conducting-polymer-assisted joining for a flexible touch-panel application *Adv. Funct. Mater.* **23** 4171-6

[51] Pang C, Lee C and Suh K Y 2013 Recent advances in flexible sensors for wearable and implantable devices *J. Appl. Polym. Sci.* **130** 1429-41

[52] Na S I, Kim S S, Jo J and Kim D Y 2008 Efficient and flexible ITO-free organic solar cells using highly conductive polymer anodes *Adv. Mater.* **20** 4061-7

[53] Ha J, Park J, Ha J, Kim D, Chung S, Lee C and Hong Y 2015 Selectively modulated inkjet printing of highly conductive and transparent foldable polymer electrodes for flexible polymer light-emitting diode applications *Org. Electron.* **19** 147-56

[54] Feng C, Liu K, Wu J S, Liu L, Cheng J S, Zhang Y, Sun Y, Li Q, Fan S and Jiang K 2010 Flexible, stretchable, transparent conducting films made from superaligned carbon nanotubes *Adv. Funct. Mater.* **20** 885-91

[55] Kim S M, Jo Y W, Kim K K, Duong D L, Shin H-J, Han J H, Choi J-Y, Kong J and Lee Y H 2010 Transparent organic P-Dopant in carbon nanotubes: Bis (trifluoromethanesulfonyl) imide *ACS Nano* **4** 6998-7004

[56] Bae S, Kim H, Lee Y, Xu X, Park J-S, Zheng Y, Balakrishnan J, Lei T, Ri Kim H and Song Y I 2010 Roll-to-roll production of 30-inch graphene films for transparent electrodes *Nat. Nanotechnol.* **5** 574-8

[57] Kim Y C, Lee S J, Jung H, Park B-E, Kim H, Lee W and Myoung J-M 2015 Optimization and device application potential of oxide–metal–oxide transparent electrode structure *RSC Adv.* **5** 65094-9

[58] Wu H, Kong D, Ruan Z, Hsu P-C, Wang S, Yu Z, Carney T J, Hu L, Fan S and Cui Y 2013 A transparent electrode based on a metal nanotrough network *Nat. Nanotechnol.* **8** 421-5

[59] Madaria A R, Kumar A, Ishikawa F N and Zhou C 2010 Uniform, highly conductive, and patterned transparent films of a percolating silver nanowire network on rigid and flexible substrates using a dry transfer technique *Nano Res.* **3** 564-73

[60] Kim S, Kim S Y, Kim J and Kim J H 2014 Highly reliable AgNW/PEDOT: PSS hybrid films: efficient methods for enhancing transparency and lowering resistance and haziness *J. Mater. Chem. C* **2** 5636-43

[61] Lee S J, Kim Y-H, Kim J K, Baik H, Park J H, Lee J, Nam J, Park J H, Lee T-W and Yi G-R 2014 A roll-to-roll welding process for planarized silver nanowire electrodes *Nanoscale* **6** 11828-34

[62] Vosgueritchian M, Lipomi D J and Bao Z 2012 Highly conductive and transparent PEDOT: PSS films with a fluorosurfactant for stretchable and flexible transparent electrodes *Adv. Funct. Mater.* **22** 421-8

[63] Langley D, Lagrange M, Giusti G, Jiménez C, Bréchet Y, Nguyen N D and Bellet D 2014 Metallic nanowire networks: effects of thermal annealing on electrical resistance *Nanoscale* **6** 13535-43

[64] Jiu J, Araki T, Wang J, Nogi M, Sugahara T, Nagao S, Koga H, Suganuma K, Nakazawa E and Hara M 2014 Facile synthesis of very-long silver nanowires for transparent electrodes *J. Mater. Chem. A* **2** 6326-30

[65] Lee J, Lee I, Kim T S and Lee J Y 2013 Efficient welding of silver nanowire networks without post-processing *Small* **9** 2887-94

[66] Kang S, Kim T, Cho S, Lee Y, Choe A, Walker B, Ko S-J, Kim J Y and Ko H 2015 Capillary printing of highly aligned silver nanowire transparent electrodes for high-performance optoelectronic devices *Nano Lett.* **15** 7933-42

[67] Jin Y, Li L, Cheng Y, Kong L, Pei Q and Xiao F 2015 Cohesively enhanced conductivity and adhesion of flexible silver nanowire networks by biocompatible polymer sol–gel transition *Adv. Funct. Mater.* **25** 1581-7

[68] Zhu G-J, Ren P-G, Guo H, Jin Y-L, Yan D-X and Li Z-M 2019 Highly sensitive and stretchable polyurethane fiber strain sensors with embedded silver nanowires *ACS Appl. Mater. Interfaces* **11** 23649-58

[69] Duan Y-H, Duan Y, Wang X, Yang D, Yang Y-Q, Chen P, Sun F-B, Xue K-W and Zhao Y 2015 Highly flexible peeled-off silver nanowire transparent anode using in organic light-emitting devices *Appl. Surf. Sci.* **351** 445-50

[70] Ye T, Jun L, Kun L, Hu W, Ping C, Ya-Hui D, Zheng C, Yun-Fei L, Hao-Ran W and Yu D 2017 Inkjet-printed Ag grid combined with Ag nanowires to form a transparent hybrid electrode for organic electronics *Org. Electron.* **41** 179-85

[71] Liu Y-s, Feng J, Ou X-L, Cui H-f, Xu M and Sun H-B 2016 Ultrasmooth, highly conductive and transparent PEDOT: PSS/silver nanowire composite electrode for flexible organic light-emitting devices *Org. Electron.* **31** 247-52

[72] Kim D, Ko Y, Kwon G, Kim U-J and You J 2018 Micropatterning silver nanowire networks on cellulose nanopaper for transparent paper electronics

ACS Appl. Mater. Interfaces **10** 38517-25

[73] Shin K, Park J S, Han J H, Choi Y, Chung D S and Kim S H 2017 Patterned transparent electrode with a continuous distribution of silver nanowires produced by an etching-free patterning method *Sci. Rep.* **7** 1-10

[74] Kim S, Kim B, Cho S M, Lee H-J and Hwang B 2017 Etchant-free patterning of silver nanowire transparent electrode using dry-film photoresists for organic light-emitting diodes *Mater. Lett.* **209** 433-6

[75] Kim Y U, Kwon N Y, Park S H, Kim C W, Chau H D, Hoang M H, Cho M J and Choi D H 2021 Patterned sandwich-type silver nanowire-based flexible electrode by photolithography *ACS Appl. Mater. Interfaces* **13** 61463-72

[76] Liu S, Ho S and So F 2016 Novel patterning method for silver nanowire electrodes for thermal-evaporated organic light emitting diodes *ACS Appl. Mater. Interfaces* **8** 9268-74

[77] Liu G-S, Liu C, Chen H-J, Cao W, Qiu J-S, Shieh H-P D and Yang B-R 2016 Electrically robust silver nanowire patterns transferrable onto various substrates *Nanoscale* **8** 5507-15

[78] Jung S Y, Kim J Y, Choe G, Choi B S, Kim S J, An T K and Jeong Y J 2021 Enhanced contact properties of spray-coated AgNWs source and drain electrodes in oxide thin-film transistors *Curr. Appl. Phys.* **21** 155-60

[79] Song J Y, Oh J H, Choi D and Park S M 2021 Highly efficient patterning technique for silver nanowire electrodes by electrospray deposition and its application to self-powered triboelectric tactile sensor *Sci. Rep.* **11** 1-12

[80] Um D-S, Lee Y, Kim T, Lim S, Lee H, Ha M, Khan Z, Kang S, Kim M P and Kim J Y 2020 High-resolution filtration patterning of silver nanowire

electrodes for flexible and transparent optoelectronic devices *ACS Appl. Mater. Interfaces* **12** 32154-62

[81] Miller M S, O'Kane J C, Niec A, Carmichael R S and Carmichael T B 2013 Silver nanowire/optical adhesive coatings as transparent electrodes for flexible electronics *ACS Appl. Mater. Interfaces* **5** 10165-72

[82] Ahn J, Seo J-W, Lee T-I, Kwon D, Park I, Kim T-S and Lee J-Y 2016 Extremely robust and patternable electrodes for copy-paper-based electronics *ACS Appl. Mater. Interfaces* **8** 19031-7

[83] Ahn J, Seo J-W, Kim J Y, Lee J, Cho C, Kang J, Choi S-Y and Lee J-Y 2016 Self-supplied nano-fusing and transferring metal nanostructures via surface oxide reduction *ACS Appl. Mater. Interfaces* **8** 1112-9

[84] Wang P-H, Chen S-P, Su C-H and Liao Y-C 2015 Direct printed silver nanowire thin film patterns for flexible transparent heaters with temperature gradients *RSC Adv.* **5** 98412-8

[85] Maisch P, Tam K C, Lucera L, Egelhaaf H-J, Scheiber H, Maier E and Brabec C J 2016 Inkjet printed silver nanowire percolation networks as electrodes for highly efficient semitransparent organic solar cells *Org. Electron.* **38** 139-43

[86] Huang Q, Al-Milaji K N and Zhao H 2018 Inkjet printing of silver nanowires for stretchable heaters *ACS Appl. Nano Mater.* **1** 4528-36

[87] Li X, Kim K, Oh H, Moon H C, Nam S and Kim S H 2019 Cone-jet printing of aligned silver nanowire/poly (ethylene oxide) composite electrodes for organic thin-film transistors *Org. Electron.* **69** 190-9

[88] Li X, Lee G S, Park S H, Kong H, An T K and Kim S H 2018 Direct writing of silver nanowire electrodes via dragging mode electrohydrodynamic jet

printing for organic thin film transistors *Org. Electron.* **62** 357-65

[89] Lee H, Seong B, Kim J, Jang Y and Byun D 2014 Direct alignment and patterning of silver nanowires by electrohydrodynamic jet printing *Small* **10** 3918-22

[90] Ouyang J and Yang Y 2006 Conducting polymer as transparent electric glue *Adv. Mater.* **18** 2141-4

[91] Huang J, Li G and Yang Y 2008 A semi-transparent plastic solar cell fabricated by a lamination process *Adv. Mater.* **20** 415-9

[92] Shimada C and Shiratori S 2013 Viscous conductive glue layer in semitransparent polymer-based solar cells fabricated by a lamination process *ACS Appl. Mater. Interfaces* **5** 11087-92

[93] Park J, Kim G, Lee B, Lee S, Won P, Yoon H, Cho H, Ko S H and Hong Y 2020 Highly Customizable Transparent Silver Nanowire Patterning via Inkjet-Printed Conductive Polymer Templates Formed on Various Surfaces *Adv. Mater. Technol.* **5** 2000042

[94] Spyropoulos G D, Quiroz C O R, Salvador M, Hou Y, Gasparini N, Schweizer P, Adams J, Kubis P, Li N and Spiecker E 2016 Organic and perovskite solar modules innovated by adhesive top electrode and depth-resolved laser patterning *Energy Environ. Sci.* **9** 2302-13

[95] Cohen D, Bostian M E, Nguyen L and Walter M G 2018 Conductive poly (3, 4-ethylenedioxythiophene): poly (styrene sulfonate) polymer glue as an ohmic and rectifying electrical contact for H-terminated n-Si and p-Si wafers *Polym. Int.* **67** 853-8

[96] Park J, Yoon H, Kim G, Lee B, Lee S, Jeong S, Kim T, Seo J, Chung S and Hong Y 2019 Highly customizable all solution–processed polymer light

emitting diodes with inkjet printed Ag and transfer printed conductive polymer electrodes *Adv. Funct. Mater.* **29** 1902412

[97] Lee K M, Fardel R, Zhao L, Arnold C B and Rand B P 2017 Enhanced outcoupling in flexible organic light-emitting diodes on scattering polyimide substrates *Org. Electron.* **51** 471-6

[98] Kang H, Kim Y, Cheon S, Yi G-R and Cho J H 2017 Halide welding for silver nanowire network electrode *ACS Appl. Mater. Interfaces* **9** 30779-85

[99] Tooley W W, Feghhi S, Han S J, Wang J and Sniadecki N J 2011 Thermal fracture of oxidized polydimethylsiloxane during soft lithography of nanopost arrays *J. Micromech. Microeng.* **21** 054013

[100] Yu S, Sun Y, Ni Y, Zhang X and Zhou H 2016 Controlled formation of surface patterns in metal films deposited on elasticity-gradient PDMS substrates *ACS Appl. Mater. Interfaces* **8** 5706-14

[101] Haacke G 1976 New figure of merit for transparent conductors *J. Appl. Phys.* **47** 4086-9

[102] Serrano I G, Panda J, Edvinsson T and Kamalakar M V 2020 Flexible transparent graphene laminates via direct lamination of graphene onto polyethylene naphthalate substrates *Nanoscale Adv.* **2** 3156-63

[103] Weijtens C 1991 Influence of the deposition and anneal temperature on the electrical properties of indium tin oxide *J. Electrochem. Soc.* **138** 3432

[104] Fang Y, Wu Z, Li J, Jiang F, Zhang K, Zhang Y, Zhou Y, Zhou J and Hu B 2018 High-performance hazy silver nanowire transparent electrodes through diameter tailoring for semitransparent photovoltaics *Adv. Funct. Mater.* **28** 1705409

[105] Tokuno T, Nogi M, Karakawa M, Jiu J, Nge T T, Aso Y and Suganuma K

2011 Fabrication of silver nanowire transparent electrodes at room temperature *Nano Res.* **4** 1215-22

[106] Liu H-S, Pan B-C and Liou G-S 2017 Highly transparent AgNW/PDMS stretchable electrodes for elastomeric electrochromic devices *Nanoscale* **9** 2633-9

[107] Zhu Y, Deng Y, Yi P, Peng L, Lai X and Lin Z 2019 Flexible transparent electrodes based on silver nanowires: Material synthesis, fabrication, performance, and applications *Adv. Mater. Technol.* **4** 1900413

[108] Wu T, Sher C-W, Lin Y, Lee C-F, Liang S, Lu Y, Huang Chen S-W, Guo W, Kuo H-C and Chen Z 2018 Mini-LED and micro-LED: promising candidates for the next generation display technology *Appl. Sci.* **8** 1557

[109] Huang Y, Hsiang E-L, Deng M-Y and Wu S-T 2020 Mini-LED, Micro-LED and OLED displays: Present status and future perspectives *Light Sci. Appl.* **9** 1-16

[110] Pan Z, Guo C, Wang X, Liu J, Cao R, Gong Y, Wang J, Liu N, Chen Z and Wang L 2020 Wafer-Scale Micro-LEDs Transferred onto an Adhesive Film for Planar and Flexible Displays *Adv. Mater. Technol.* **5** 2000549

[111] Kishino K, Sakakibara N, Narita K and Oto T 2019 Two-dimensional multicolor (RGBY) integrated nanocolumn micro-LEDs as a fundamental technology of micro-LED display *Appl. Phys. Express* **13** 014003

[112] Ho D H, Hong P, Han J T, Kim S Y, Kwon S J and Cho J H 2020 3D-printed sugar scaffold for high-precision and highly sensitive active and passive wearable sensors *Adv. Sci.* **7** 1902521

[113] Oren S, Ceylan H, Schnable P S and Dong L 2017 High-resolution patterning and transferring of graphene-based nanomaterials onto tape toward roll-to-

roll production of tape-based wearable sensors *Adv. Mater. Technol.* **2** 1700223

[114] Biswas S, Schoeberl A, Hao Y, Reiprich J, Stauden T, Pezoldt J and Jacobs H O 2019 Integrated multilayer stretchable printed circuit boards paving the way for deformable active matrix *Nat. Commun.* **10** 1-8

[115] Lopes P A, Santos B C, de Almeida A T and Tavakoli M 2021 Reversible polymer-gel transition for ultra-stretchable chip-integrated circuits through self-soldering and self-coating and self-healing *Nat. Commun.* **12** 1-10

[116] Linghu C, Zhang S, Wang C and Song J 2018 Transfer printing techniques for flexible and stretchable inorganic electronics *npj Flex. Electron.* **2** 1-14

[117] Li W, Meredov A and Shamim A 2019 Coat-and-print patterning of silver nanowires for flexible and transparent electronics *npj Flex. Electron.* **3** 1-7

[118] Wan T, Guan P, Guan X, Hu L, Wu T, Cazorla C and Chu D 2020 Facile patterning of silver nanowires with controlled polarities via inkjet-assisted manipulation of interface adhesion *ACS Appl. Mater. Interfaces* **12** 34086-94

[119] Inoue A, Yuk H, Lu B and Zhao X 2020 Strong adhesion of wet conducting polymers on diverse substrates *Sci. Adv.* **6** eaay5394

[120] Park B, Jang J, Kim H, Seo J, Yoo H, Kim T and Hong Y 2020 Dense assembly of finely patterned semiconducting single-walled carbon nanotubes via a selective transfer method of nanotube-attracting layers *ACS Appl. Mater. Interfaces* **12** 38441-50

[121] De S, Higgins T M, Lyons P E, Doherty E M, Nirmalraj P N, Blau W J, Boland J J and Coleman J N 2009 Silver nanowire networks as flexible, transparent, conducting films: extremely high DC to optical conductivity

ratios *ACS Nano* **3** 1767-74

[122] Kim T-W, Lee J-S, Kim Y-C, Joo Y-C and Kim B-J 2019 Bending strain and bending fatigue lifetime of flexible metal electrodes on polymer substrates *Materials* **12** 2490

[123] Lim S, Park S H, An T K, Lee H S and Kim S H 2016 Electrohydrodynamic printing of poly (3, 4-ethylenedioxythiophene): poly (4-styrenesulfonate) electrodes with ratio-optimized surfactant *RSC Adv.* **6** 2004-10

[124] Yoon J, Joo Y, Oh E, Lee B, Kim D, Lee S, Kim T, Byun J and Hong Y 2019 Soft Modular Electronic Blocks (SMEBs): A Strategy for Tailored Wearable Health-Monitoring Systems *Adv. Sci.* **6** 1801682

[125] Byun J, Lee B, Oh E, Kim H, Kim S, Lee S and Hong Y 2017 Fully printable, strain-engineered electronic wrap for customizable soft electronics *Sci. Rep.* **7** 1-11

[126] Jang H J, Lee J Y, Kwak J, Lee D, Park J-H, Lee B and Noh Y Y 2019 Progress of display performances: AR, VR, QLED, OLED, and TFT *J. Inf. Disp.* **20** 1-8

[127] Geum D-M, Kim S K, Kang C-M, Moon S-H, Kyhm J, Han J, Lee D-S and Kim S 2019 Strategy toward the fabrication of ultrahigh-resolution micro-LED displays by bonding-interface-engineered vertical stacking and surface passivation *Nanoscale* **11** 23139-48

[128] Xiong J, Hsiang E-L, He Z, Zhan T and Wu S-T 2021 Augmented reality and virtual reality displays: emerging technologies and future perspectives *Light Sci. Appl.* **10** 1-30

[129] Sun Y, Fan J, Liu M, Zhang L, Jiang B, Zhang M and Zhang X 2020 Highly transparent, ultra-thin flexible, full-color mini-LED display with indium–

gallium–zinc oxide thin-film transistor substrate *J. Soc. Inf. Disp.* **28** 926-35

[130] Tan G, Huang Y, Li M-C, Lee S-L and Wu S-T 2018 High dynamic range liquid crystal displays with a mini-LED backlight *Opt. Express* **26** 16572-84

[131] Lu B, Wang Y, Hyun B-R, Kuo H-C and Liu Z 2020 Color difference and thermal stability of flexible transparent InGaN/GaN multiple quantum wells mini-LED arrays *IEEE Electron Device Lett.* **41** 1040-3

[132] Kang C-M, Kong D-J, Shim J-P, Kim S, Choi S-B, Lee J-Y, Min J-H, Seo D-J, Choi S-Y and Lee D-S 2017 Fabrication of a vertically-stacked passive-matrix micro-LED array structure for a dual color display *Opt. Express* **25** 2489-95

[133] Lin R, Liu X, Zhou G, Qian Z, Cui X and Tian P 2021 InGaN Micro-LED Array Enabled Advanced Underwater Wireless Optical Communication and Underwater Charging *Adv. Opt. Mater.* **9** 2002211

[134] Zhang X, Qi L, Chong W C, Li P, Tang C W and Lau K M 2021 Active matrix monolithic micro-LED full-color micro-display *J. Soc. Inf. Disp.* **29** 47-56

[135] Paranjpe A, Montgomery J, Lee S M and Morath C 2018 45-2: invited paper: micro-LED displays: key manufacturing challenges and solutions *SID Symp. Dig. Tech. Pap.* **49** 597-600

[136] Ma T, Chen J, Chen Z, Liang L, Hu J, Shen W, Li Z and Zeng H 2023 Progress in Color Conversion Technology for Micro-LED *Adv. Mater. Technol.* **8** 2200632

[137] Kim W H, Jang Y J, Kim J-Y, Han M, Kang M, Yang K, Ryou J-H and Kwon M-K 2020 High-performance color-converted full-color micro-LED arrays *Appl. Sci.* **10** 2112

[138] Qi L, Zhang X, Chong W C, Li P and Lau K M 2021 848 ppi high-brightness active-matrix micro-LED micro-display using GaN-on-Si epi-wafers towards mass production *Opt. Express* **29** 10580-91

[139] Wang Z, Zhu S, Shan X, Yuan Z, Cui X and Tian P 2021 Full-color micro-LED display based on a single chip with two types of InGaN/GaN MQWs *Opt. Lett.* **46** 4358-61

[140] Lee T-Y, Chen L-Y, Lo Y-Y, Swayamprabha S S, Kumar A, Huang Y-M, Chen S-C, Zan H-W, Chen F-C and Horng R-H 2022 Technology and Applications of Micro-LEDs: Their Characteristics, Fabrication, Advancement, and Challenges *ACS Photonics* **9** 2905-30

[141] Liu Y, Hyun B-R, Wang Y, Zhang K, Kwok H S and Liu Z 2020 R/G/B Micro-LEDs for In-Pixel Integrated Arrays and Temperature Sensing *ACS Appl. Electron. Mater.* **3** 3-10

[142] Gou F, Hsiang E L, Tan G, Lan Y F, Tsai C Y and Wu S T 2019 High performance color-converted micro-LED displays *J. Soc. Inf. Disp.* **27** 199-206

[143] Yin Y, Hu Z, Ali M U, Duan M, Gao L, Liu M, Peng W, Geng J, Pan S and Wu Y 2020 Full-color micro-LED display with $CsPbBr_3$ perovskite and CdSe quantum dots as color conversion layers *Adv. Mater. Technol.* **5** 2000251

[144] Mun S H, Kang C M, Min J H, Choi S Y, Jeong W L, Kim G G, Lee J S, Kim K P, Ko H C and Lee D S 2021 Highly Efficient Full-Color Inorganic LEDs on a Single Wafer by Using Multiple Adhesive Bonding *Adv. Mater. Interfaces* **8** 2100300

[145] Wijayantha K, Peter L M and Otley L 2004 Fabrication of CdS quantum dot

sensitized solar cells via a pressing route *Sol. Energy Mater. Sol. Cells* **83** 363-9

[146] Chan W C and Nie S 1998 Quantum dot bioconjugates for ultrasensitive nonisotopic detection *Science* **281** 2016-8

[147] Moon H, Lee C, Lee W, Kim J and Chae H 2019 Stability of quantum dots, quantum dot films, and quantum dot light-emitting diodes for display applications *Adv. Mater.* **31** 1804294

[148] Yang J, Choi M K, Yang U J, Kim S Y, Kim Y S, Kim J H, Kim D-H and Hyeon T 2020 Toward full-color electroluminescent quantum dot displays *Nano Lett.* **21** 26-33

[149] Mashford B S, Stevenson M, Popovic Z, Hamilton C, Zhou Z, Breen C, Steckel J, Bulovic V, Bawendi M and Coe-Sullivan S 2013 High-efficiency quantum-dot light-emitting devices with enhanced charge injection *Nat. Photonics* **7** 407-12

[150] Castan A, Kim H-M and Jang J 2014 All-solution-processed inverted quantum-dot light-emitting diodes *ACS Appl. Mater. Interfaces* **6** 2508-15

[151] Yu Y, Liang Y, Yong J, Li T, Hossain M S, Liu Y, Hu Y, Ganesan K and Skafidas E 2022 Low-Temperature Solution-Processed Transparent QLED Using Inorganic Metal Oxide Carrier Transport Layers *Adv. Funct. Mater.* **32** 2106387

[152] Liu Y, Jiang C, Song C, Wang J, Mu L, He Z, Zhong Z, Cun Y, Mai C and Wang J 2018 Highly efficient all-solution processed inverted quantum dots based light emitting diodes *ACS Nano* **12** 1564-70

[153] Ko Y-H, Prabhakaran P, Choi S, Kim G-J, Lee C and Lee K-S 2020 Environmentally friendly quantum-dot color filters for ultra-high-definition

liquid crystal displays *Sci. Rep.* **10** 1-8

[154] Hu Z, Yin Y, Ali M U, Peng W, Zhang S, Li D, Zou T, Li Y, Jiao S and Chen S-j 2020 Inkjet printed uniform quantum dots as color conversion layers for full-color OLED displays *Nanoscale* **12** 2103-10

[155] Dupont D, Tessier M D, Smet P F and Hens Z 2017 Indium phosphide-based quantum dots with Shell-enhanced absorption for luminescent down-conversion *Adv. Mater.* **29** 1700686

[156] Yoon H C, Kang H, Lee S, Oh J H, Yang H and Do Y R 2016 Study of perovskite QD down-converted LEDs and six-color white LEDs for future displays with excellent color performance *ACS Appl. Mater. Interfaces* **8** 18189-200

[157] Wood V, Panzer M J, Chen J, Bradley M S, Halpert J E, Bawendi M G and Bulović V 2009 Inkjet-printed quantum dot–polymer composites for full-color ac-driven displays *Adv. Mater.* **21** 2151-5

[158] Haverinen H M, Myllylä R A and Jabbour G E 2009 Inkjet printing of light emitting quantum dots *Appl. Phys. Lett.* **94** 073108

[159] Yang P, Zhang L, Kang D J, Strahl R and Kraus T 2020 High-resolution inkjet printing of quantum dot light-emitting microdiode arrays *Adv. Opt. Mater.* **8** 1901429

[160] Bae W K, Kwak J, Lim J, Lee D, Nam M K, Char K, Lee C and Lee S 2010 Multicolored light-emitting diodes based on all-quantum-dot multilayer films using layer-by-layer assembly method *Nano Lett.* **10** 2368-73

[161] Jiang C, Zhong Z, Liu B, He Z, Zou J, Wang L, Wang J, Peng J and Cao Y 2016 Coffee-ring-free quantum dot thin film using inkjet printing from a mixed-solvent system on modified ZnO transport layer for light-emitting

devices *ACS Appl. Mater. Interfaces* **8** 26162-8

[162] Liu Y, Li F, Xu Z, Zheng C, Guo T, Xie X, Qian L, Fu D and Yan X 2017 Efficient all-solution processed quantum dot light emitting diodes based on inkjet printing technique *ACS Appl. Mater. Interfaces* **9** 25506-12

[163] Li H, Duan Y, Shao Z, Zhang G, Li H, Huang Y and Yin Z 2020 High-Resolution Pixelated Light Emitting Diodes Based on Electrohydrodynamic Printing and Coffee-Ring-Free Quantum Dot Film *Adv. Mater. Technol.* **5** 2000401

[164] Dement D B, Quan M K and Ferry V E 2019 Nanoscale patterning of colloidal nanocrystal films for nanophotonic applications using direct write electron beam lithography *ACS Appl. Mater. Interfaces* **11** 14970-9

[165] Nakanishi Y, Takeshita T, Qu Y, Imabayashi H, Okamoto S, Utsumi H, Kanehiro M, Angioni E, Boardman E A and Hamilton I 2020 Active matrix QD-LED with top emission structure by UV lithography for RGB patterning *J. Soc. Inf. Disp.* **28** 499-508

[166] Kang H, Kim S, Oh J H, Yoon H C, Jo J H, Yang H and Do Y R 2018 Color-by-blue QD-emissive LCD enabled by replacing RGB color filters with narrow-band GR InP/ZnSeS/ZnS QD films *Adv. Opt. Mater.* **6** 1701239

[167] Nazim M, Kim B, Lee S, Min B K and Kim J H 2020 UV-Curable Polymer–QD Flexible Films as the Downconversion Layer for Improved Performance of Cu (In, Ga) Se2 Solar Cells *Energy Fuels* **34** 14581-90

[168] Elliott A M, Ivanova O S, Williams C B and Campbell T A 2013 Inkjet printing of quantum dots in photopolymer for use in additive manufacturing of nanocomposites *Adv. Eng. Mater.* **15** 903-7

[169] Li X, Kundaliya D, Tan Z J, Anc M and Fang N X 2019 Projection

lithography patterned high-resolution quantum dots/thiol-ene photo-polymer pixels for color down conversion *Opt. Express* **27** 30864-74

[170] Zou W, Yu H, Lv X, Zhou P, Guo H, Zhong Y and Liu L 2022 Electrohydrodynamic Direct-Writing Fabrication of Microstructure-Enhanced Microelectrode Arrays for Customized and Curved Physiological Electronics *Adv. Mater. Interfaces* **9** 2201197

[171] Tang L, Min J, Lee E-C, Kim J S and Lee N Y 2010 Targeted cell adhesion on selectively micropatterned polymer arrays on a poly (dimethylsiloxane) surface *Biomed. Microdevices* **12** 13-21

[172] Kim J Y, Pfeiffer K, Voigt A, Gruetzner G and Brugger J 2012 Directly fabricated multi-scale microlens arrays on a hydrophobic flat surface by a simple ink-jet printing technique *J. Mater. Chem.* **22** 3053-8

[173] Lee Y, Bae S, Hwang B, Schroeder M, Lee Y and Baik S 2019 Considerably improved water and oil washability of highly conductive stretchable fibers by chemical functionalization with fluorinated silane *J. Mater. Chem. C* **7** 12297-305

[174] Xiang H and Komvopoulos K 2013 Effect of fluorocarbon self-assembled monolayer films on sidewall adhesion and friction of surface micromachines with impacting and sliding contact interfaces *J. Appl. Phys.* **113** 224505

[175] Koh T-W, Cho H, Yun C and Yoo S 2012 ITO-free down-conversion white organic light-emitting diodes with structured color conversion layers for enhanced optical efficiency and color rendering *Org. Electron.* **13** 3145-53

[176] Kim Y H, Lee H, Kang S-M, Lee Y and Bae B-S 2020 Long-term stable microlens array-integrated quantum dot/siloxane film for thin white backlight units *ACS Appl. Nano Mater.* **3** 10261-9

[177] Smith M J, Malak S T, Jung J, Yoon Y J, Lin C H, Kim S, Lee K M, Ma R, White T J and Bunning T J 2017 Robust, uniform, and highly emissive quantum dot–polymer films and patterns using thiol–ene chemistry *ACS Appl. Mater. Interfaces* **9** 17435-48

[178] Kim Y H, Koh S, Lee H, Kang S-M, Lee D C and Bae B-S 2019 Photo-patternable quantum dots/siloxane composite with long-term stability for quantum dot color filters *ACS Appl. Mater. Interfaces* **12** 3961-8

[179] Shiraishi M, Iso Y and Isobe T 2022 Transparent Nanocomposites Comprising Ligand-Exchanged CuInS2/ZnS Quantum Dots and UV-Cured Resin for Wavelength Converters *ACS Omega* **7** 33039-45

[180] Smith M J, Lin C H, Yu S and Tsukruk V V 2019 Composite structures with emissive quantum dots for light enhancement *Adv. Opt. Mater.* **7** 1801072

[181] Kim T, Yoon C, Song Y-G, Kim Y-J and Lee K 2016 Thermal stabilities of cadmium selenide and cadmium-free quantum dots in quantum dot–silicone nanocomposites *J. Lumin.* **177** 54-8

[182] Liu C-Y, Chen T-P, Kao T S, Huang J-K, Kuo H-C, Chen Y-F and Chang C-Y 2016 Color-conversion efficiency enhancement of quantum dots via selective area nano-rods light-emitting diodes *Opt. Express* **24** 19978-87

[183] Hyun B-R, Sher C-W, Chang Y-W, Lin Y, Liu Z and Kuo H-C 2021 Dual role of quantum dots as color conversion layer and suppression of input light for full-color micro-LED displays *J. Phys. Chem. Lett.* **12** 6946-54

[184] Khan Y, Hwang S, Braveenth R, Jung Y H, Walker B and Kwon J H 2022 Synthesis of fluorescent organic nano-dots and their application as efficient color conversion layers *Nat. Commun.* **13** 1-9

[185] Su M, Qin F, Zhang Z, Chen B, Pan Q, Huang Z, Cai Z, Zhao Z, Hu X and

Derome D 2020 Non-lithography hydrodynamic printing of micro/nanostructures on curved surfaces *Angew. Chem. Int. Ed.* **59** 14234-40

[186] Adams J J, Duoss E B, Malkowski T F, Motala M J, Ahn B Y, Nuzzo R G, Bernhard J T and Lewis J A 2011 Conformal printing of electrically small antennas on three-dimensional surfaces *Adv. Mater.* **23** 1335-40

[187] Senior M 2014 Novartis signs up for Google smart lens *Nat. Biotechnol.* **32** 856-7

[188] Wu H, Tian Y, Luo H, Zhu H, Duan Y and Huang Y 2020 Fabrication techniques for curved electronics on arbitrary surfaces *Adv. Mater. Technol.* **5** 2000093

[189] Seong B, Yoo H, Nguyen V D, Jang Y, Ryu C and Byun D 2014 Metal-mesh based transparent electrode on a 3-D curved surface by electrohydrodynamic jet printing *J. Micromech. Microeng.* **24** 097002

[190] An B W, Kim K, Kim M, Kim S Y, Hur S H and Park J U 2015 Direct printing of reduced graphene oxide on planar or highly curved surfaces with high resolutions using electrohydrodynamics *Small* **11** 2263-8

[191] Shi J, Ge W, Zhu J, Saruyama M and Teranishi T 2020 Core–Shell $CsPbBr_3$@ CdS Quantum Dots with Enhanced Stability and Photoluminescence Quantum Yields for Optoelectronic Devices *ACS Appl. Nano Mater.* **3** 7563-71

[192] Abe S, Joos J J, Martin L I, Hens Z and Smet P F 2017 Hybrid remote quantum dot/powder phosphor designs for display backlights *Light Sci. Appl.* **6** e16271-e

[193] Li Z-T, Li J-X, Li J-S, Deng Z-H, Deng Y-H and Tang Y 2020 Scattering

effect on optical performance of quantum dot white light-emitting diodes incorporating SiO_2 nanoparticles *IEEE J. Quantum Electron.* **56** 1-9

[194] Kim H C, Hong H-G, Yoon C, Choi H, Ahn I-S, Lee D C, Kim Y-J and Lee K 2013 Fabrication of high quantum yield quantum dot/polymer films by enhancing dispersion of quantum dots using silica particles *J. Colloid Interface Sci.* **393** 74-9

Publication List

[1] International Journals

1. J. Park†, **G. Kim**†, B. Lee, S. Lee, P. Won, H. Yoon, H. Cho, S. Ko, Y. Hong*, “Highly Customizable Transparent Silver Nanowire Patterning via Inkjet-printed Conductive Polymer Templates Formed on Various Surfaces”, *Advanced Materials Technologies* **5**, 2000042 (2020) (Equally contributed article)
2. **G. Kim,** J. Yoon, H. Yoon, H. Cho, J. Seo, Y. Hong*, “High-resolution maskless patterning of AgNWs based on adhesion enhancement of printed conductive polymer”, *Flexible & Printed Electronics* **7**, 045009 (2022)
3. **G.Kim** et al., “High-resolution patterning of uniform polymer/QD composites by ink optimization” (manuscript in preparation)

i. S. Lee, S. Lee, H. Yoon, C.-K. Lee, C. Yoo, J. Park, J. Byun, **G. Kim**, B. Lee, B. Lee, and Y. Hong*, “Printed cylindrical lens pair for application to the seam concealment in tiled displays”, *Optics Express* **26**, 824 (2018)

ii. J. Park, H. Yoon, **G. Kim**, B. Lee, S. Lee, S. Jeong, T. Kim, J. Seo, S. Chung, Y. Hong*, “Highly Customizable All Solution–Processed Polymer Light Emitting Diodes with Inkjet Printed Ag and Transfer Printed Conductive Polymer Electrodes”, *Advanced Functional Materials* **29**, 1902412 (2019)

iii. D. Kim, D. K. Lee, J. Yoon, D. Hahm, B. Lee, E. Oh, **G. Kim**, J. Seo, and Y. Hong*, “Electronic Skin Based on Cellulose/Carbon Nanotube Fiber

Network for Large-Area 3D Touch and Real-Time 3D Surface Scanning", *ACS Applied Materials & Interfaces* **13**, 53111 (2021)

iv. S. Lee, C. Yoo, H. Yoon, D. Kim, **G. Kim**, B. Lee, and Y. Hong*, "3D printing-based mirrored image component for seamless modular curved-edge displays", *Optics Express* **29**, 14745 (2021)

[2] International Conference

1. **G. Kim**, J. Park, J. Ha, J. Ha, C. Lee, and Y. Hong*, "ITO PEDOT PSS Bilayer Electrodes with Superior Flexibility and Their Application to Solution-Processed Polymer Light-Emitting Diodes", The 8th International Workshop on Flexible & Printable Electronics (IWFPE 2016), Jeonju, Korea, November (2016) (Poster)
2. **G. Kim**, J. Park, J. Ha, C. Lee, and Y. Hong*, "Fabrication of solution-processed flexible polymer light-emitting diodes with ITO/PEDOT:PSS bilayer transparent electrodes", The 8th International Conference on Flexible and Printed Electronics (ICFPE 2017), Jeju island, Korea, September (2017) (Poster)
3. **G. Kim**, J. Park, S. Lee, C. Lee, and Y. Hong*, "ITO-free solution-processed polymer light-emitting diodes with embedded AgNW-transferred PEDOT:PSS", SPIE Photonics West 2019, San Francisco, February (2019) (Oral)
4. **G. Kim**, J. Park, S. Jeong, H. Yoon, S. Lee, and Y. Hong*, "All-solution-processed transparent polymer light-emitting diodes with transferred PEDOT:PSS electrodes", The 19th International Meeting on Information

Display 2019 (IMID 2019), Gyeongju, Korea, August (2019) (Poster)

5. **G. Kim**, J. Park, J. Yoon, S. Lee, and Y. Hong*, “Micro-Patternable AgNW-PEDOT:PSS Hybrid Electrodes for All-Solution-Processed Polymer Light-Emitting Diodes”, SID Display Week 2020, Virtual Conference, August (2020) (Poster)
6. **G. Kim**, J. Yoon, S. Lee, D. Kim, and Y. Hong*, “Electrohydrodynamic Inkjet Printed Micro-Rigid Island Arrays for Application to Stretchable Platform”, The 20th International Meeting on Information Display 2020 (IMID 2020), Virtual Conference, August (2020) (Oral)
7. **G. Kim**, J. Yoon, and Y. Hong*, “Precise Subtractive Patterning Method of AgNWs on Deformable Platform”, The 21st International Meeting on Information Display 2021 (IMID 2021), Seoul/Online, Korea, August (2021) (Poster)
8. **G. Kim**, H. Yoon, D. Hahm, J. Yoon, S. Lee, W. K. Bae, and Y. Hong*, “Electrohydrodynamic Printing of Quantum Dot/Polymer Composite for Color-Conversion Micro-Structure on Flexible Platform”, 2022 Materials Research Society (MRS) Spring Meeting & Exhibit, Honolulu, USA, May (2022) (Poster)

[3] Patent

1. Y. Hong, J. Park, **G. Kim** (SNU R&DB Foundation), “Silver nanowire thin-film patterning method”, US 17/254,261, 2021 (Application)
2. 홍용택, 박종장, **김건희** (서울대학교 산학협력단), “실버 나노와이어 박막 패터닝 방법”, 대한민국, 10-2087835, 2020 (등록)

3. 홍용택, 이승환, **김건희** (서울대학교 산학협력단), “양자점/고분자 복합재료의 미세 프린팅을 이용한 색전환 마이크로 렌즈 및 그 제조방법”, 대한민국, 10-2362061, 2022 (등록)
4. 홍용택, **김건희** (서울대학교 산학협력단), “전도성 폴리머 인쇄 기술 기반의 고해상도 마스크리스 나노 와이어 박막 패터닝 방법”, 대한민국, 10-2022-0138710, 2022 (출원)
5. 홍용택, **김건희**, 이승환, 윤형수 (서울대학교 산학협력단), “색전환 마이크로 렌즈 어레이 시트 및 그 제조 방법”, 대한민국, 10-2022-0029077, 2022 (가출원)

국문 초록

디스플레이 구성 요소들의 발전이 유연 신축성 기판 하에서의 장치의 안정적 동작에 초점을 맞추고 있음에 따라, 용액 공정이 기존의 공정의 단점을 보완하기 위한 유망한 박막 형성 공정으로 주목을 받아왔다. 그 중에서, 잉크 재료를 직접 인쇄하는 방식은 공정 시 패터닝 마스크가 필요 없어 패터닝 자유도가 높은 공정이라는 점에서 많은 연구자들이 주목하여 다양한 연구 성과가 보고되었다. 인쇄 공정 중 하나인 잉크젯 프린팅 방식은 매우 신뢰성 있는 인쇄 방식임에도 불구하고, 패터닝의 해상도의 증가가 요구됨에 따라 새로운 고해상도 패터닝 기술 중 하나인 EHD 프린팅 공정 방식이 새로운 대안으로 제시되어 왔다. 본 논문에서는, 원하는 해상도에 따라 잉크젯 프린팅 공정이나 EHD 공정 기술을 선택하여 차세대 디스플레이의 다양한 구성요소들을 손쉽게 패터닝하는 기술에 대하여 제안하였다.

첫 번째로, 잉크젯 프린팅과 전사 공정을 결합한 은 나노와이어 투명 전극의 패터닝 기술을 제시하였다. 복잡한 은 나노와이어의 패터닝 기술은 은나노와이어 투명 전극의 상품화를 가로막고 있다. 은 나노와이어의 경우 훌륭한 전기적 광학적 특성과 기계적 안정성을 가지고 있어 ITO의 대체제로 언급되고 있음에도, 공정 시 패터닝 마스크를 교체해야 하고 고해상도의 마스크 제작시에는 높은 공정

단가가 필요하다는 단점이 존재한다. 이러한 문제를 해결하기 위해, 접착 물질이 섞인 PEDOT:PSS 전도성 폴리머를 원하는 기판에 프린팅하고 그 위에 은 나노와이어가 코팅된 스탬프를 부착시켜, 스탬프로부터 은 나노와이어를 선택적으로 전사시키는 직관적인 패터닝 공정을 개발하였다. 접착물질이 포함되어 있는 PEDOT:PSS를 원하는 패턴으로 인쇄하고, 그 위에 은 나노와이어를 선택적으로 전사함으로써 패터닝 마스크가 필요하지 않으며, 유연 기판 위에 손쉽게 패터닝할 수 있는 길을 열었다. 단순한 투명전극 패터닝 기술을 통해, 훌륭한 유연성을 가지는 디스플레이에 응용할 수 있다.

둘 째로, 은 나노와이어 전극 패턴의 해상도를 높이기 위한 최적화된 고수율 패터닝 기술을 개발하였다. 잉크젯 프린팅의 해상도의 한계와 전사 공정 시에 가해지는 외력에 의한 패턴의 손상은 30 마이크로미터 이하의 미세공정을 방해해왔다. 따라서 은 나노와이어 패턴의 해상도를 향상시키기 위한 최적화된 패터닝 공정이 필요하였고, PVA 물질을 은 나노와이어 층 아래 위치시키는 접착 물질로 선택하였다. PEDOT:PSS를 은 나노와이어 층 위에 프린팅하면, 프린팅된 PEDOT:PSS와 PVA층이 상호 침투 과정을 거쳐 강하게 결합한다. 은 나노와이어는 PEDOT:PSS 와 PVA 층 사이에 붙잡히기 때문에, PEDOT:PSS 패턴 아래에 존재하는 은 나노와이어는 패터닝 공정을 진행하는 동안 손실 없이 남아있게 된다. 본 공정에서 EHD 프린팅을 도입하여, PEDOT:PSS 잉크를 15 마이크로미터 너비의 미세한 패턴형태로 토출할 수 있다. PVA를 이용한 공정 방식의 또다른

장점은 신축성 기판위에 정밀한 패터닝이 가능하다는 점이다. 그러므로 이러한 패터닝 방식은 고해상도를 가지는 고전도도의 신축성 전자소자에 응용 가능하다.

마지막으로, QD가 섞인 폴리머 물질을 EHD 프린팅 공정을 통해 미세 패터닝하여 최적화된 색전환 구조의 제작을 진행하였다. 인쇄된 QD 층의 균일성을 높이기 위해, QD와 광경화 가능한 폴리머 물질을 섞는 공정이 선행되었다. 폴리머 내부에서의 QD의 뭉침 현상과 그에 따른 EHD 공정에서의 노즐 막힘을 방지하기 위해 ligand exchange 공정이 수행되었다. 공정이 수행된 QD의 경우 발광 파장과 흡광 스펙트럼과 같은 QD의 광특성을 유지하였다. 또한, 폴리머와 QD의 혼합물의 경우 고농도의 QD의 경우에도 안정적으로 토출되었다. 적절한 표면처리를 통해 인쇄된 색전환 구조의 경우 렌즈의 형태를 띄고 있었으며, 그 직경은 40 마이크로미터에서부터 20 마이크로 미터까지 조절되었다. 마이크로 LED 광원위에 원하는 두께로 QD 혼합물을 인쇄하였을 때, 혼합물층에 의한 효과를 확인하였으며, 혼합물 잉크는 폴리이미드나 엘라스토머 위에도 프린팅 할 수 있어 차세대 발광소자로 응용할 수 있는 길을 열었다.

주요어: 은 나노와이어, PEDOT:PSS, 잉크젯 프린팅, EHD 프린팅, 퀀텀 닷, 유연 & 신축성 전자소자

학번: 2016-20865